TID-4500, UC-4
Chemistry

LAWRENCE LIVERMORE LABORATORY
University of California/Livermore, California/94550

UCRL-51061, Vol. I

COMPUTERIZED QUANTITATIVE ANALYSIS BY GAMMA-RAY SPECTROMETRY. VOL. I. DESCRIPTION OF THE GAMANAL PROGRAM

R. Gunnink

J. B. Niday

Ms. date: March 1, 1972

Contents

Other Volumes

Vol. II. Source Listing of the GAMANAL Program (1971)

Vol. III. A User's Guide to GAMANAL (1971)

Vol. IV. Auxiliary Programs for GAMANAL (to be published)

Vol. V. Decay-Scheme Data Library for GAMANAL (planned revision of UCID-15439)

COMPUTERIZED QUANTITATIVE ANALYSIS BY GAMMA-RAY SPECTROMETRY. VOL. I. DESCRIPTION OF THE GAMANAL PROGRAM

Abstract

GAMANAL provides a complete qualitative and quantitative analysis of mixtures of radioactive species by computer interpretation of high-resolution gamma-ray spectra. This volume describes the methods used for determining background, resolving and fitting complex peak groupings, determining the energies and absolute intensities of the gamma rays, and determining the amounts of the source nuclides. The latter are identified with the aid of a preprocessed decay-scheme library, and all interferences are resolved by a least-squares solution of the matrix of equations for the gamma intensities.

Introduction

The extensive use at Lawrence Livermore Laboratory of lithium-drifted germanium gamma-ray detector systems for nondestructive analysis has necessitated the development of computer programs capable of accurate and complete reduction and interpretation of the spectral data. This need resulted not only from the large number of data channels typically used but also from the complexity of the spectra. We have made preliminary reports[1,2] on an earlier version of our current computer code, which gave us several years of valuable service in analyzing samples containing mixtures of fission and activation products. More recently, we have completely rewritten major portions of this program, thereby developing a second generation program that incorporates the experience gained.

In this report we describe and partially document the approach we have adopted in analyzing spectra obtained by using Ge(Li) detectors. This approach must of course reflect the types and numbers of samples, the counting equipment, and the computer facilities available at the Laboratory. As a result of the use of computer-controlled automatic sample changers (see Fig. 1), the spectra are frequently submitted to the computer for analysis without any prior inspection by the experimenter. Therefore we have written GAMANAL so that little or no man-machine interaction is required, even though the spectra may be very complex.

We also require that the program be able to interpret a spectrum regardless of the nature of the source or its physical relationship to the detector. Because of

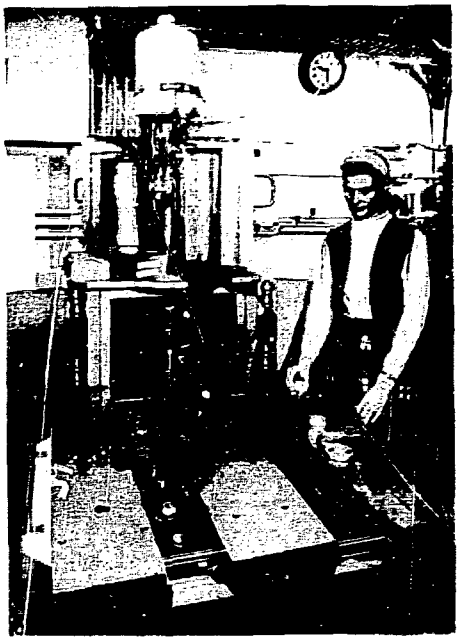

Fig. 1. View of one of the automatic sample changers for Ge(Li) counting.

the wide variety of sources encountered, the usual technique of using precalibrated counting positions is not feasible. For example, some sources are quite "cold" and must be counted at close-in geometries (~ 1 cm), whereas others require large counting distances (~ 100 cm). Some samples are point sources, whereas others are disk or solid sources composed of a variety of materials.

Equations derived from simplified models were therefore formulated and tested to account for this range of geometry and counting conditions and to correct for self-attenuation of gamma rays within the sample. In this way we were able to calibrate the counting systems so that the procedures for final analytical interpretation of the resulting data could be the same for all systems. Furthermore, this calibration is semipermanent and requires only a good set of absolute gamma ray

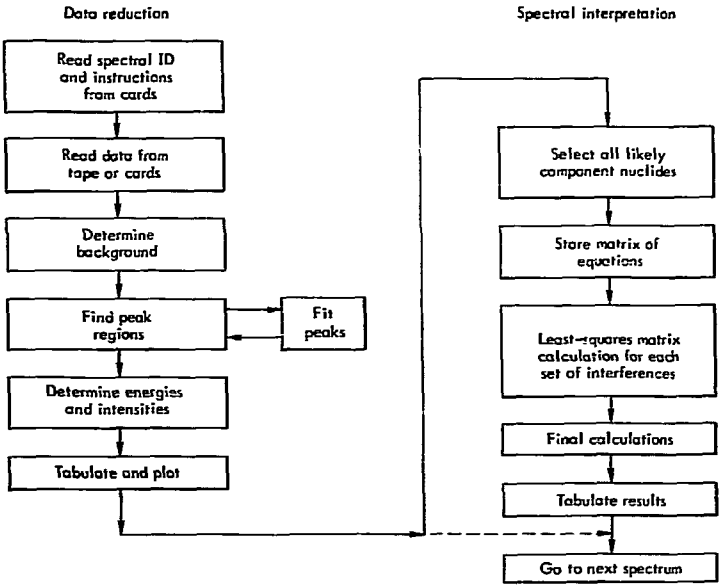

Fig. 2. Diagram of the GAMANAL program.

standards, which are available commercially or can be readily prepared.

A complete spectral analysis can be separated into two parts, first, the input and reduction of the spectral data into entities such as photopeak energies and intensities, and second, the quantitative interpretation of these items as disintegration rates, atoms, or grams of specific nuclides or materials.

Figure 2 shows a diagram outlining the computer program. The requirements and procedures for data input are detailed in Volume III of this report,[3] but a few features will be discussed briefly in the next section. A complete source listing of GAMANAL is to be found in Volume II.[4] Several auxiliary programs to be mentioned later will be listed and discussed in Volume IV.[5]

Data Handling

We have attempted to make the program flexible with respect to the input of data, control of the flow of the analysis, and output provided. Because it is a "hands-off" program, running primarily in the batch-production mode, this flexibility is obtained by use of a number of control instructions and parameter cards. The assembling of the data and instructions is handled by subroutine INTAKE, which has been split off from the main program for convenience only. Up to 17 different types of cards, each identified by a character (NCARD) punched in column 1, have been described in detail in the User's Guide.[3]

The basic card controlling the analysis of a specific spectrum has a 2 in the first column and must carry the detector and system labels and a unique six-character label (named NSPEC) for the spectrum. This Type 2 card usually supplies additional information, such as a name for the sample and data on its weight, timing, and geometry, as well as a coded set of instructions for the handling and analysis of the pulse-height data and output of the results.

This control card may be followed by other cards supplying information on the sample or its spectrum. However, the calibration parameter cards are identified by such items as detector or system, and for convenience are usually submitted as a group in front of the first sample control card. These parameters are stored with the aid of subroutine FSLOT and selected later as required by INTAKE.

After a Type 2 card has been interpreted, the specified pulse-height data are acquired from any of a variety of sources—data cards, binary or BCD magnetic tapes, or permanent storage tapes previously written by GAMANAL. The tape routines are heavily oriented toward this installation and will not be described here, but some discussion of them may be found in the User's Guide.[3]

Once the pulse-height data are stored, the reading of any additional cards is resumed until another sample control card is detected. However, this card is not interpreted until the analysis of the data already obtained has been completed and INTAKE has been reentered. The collected information is summarized (see

Appendix A) and usually stored on a permanent storage tape before the data-reduction phase begins.

If any essential information is missing, or if serious errors occur anywhere in the program, an exit is taken through subroutine EMERGX to skip the processing of the current sample rather than to risk aborting the remainder of the computer run. A call to the entry point PASS has the same effect, except that no memory dump is taken. After cleaning up some flags, this routine examines NCARD and NSPEC, determines the proper reentry point in INTAKE, and proceeds to the next sample.

Subroutine GRAPH utilizes the Laboratory facilities for obtaining hard copy from computer-generated cathode ray tube (CRT) pictures. The various plotting options available[3] in GAMANAL include plotting the raw data only, plotting the results of the fitting of individual peak groupings, and plotting the complete spectrum with a tracing of the background used and of the peaks located and their energies (see Appendix B). The last type of plot has proved very useful and corresponds with the tabulation of a summary of the peaks (see Appendix A) at the completion of the data reduction phase.

Data Reduction

DETERMINATION OF BACKGROUND

Subroutine BKGRD determines the background or Compton continuum under the peaks in a spectrum prior to the detailed examination of peak regions. The logic used is quite subjective and is based largely upon experience. Because of the multitude of tests and choices involved, it is difficult to follow the flow of data through this subroutine, and we will discuss only some of the more salient features.

The general approach, rather than delineating peak regions, is to attempt to find all the nonpeak regions in a spectrum by applying various tests to the slopes between points or groups of points. These tests take into account the resolution of the detector and the gain used, as well as the counting statistics. Regions which fail these tests are assumed to contain peaks, and the underlying background continuum for such regions is estimated by an interpolation method to be discussed later in this section.

An important feature of this approach is that we converge upon the final background curve in three stages. In the first we attempt to get a global view of the background of the entire spectrum, similar to the subjective view one gets from viewing a large graphic display. The details are overlooked, but the sign and magnitude of the slope are ascertained for all regions of the spectrum. Once this has been done, the succeeding stages can employ more rigorous criteria permitting correct decisions at the microscopic level.

The first stage is accomplished by generating a crude background curve using the technique of Ralston and Wilcox.[6] The original spectrum is smoothed as shown in Fig. 3, and each new data point compared with the original, which is always preserved. A new spectrum is generated by using the smoothed values instead of

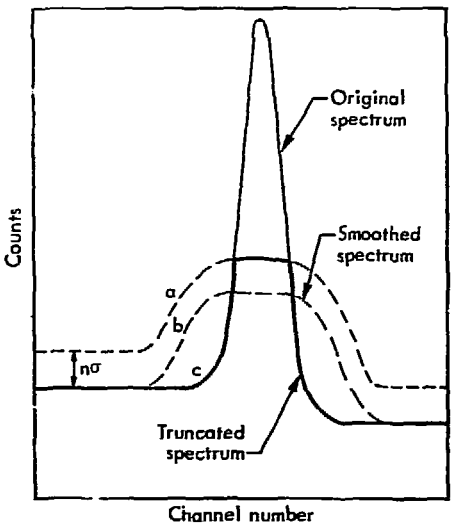

Fig. 3. Detail of the smoothing and truncation processes in the first stage of the background determination. A new "spectrum" (curve c) is formed by truncating the previous spectrum wherever it exceeds the smooth spectrum (curve b) by more than n standard deviations.

the original data points whenever the latter exceed the former by more than a specified number of standard deviations. This modified spectrum is now smoothed in turn and the process repeated, but the size of the allowable deviation is reduced. After several cycles of this process (seven are currently used) a fairly good general picture of the background continuum emerges, as illustrated in Fig. 4.

The second stage begins with a detailed comparison of the slopes between adjacent points or groups of points in this approximate background array and the corresponding slopes in the original data. A new background array is built up from points not showing statistically-significant differences.

We now will describe a second and somewhat unique feature of this subroutine, i.e., the method of interpolation between background regions. Instead of the simple straight-line or polynomial curve usually used to describe the shape of the background under a peak, we have chosen a smoothed step taken at the center of the peak, as shown in Fig. 5. We feel that this choice has a good basis in principle and in practice.

If we consider a hypothetical detector system exhibiting no instrumental noise or statistical effects, all the full-energy pulses corresponding to a given gamma ray could be made to appear in one channel rather than as a broadened distribution. The background just before the peak (i.e., the additional counts that one observes between the Compton edge and the low-energy side of a peak) presumably consists of degraded full-energy events resulting from such causes as detector edge effect or small-angle scattering by material between the sample and the detector. If such processes continue to contribute pulses up to the full energy of the peak, then, in our hypothetical case, a sharp step would be observed at the peak location. In actuality, the same line-broadening processes that spread the peak will affect these pulses, which we have chosen to consider part of the Compton background. The effect of this dispersion on the step is approximated by the two or three cycles of linear smoothing carried out later on the entire background array.

There is, moreover, an important practical reason for the interpolation by a smoothed-step function. In the case of a peak multiplet such as that in Fig. 6, background information can be obtained only

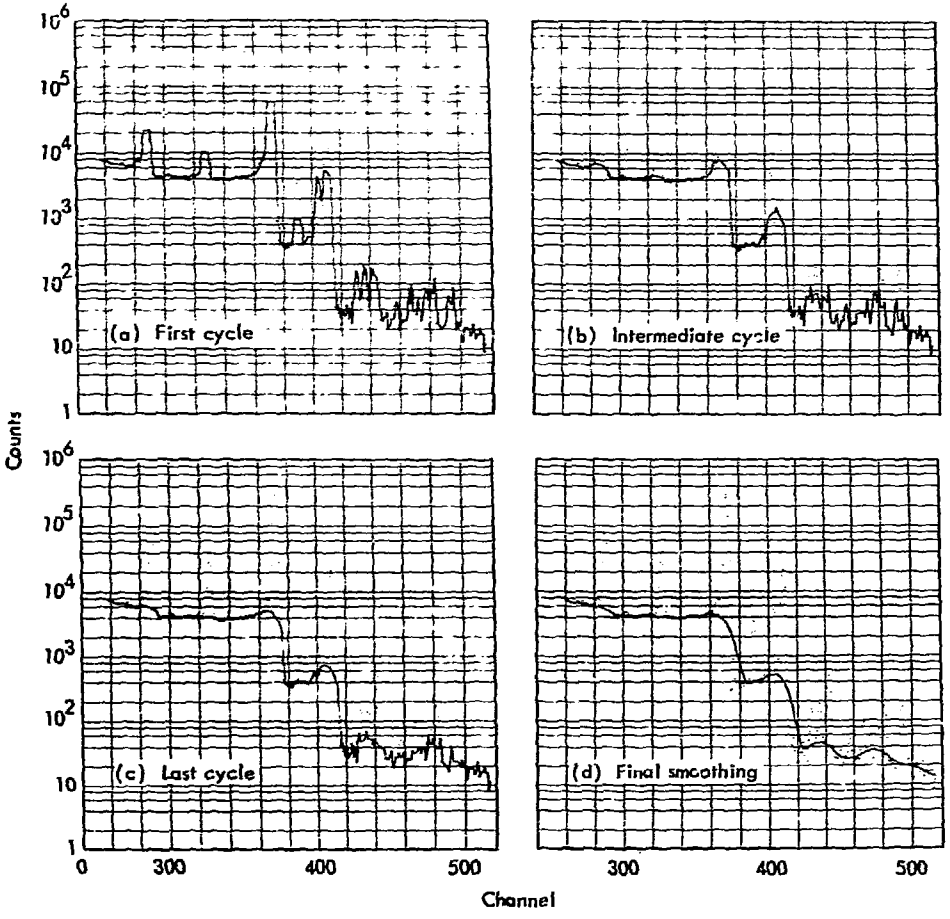

Fig. 4. The results of the first stage processes for a typical spectrum.

from the extreme ends of this peak region. Obviously, the simple straight-line interpolation shown as curve (a) will give incorrect results. An earlier version of GAMANAL, which used the straight line and apportioned the total area on the basis of the relative heights of the peaks without taking the peak shapes into account, gave unsatisfactory results in many cases.

In our present approach a step function is generated as shown in curve (b) and the subsequent smoothing produces the desired result (curve (c)). Note that this interpolation takes into account both the relative heights of the peaks and the previously-determined general slope of the background. Not only are the areas now determined more consistently, but

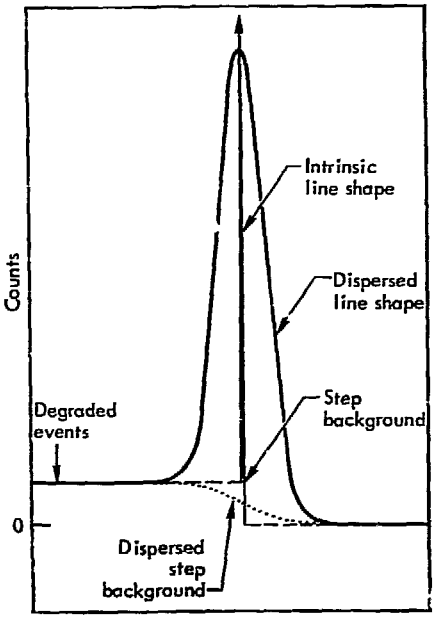

Fig. 5. Diagram of the effect of energy dispersion on the background under a peak. The same processes that broaden the intrinsic line shape will disperse the proposed sharp step in the background.

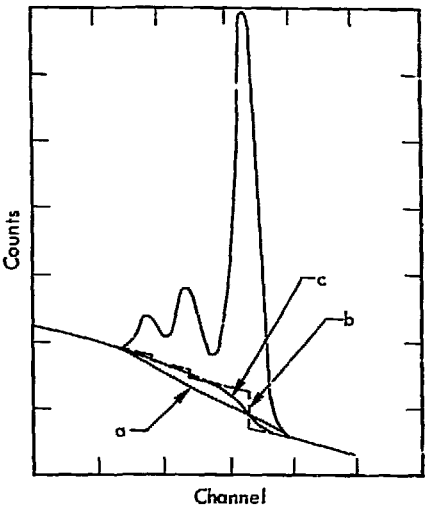

Fig. 6. Comparison of the straight-line interpolation (curve a) with the stepwise interpolation method (curve b and c) now used in GAMANAL. The final background (curve c) is produced by smoothing curve b.

the subsequent fit to standardized peak shapes is much more satisfactory.

Among the many precautions that must be taken in BKGRD are those against using "dropped" or overflowed channel counts. Part of the logic of this subroutine is that the background cannot exceed the data points to a statistically-significant degree (or else, presumably, the true background was missed). If this occurs in making an interpolation, checks for overflows are made before the intervening low points are accepted as background. If they are accepted, new interpolations are made, which will have the effect of breaking up any peak grouping involved.

For the third stage of the background determination, the entire second stage process is repeated with tightened criteria because better information is now available on the slope of the background.

Figure 7 demonstrates the results of this approach on a section of spectral data.

The peak regions of the spectrum can now be located by subtracting the background data from the original spectrum. Some upward adjustment of the background may occur later during the peak-shape analysis of these regions (see subroutine FIT).

DELINEATION OF PHOTOPEAKS

Determination of Standard Peak Shape

Before discussing how each peak region is analyzed, we will describe the

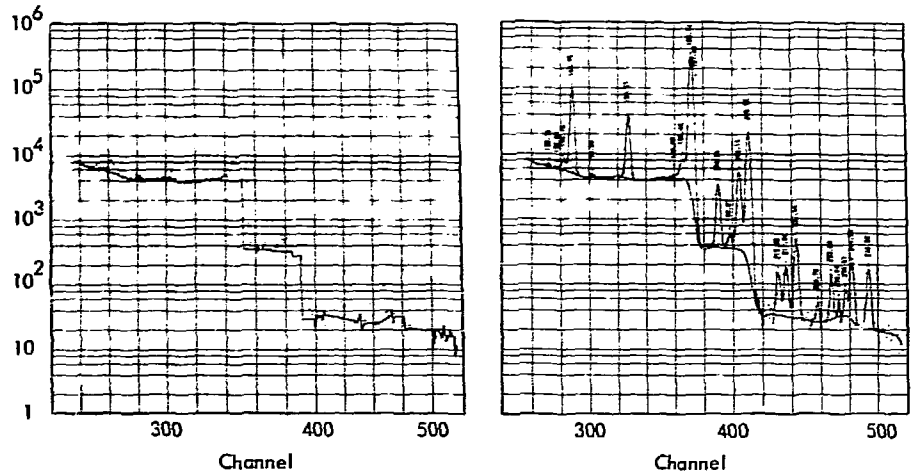

(a) Interpolated background before smoothing

(b) Final smoothed background

Fig. 7. The application of the stepwise interpolation method to a typical spectrum.

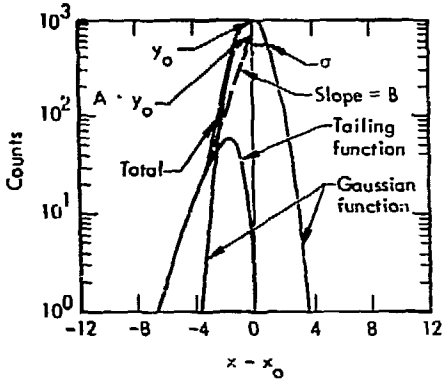

Fig. 8. A detail showing the components used to describe a peak shape.

mathematical function and procedures used to characterize peak shapes.

The shape analysis function used is taken in part from that described by Sanders and Holm.[7] The peak shape (net counts) is described as the sum of a Gaussian and a tailing term. This is shown schematically in Fig. 8, and can be written as

$$y_i = y_o \cdot e^{\alpha(x_i - x_o)^2} + A y_o \cdot e^{B(x_i - x_o)} \times \left[1 - e^{C \cdot \alpha (x_i - x_o)^2}\right]^{\delta} \qquad (1)$$

where

y_i = net data counts

y_o = peak height

$\alpha = -\frac{1}{2\sigma^2}$ (σ = peak width parameter)

x_i = channel value of ith point

x_o = peak position

A, B, and C are parameters used in describing the tailing function

$\delta = 1$ for $(x_i - x_o) < 0$

$\delta = 0$ for $(x_i - x_o) > 0$.

We see that six parameters (y_o, x_o, α, A, B, and C) characterize a peak completely.

The data points [(Y(i)] in an overlapping peak multiplet are considered to be linear combinations of the contributions from each peak j so that

$$Y(i) = \sum_{j=i}^{n} y_{ji} . \qquad (2)$$

In analyzing a multiplet, we allow only y_o, the peak height, and x_o, the peak position, to differ for the individual peaks, since the other parameters (α, A, B, C) do not change rapidly with energy. Furthermore, since y_o and x_o are the only quantities of interest for analytical purposes, we generally use predetermined values of the other four parameters, which are then held constant for any given fitting operation. In general, the values of these four parameters are dependent on the detector, the electronic system, the gamma-ray energy, and the amplifier gain.

A separate computer program could have been written to determine and study these parameters. Instead, we have chosen to include subroutine SHAPE in our working program. Its function is to characterize the parameters α, A, B, and C for the 2 to 15 peaks specified on Type 3 cards.[3] Each peak used for shape analysis is first located by PKSCH and then sent to subroutine FIT for the actual fitting. The independent answers are assembled by SHAPE for characterization of the various shape parameters.

We will now discuss each of these parameters in greater detail.

The peak width is normally the most sensitive parameter in a peak-fitting operation and is commonly specified by the full width at half maximum (FWHM = 2.355σ). This is related to α by

$$\alpha = -1/(2\sigma^2). \qquad (3)$$

The width of a photopeak results primarily from the summing of the instrumental noise (ΔE_n) and an energy-dependent term (ΔE_s) resulting from statistical fluctuations in the number of ion pairs formed in the detector. For a more detailed discussion of these quantities, see Ref. 8.

To a first approximation, the statistical term is a linear function of energy and the noise contribution is constant. Thus, we may express the observed total peak width (ΔE_t) as follows:

$$\Delta E_t^2 = \Delta E_n^2 + \Delta E_s^2 = k_1 + k_2 E . \qquad (4)$$

Although k_2 involves the Fano factor, we treat it as a quantity which, along with k_1, must be determined for each detector system. The values of k_1 and k_2 are determined by the method of linear least squares when more than two peaks are used.

The quantities observed and measured, such as peak widths, are in terms of channels rather than energies. To accommodate different amplifier gains, it is desirable to separate the gain dependence from the equations that describe the shape parameters. For the width parameters, we write

$$\Delta E^2 = (\Delta CH^2 - C_s) \cdot (GAIN)^2 \qquad (5)$$

where gain is expressed in keV/channel and C_s is a Sheppard's correction for the error resulting from treating all counts in a given channel as though concentrated at the channel center. It can be shown that the value of C_s is approximately 0.46

when expressed in terms of the full width at half maximum (FWHM).

The above equation now becomes

$$\left[(\mathrm{FWHM})^2 - 0.46\right] \cdot (\mathrm{GAIN})^2 = k_1 + k_2 \cdot E. \qquad (6)$$

That such an equation indeed expresses the relationship between peak widths and energy was verified, as Fig. 9 shows.

The parameters A, B, and C in Eq. (1) describe the tailing term (see also Fig. 8). The quantities A and B are the amplitude and slope descriptions of an exponentially-rising term that is multiplied by

$$\left[1 - e^{\alpha C(x_1 - x_o)^2}\right]$$

to reduce its contribution to the peak back to zero at the peak position. The quantity C is a rather insensitive term, quite easily influenced by poor statistics, and is therefore difficult to measure. A value of 0.4 appears to hold quite well for all our detector systems.

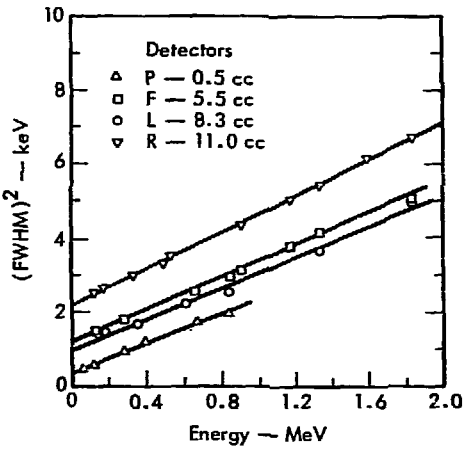

Fig. 9. Illustration of the variation of peak width with energy.

In our study of the other two tailing constants, we found that the slope parameter B is dependent only on the detector system, whereas the amplitude A is both detector and energy dependent. The parameters B and C should be determined where the tailing is most pronounced; therefore, for their measurement we use only the highest-energy peak of those specified for shape analysis. The values of B and C are thereafter held fixed for lower-energy peaks while the other parameters are being characterized.

We found a rather simple approximate relationship between the exponential slope parameter A and gamma-ray energy. It is given by

$$\ln A = C_1 + C_2 \cdot E \qquad (7)$$

Figure 10 presents the fit of this relationship to some typical data. The best values of C_1 and C_2 are determined by the method of least squares in SHAPE.

Subroutine SHAPE is called by default if the shape parameters for the particular detector and system are missing from the input deck. It may also be called by specific request on the Type 2 card[3] to determine some or all of the six parameters used. These are, respectively, the two constants each found in Eqs. (4) and (7), and the values of B and C of Eq. (1).

Although it is desirable to use single peaks for shape analyses, this is not essential. However, if a peak grouping is to be used, the individual peaks in it must all be sufficiently resolved to be detected in PKSCH by the derivative method.

Some typical printed output from a call for a shape analysis is shown in Appendix C along with a summary of results for a set of such peaks.

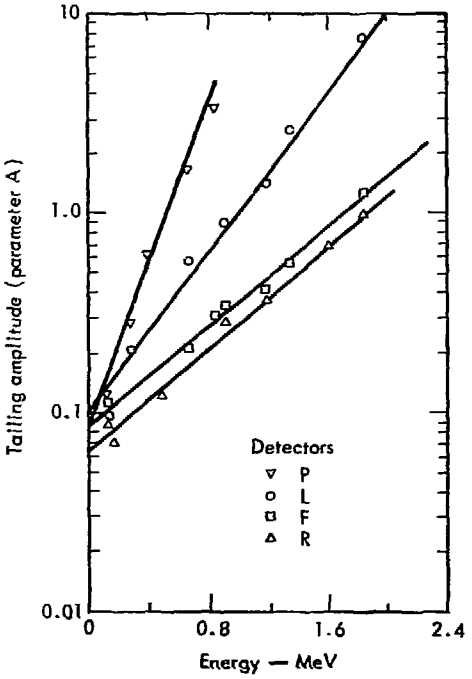

Fig. 10. Illustration of the variation of exponential tailing amplitude with energy.

Search for Peaks

Subroutine PKSCH locates the peak regions in a spectrum and supplies them individually to subroutine FIT for detailed analysis. A peak region is defined as an area of the spectrum in which all the data points are significantly higher than the previously-determined background. When the bounds of such a region have been determined, the more obvious peaks in it are located by a point-by-point examination of the first and second derivatives, using statistically-weighted tests.

The size of the peak grouping is currently restricted to 160 data points and 10 initial peaks. (FIT can accommodate an analysis of 12 peaks.) If a peak region exceeds either of these limits, PKSCH will split the peak grouping apart at the point where the net counts are lowest in value. This is done by drawing in a parabolic increment to the background; the parabola passes through this point as well as the end points where the net counts equal zero.

Intermediate results such as the net counts and weighting factors for each channel and the approximate heights and positions of the obvious peaks are now available for use in subroutine FIT. When the program returns from FIT, the final results are stored in the appropriate arrays and error calculations are made before a search for the next peak grouping is started. The calculation of combined errors is discussed in the section immediately following.

Fitting the Peaks with Standard Shapes

Subroutine FIT performs a detailed analysis of each peak region submitted to it by PKSCH, using as data the net counts in each channel, their weighting factors, and estimates of the parameters that describe the peak positions, heights, and shapes. Some of these shape parameters may be held fixed at the input estimates and the best least-squares value will be obtained for all free parameters.

Since Eqs. (1) and (2) are not of a linear form, the least-squares answers must be obtained by some iterative method. A Taylor's expansion about trial values is used to linearize the equations. The Newton-Raphson (Gauss) iterative technique is then used to find the best least-squares values of the free parameters. When only the first terms of the expansion are retained, the equation is

$$Y(i) - \sum_{j=1}^{N} f(p_1^o, p_2^o, \ldots p_k^o)$$

$$= \sum_{j=1}^{N} \left(\frac{\partial f}{\partial p_1}\right) \Delta p_1 + \sum_{j=1}^{N} \left(\frac{\partial f}{\partial p_2}\right) \Delta p_2$$

$$+ \ldots \sum_{j=1}^{N} \left(\frac{\partial f}{\partial p_k}\right) \Delta p_k \qquad (8)$$

where

$Y(i)$ = the count in channel i

p_k^o = current best estimate of the kth shape parameter

Δp_k = the change in the current best estimate of the kth shape parameter required to obtain a better fit to the data.

Under certain conditions, an additional term may be added which allows for a parabolic increment to the background. These conditions are described later in this section.

The partial derivatives with respect to the free parameters are calculated using the current best estimates for these quantities. The values of these derivatives are then used as coefficients in Eq. (8) for the next least-squares analysis in the iteration process. The estimates are updated following each iteration and the process continued until each of the free parameters changes by less than a prescribed amount. This amount is usually set at one-half the value of the error indicated for that parameter by the diagonal matrix elements.

We have encountered several situations that cause the matrix to be ill-conditioned, the answers to diverge, or that otherwise produce meaningless or poor results. We have included counteractive steps in the program for each. For example, when the initial estimates for the input parameters were poor, use of the excessive increments indicated by the answers tended to cause divergent conditions. These large swings were "damped" successfully by making only a fraction of the indicated change in any one iteration. Action was also taken to prevent crossing-over (or even too close an approach) of two neighboring peaks. In the determination of parameters other than peak heights and positions (i.e., FIT called from SHAPE), we found it desirable to free only one of these parameters at a time, starting with the most sensitive one and progressing to the least sensitive. Even so, a satisfactory analysis is generally completed in just a few iterations, although up to 15 are permitted.

If a peak height becomes negative during the iteration process, it is eliminated from further consideration. At the conclusion of this process, several tests are made, including an examination of the residuals (expressed in units of the standard deviation of the net counts). Possible extra peaks are indicated if a value in this array and also the sum of its two neighbors each exceed 4 standard deviations or the number given by OPRATR(6).[3] A peak is inserted at that position with the largest such residual (except when it is too close to an existing peak centroid), and the least-squares analysis is repeated. This process continues until the criteria for residuals are satisfied or until the maximum allowable number of peaks is reached. (This number is 12 in the normal operating program, although we have an expanded version which handles up to 20 peaks). Figure 11 shows the results of each cycle of the analysis of a multiplet.

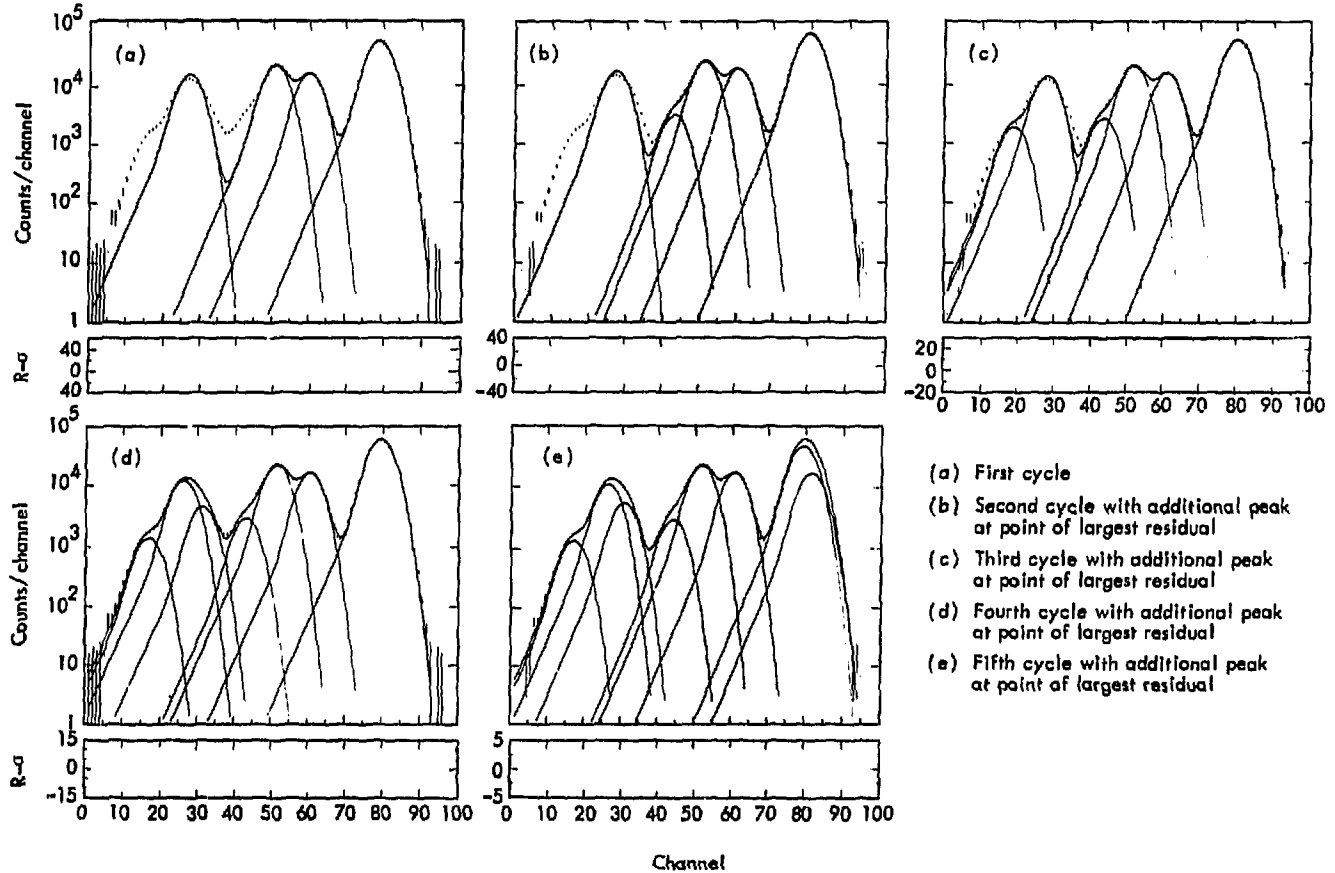

Fig. 11. Analysis of a peak multiplet by least-squares fitting using a predetermined line shape. Fig. 11(a) illustrates the first cycle using the four peaks detected by the derivative method. The successive addition of further peaks at the point of largest residual is shown in Figs. b, c, d, and e.

Further illustrations of the final fitting cycle are given in Appendix B.

Under certain conditions, a parabolic increment to the background will be incorporated into the fitting analysis. This is allowed because there are some spectral regions for which subroutine BKGRD cannot always make a good assessment of the background. For example, if a peak multiplet is quite large, it is difficult to know or predict the precise location of the background curve. Therefore, if the total number of peaks found in a peak grouping exceeds the number specified by OPRATR (3)[3] (usually three), one additional parameter will be freed. This allows for a parabola background passing through the end points, whose net counts are always zero.

Distinct and rather sharp "humps" frequently result from backscatter or 90° scatter of low-energy photons and are misconstrued by BKGRD to be a tightly-overlapping group of peaks. Such a hump will generally have only one inflection point and therefore PKSCH will find only one initial peak. However, this hump can be distinguished from a true single photopeak after the first fitting operation by comparing the area of the fitted peak to the net area under the data points. We use the rule that if the sum of the areas of the initial fitted peaks does not exceed 50% of the total area of the multiplet, a parabola background is immediately freed regardless of the number of peaks.

If this additional parameter is included in the fitting, it is required that the calculation result in a positive increment to the background, i.e., the sign of the freed parameter must be negative. If not, a change in background is dropped from further consideration. It is further required that no resultant background value be statistically greater than the corresponding data point. If it is, the background is reinterpolated between the data point of maximum overlap and the two end points. The program returns to PKSCH to restart the entire process of locating and fitting peaks for each of the two peak regions which result.

For routine analyses, the quantities of interest in the peak-fitting operation are just the peak heights (or areas) and the peak positions. Ideally, it would be desirable to fix all other parameters at their estimated values, but we have found that the peak-resolution parameter (α) should be given a certain amount of freedom. Since it is a sensitive parameter, small spectrum-to-spectrum variations can produce poor fits on statistically good peaks if α is held constant. To overcome this problem, provision has been made for specifying the maximum variation of the peak width[3] (usually about 5 to 10%) to be tolerated in any particular analysis. An exception is made for a peak occurring at approximately 511 keV. Since this peak may be considerably broadened if it is due to positron annihilation, the restraint on its width is removed. An example of this is shown in Appendix B.

A similar problem is encountered with x rays. The natural (Lorentzian) line shape of gamma rays is generally very narrow because of the relatively long lifetime of nuclear states. Consequently, this line shape does not noticeably contribute to the observed line shapes of gamma rays in the presence of much larger detector and instrumental effects. However, the short lifetimes of x-ray transitions

produce considerably broader natural line widths and result in a noticeably different peak width and shape. Since we have not attempted to account for these perturbations in this program, an acceptable fit is usually arrived at only after admitting spurious peaks into the profile of an x-ray peak (see Appendix B). The total intensity of the x ray can be obtained easily by summing the individual intensities reported.

The errors assigned to the peak areas and positions are determined from the diagonal matrix elements and from a pseudo chi-square test. That is,

$$\text{ERROR (j)} = \sqrt{\text{DM(j)} \div \text{QFIT(j)}} \qquad (9)$$

where

DM(j) = diagonal matrix element of parameter j.

$$\text{QFIT (j)} = \frac{\sum_{i=1}^{N} R_i^2 \div \left(y_{ij}/y_j^o\right)^{1/2}}{\sum_{i=1}^{N} \left(y_{ij}/y_j^o\right)^{1/2}} \qquad (10)$$

where

R_i = the weighted residual

y_{ij} = the contribution of peak j to channel i

y_j^o = the peak height of peak j.

An additional contribution to the reported error arises from the fact that the areas of peaks are calculated in two ways and the average is used in calculating gamma intensities. The first method is by integration of the areas of the fitted peak-shape profiles. The second involves proportioning the total net count of the peak multiplet according to the relative peak heights determined by FIT. These two answers, reported in the summary printout as "calc counts" and "prop. counts" respectively, should agree closely. Any discrepancies that exist between them are folded into the calculation of intensity error by PKSCH. Also, the uncertainties in the determination of the correct background at the extremities of the peak grouping are important, and because of the interpolation, they increase in effect with the size of the peak grouping. These factors have been included in the calculation of total intensity errors on a somewhat subjective basis.

One additional function performed by FIT is the determination of the starting and ending positions for each peak. These positions are used in a unique way in subroutines IDENTIFY and LDMATX to establish the energy "window" associated with the peak, but they do not physically define precise points at which peaks start or end. If the peaks in a peak multiplet are partially separated, there is seldom any problem in fitting them, and the answers have been found to be accurate. However, if the peak centroids happen to be very close together, as illustrated by the two peaks to the right in Fig. 11(e), far greater demands are placed upon the statistics of the data points and the accuracy of the parameters that describe the peak shape. Thus, even for statistically good peaks the error in the intensity analysis of the individual peaks may become quite large. Although such close-lying peaks are reported individually in the intermediate summary table, their intensities may be added back together by LDMATX. The reason for this, as will become clearer in our discussion of subroutines LDMATX and EVAL, is that additional information

regarding the makeup of the observed peak intensities is usually available in the final stages of the calculation. The contributions of individual nuclides to the peaks of a close-lying multiplet are determined at that time. The peaks that should be recombined in this way are appropriately flagged by FIT. They are identified in the printout by the blank spaces that appear in the peak START and END columns in the intermediate summary table (see Appendix A).

DETERMINATION OF PHOTOPEAK ENERGIES

The quantities determined by FIT and stored by PKSCH characterize the peaks as they are observed in the pulse height spectrum. It is the purpose of subroutines FINDE, CALGPM and CALCMU to interpret these measurements as gamma-ray energies and intensities and related quantities.

To calculate precise energies from the observed peak positions, we require as input two or more energy-scaling markers and a description of the nonlinearity of the electronic system. The nonlinearity can be characterized by the use of a precision pulse generator or a source (or sources) emitting a convenient set of gamma rays of known energy. A description of the nonlinearity is achieved by a supplementary program called LINEARITY,[5] which makes a least-squares fit of a set of peak positions and energies to a polynomial equation of the form

$$P_i = \sum_{j=1}^{N} a_j (CL)_i^{(j-1)} \qquad (11)$$

where

P_i = pulser voltages or gamma-ray energies

CL_i = channel positions of peaks

a_j = coefficients of the polynomial

The first two terms of the polynomial specify the zero energy intercept and the gain, respectively, whereas the higher order terms describe the nonlinearity. Figure 12 shows the nonlinearity of one of our systems along with a polynomial fit of the data.

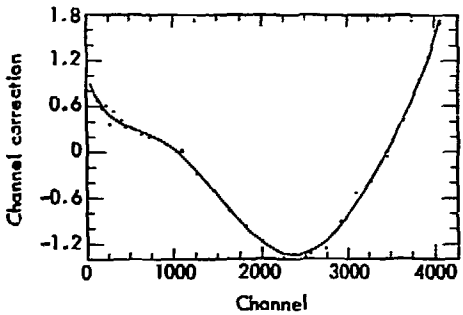

Fig. 12. Description of the nonlinearity of a typical system. The solid curve is a fit of a seventh-order polynomial to the data.

Although a fifth- or sixth-order polynomial equation generally provides an adequate description of the nonlinearity, this was not true for those of our older systems that contained a pronounced nonlinearity below channel 400. This perturbation could be accommodated by applying a linear correction term to the lower channel data before fitting a polynomial and later restoring this correction during the running of a problem in GAMANAL. For example, in Fig. 12 a straight line, whose y intercept was 1.4 and x intercept was

360, was subtracted from all pulser data below channel 360 before the least-squares fit was made. If such a linear correction is used in the LINEARITY program, the intercepts must also be submitted on the Type 4 card[3] along with the polynomial coefficients, a_j, of Eq. (11).

For some detector systems, we have found a subtle variation of the nonlinearity with gain. In these cases, measurements are made for all the most frequently used gains. The sets of coefficients placed in the Type 4 card library are identified by gain as well as by system and detector.[3]

A linear relationship is assumed to exist between the pulser or gamma-ray energies described in Eq. (11) and the peak energies in any other spectrum taken on the same system. That is,

$$E_k = A + B \cdot P_k \qquad (12)$$

where

E_k = gamma-ray energy of kth peak in the spectrum

A and B = constants (to be determined) used in describing the zero energy intercept and slope for the current analysis.

Information on the exact energies corresponding to two locations is sufficient to determine the parameters A and B, but the best line is determined by least squares if a larger number is available (up to 15 may be submitted[3]). If internal peaks are specified, only approximate channel positions are required on the Type 3 card, since the precise channel locations have already been determined in PKSCH. An option to use an external calibration is available but requires exact channel values. A summary of the fitting of the energy standards appears on the intermediate printout as shown in Appendix A. Once the values of A and B have been determined, the energies of all the peaks can be calculated.

Energies corresponding to boundary conditions of the analysis, such as the energies of the lowest and highest channels to be used, are also calculated at this time.

DETERMINATION OF PHOTON EMISSION RATES OF THE SOURCE

The second function performed by FINDE (in conjunction with subroutines CALGPM and CALCMU) is the conversion of the observed peak areas into gamma-ray intensities, expressed as photons/min emitted by the sample. This requires a knowledge of the absolute efficiency of the detector as a function of photon energy for the physical arrangement used.

The efficiencies of Ge(Li) detectors are usually determined by using radioactive sources that emit one or more gamma rays of known intensity. If the efficiency curve is to be determined for a single geometry (fixed sample size at a fixed distance), this method is quite adequate and simple to carry out. However, the intolerable restrictions of a single geometry forced us to look for a more flexible approach.

Characterization of Detector Efficiency

We may attack the problem by first separating the total counting efficiency into two components—the intrinsic efficiency of the detector (ϵ) and the geometry factor (G). That is,

$$\text{Efficiency} = \epsilon \times G. \qquad (13)$$

For the idealized case of a point source and a point detector, the solution is simple since the geometry term is then merely

the reciprocal of the square of the distance from source to detector. We define the intrinsic detector efficiency to be the observed counts normalized to a fictitious 1 cm from the detector divided by the source strength. That is,

$$\epsilon_E \equiv \frac{(\text{cpm})_E}{(\gamma\text{pm})_E} \times d^2 \qquad (14)$$

where

$(\text{cpm})_E$ = observed counts/min in calibration peak of energy E

$(\gamma\text{pm})_E$ = *known gamma emission rate* of energy E

d = source to detector distance.

Since detectors have finite sizes, this equation holds only if the distance d is very large. When this is true, the gamma emission rate from any point source can be determined by rewriting the above equation so that

$$(\gamma\text{pm})_E = \frac{(\text{cpm})_E \times d^2}{\epsilon_E} \cdot \qquad (15)$$

This simple description of the detector efficiency is quite limited in applicability but becomes a very useful basis for representing the actual total counting efficiency. We may use Eqs. (14) and (15) if we can first establish geometric models capable of representing the detector and the source as equivalent points in space. For the purposes of the present discussion we will consider this as two separate problems, first assuming a point source and seeking a representation of the detector as an equivalent point in space.

Model Used for Detector Geometry

A typical configuration for a cylindrical detector and a point source is shown in Fig. 13. To use Eq. (15), the parameter d must be assessed by using measured or calculated values for x, w, p and r, defined as

x = distance from source to detector window

w = distance from window to "active" detector surface

p = effective penetration of gamma ray into the detector

r = effective radius of interaction

d = distance from source to effective zone of interaction

From simple geometry we have

$$d^2 = (x + w + p)^2 + r^2 \, . \qquad (16)$$

Of these, x is the only easily-measured parameter. The others must be experimentally or empirically determined. Our studies of these parameters were made on a variety of detectors ranging from small x-ray detectors to a 38 cc coaxial detector. Obviously, the model is tested most severely in the case of the largest detector.

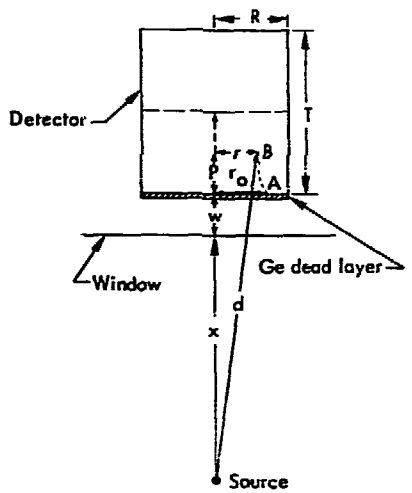

Fig. 13. Schematic illustration of a point source and a cylindrical detector.

Before the advent of large coaxial detectors, several simplifying assumptions were made which are still reasonably valid for smaller detectors. For example, the effective interaction radius r can be approximated as $R/\sqrt{2}$ and p as T/2. R and T are the physical radius and thickness of the detector, respectively. The sum, (w + p), can then be experimentally determined by simply counting a suitable source at two different distances.

For several years, these approximations proved satisfactory. However, certain limitations became apparent when larger detectors (> 10 cc) came into use. We were then forced to study more carefully the penetration parameter p and the effective interaction radius parameter r.

The gamma-ray penetration p is obviously dependent upon the energy and has limiting values of zero at low energy and one-half the detector thickness, T, at very high energies. We used the following equation to describe an effective distance of penetration p into a detector for gamma rays of some given energy

$$p = \frac{\int_0^T p\left(\frac{dI}{dp}\right) dp}{\int_0^T \left(\frac{dI}{dp}\right) dp} . \qquad (17)$$

Since

$$-\frac{dI}{dp} = \mu I , \qquad (18)$$

one can derive the equation

$$p = \frac{1}{\mu}\left[1 - \frac{\mu T e^{-\mu T}}{1 - e^{-\mu T}}\right] \qquad (19)$$

where μ is an appropriate absorption coefficient (which is energy dependent). The shape of this relationship is depicted in Fig. 14.

Although the form of this equation appears reasonable, one must now decide upon appropriate absorption coefficients. Quite precise values can be found for the photoelectric, Compton, and total attenuation coefficients.[9] However, it is not clear which, if any, of these should be used in the above equations. This is because the only interactions that concern us are those that eventually result in full energy deposition in the detector, whether by photoelectric or multiple Compton scattering processes. Since the latter process is complex, no rigorous meaning should be assigned to the penetration parameter p or to the absorption coefficient μ. However, we have found an adequate empirical function

$$\ln \mu = -2.316 + 4.2 \exp\left[-0.478 \ln E - 1.434\right]. \qquad (20)$$

The dashed line in Fig. 15 compares this curve with the other linear absorption curves.

It is important to take into account the dependence of gamma-ray penetration on

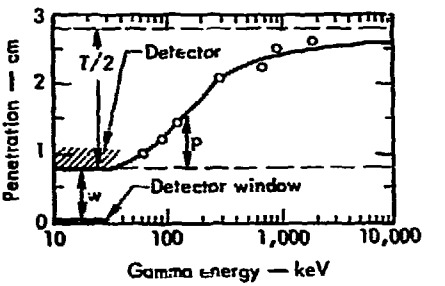

Fig. 14. Measured effective penetration of gamma rays of various energies into a 38 cc coaxial detector. The solid curve represents Eq. (19) for this detector.

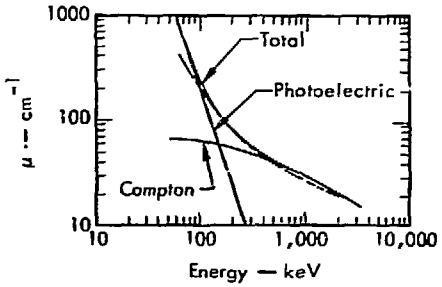

Fig. 15. Linear absorption cross sections for germanium. Eq. (20) is represented by the dashed curve.

energy even when establishing relative efficiency curves. These variations in penetration result in efficiency curves of different shape for different detector geometries, an effect that becomes very pronounced at close-in counting geometries.

The effective interaction radius r is more difficult to characterize. A rigorous meaning can be attached to it only for low energies, in which case the interaction is primarily photoelectric and occurs at the surface of the detector. This case can be used for normalizing purposes since the exact detector efficiency and the effective radius (r_o) can be computed from simple geometry (see Fig. 13). That is,

Physical geometry

$$= 1/2 \left[1 - \ell/\sqrt{\ell^2 + R^2}\right] \qquad (21)$$

where $\ell = x + w$.

However, in our model, the geometry is described by

$$G = \frac{k}{\ell^2 + r_o^2} \quad . \qquad (22)$$

A value of $k = R^2/4$ is determined by normalizing the two expressions as ℓ goes to infinity. The relationship between the effective interaction radius (r_o) and the detector radius can now be given by:

$$r_o^2 = (1 - C\ell^2)/C$$

where

$$C = \left(1 - \ell/\sqrt{\ell^2 + R^2}\right) \frac{2}{R^2} \qquad (23)$$

Some close-in geometry (ℓ) must now be chosen to fix the relationship between r_o and R. For convenience we have chosen $\ell = 1$ cm as our convention.

Since it was not clear that the effective interaction radius should be the same for higher energies, a small computer program called XDET[5] using the Newton-Raphson iterative technique for nonlinear least squares was written to evaluate the parameters (w + p) and r by Eq. (16). Input data consisted of peak counts and the corresponding sample-to-detector distances, x. Extreme care was taken to avoid inconsistencies in the peak area integration methods used and electronic problems related to pulse-pileup and live-time errors.

It became apparent that the interaction radius is markedly affected by gamma-ray energy. Table 1 illustrates this effect for a 38-cc coaxial detector counting 661 keV gamma rays. Holding the value of r constant at r_o (1.41 cm) resulted in a poor fit to Eq. (16) and the systematic errors shown in column 5 of Table 1. The best least-squares fit was obtained with a much smaller value for r, as shown in columns 6 and 7. Although the determination of

Table 1. The effect of radius of interaction on goodness of fit.*

Observed Count	Time (min)	Distance x (cm)	Calculated Count (r_o = 1.41)	Difference (%)	Calculated Count (r_o = 0.35)	Difference (%)
318864	19.67	0.225	310741	2.55	318516	0.11
254690	19.77	0.540	255169	- 0.19	255022	- 0.13
172517	19.93	1.180	177157	- 2.69	173060	- 0.31
124862	19.97	1.825	127830	- 2.38	124277	0.47
94278	20.04	2.450	96969	- 2.85	94486	- 0.22
59168	20.03	3.730	59833	- 1.12	58961	0.35
80780	40.08	5.000	81002	- 0.27	80802	- 0.03
58965	40.14	6.280	58233	1.24	58727	0.40
51500	80.22	10.650	50000	2.91	51758	- 0.50
32850	160.75	20.750	30879	6.00	32858	- 0.02

*Data are for ^{137}Cs (661 keV) counted on a 38 cc five-sided coaxial detector.

Table 2. Experimental effective interaction radius vs energy for 38 cc coaxial detector.

Energy (keV)	r	Source
60	0.49	^{241}Am
91	1.38	^{147}Nd
122	1.28	^{57}Co
279	0.61	^{203}Hg
661	0.35	^{137}Cs

the radius parameter is extremely sensitive to statistical and other sources of error, a definite trend of r with energy can be shown (see Table 2).

We believe that this trend may be qualitatively explained by the increased importance of multiple Compton scattering within the detector for production of full-energy pulses from the higher energy gamma rays. Compton gamma rays escape from the detector more easily after an interaction near the outer surface than after one near the center of the detector. The net result is that the effective radius of interaction for production of photopeaks decreases as the penetration depth increases. This is shown by the curve A-B in Fig. 13 as well as in Table 2. The magnitude of the trend indicates that other surface and edge effects undoubtedly also modify the radius parameter.

By evaluating data acquired on several detectors, we found that the following empirical relationship gives an adequate description of the effective interaction radius for use in our model

$$r^2 = r_o^2 - 0.4\, r_o^2 \sqrt{T}\, [S^2/(1 + S^2)] \qquad (24)$$

where r, r_o and T have the meanings discussed earlier and shown in Fig. 13 and where

S = (E - 60)/100

E = gamma energy in keV.

The window-to-detector distance w is also assessed from the output of the computer program XDET, along with the penetration and effective radius parameters.

Since the measurements in the design specifications do not describe w accurately enough, determination of w is always the first requirement in calibrating the total detector efficiency. It is accomplished by counting sources of different energy at several distances. The sets of data at each energy are used to calculate (w + p) values, which are plotted as shown in Fig. 14. The idealized curve derived from Eq. (19) is fitted to these data points and the y axis intercept is taken to be the window-to-detector distance.

Since no standardization of Ge(Li) detector sizes or shapes exists, care must be taken in applying the model to each new detector. At times, empirical estimations or adjustments of the model parameters must be made in order to obtain a better fit to the observed data. For example, when rectangular planar detectors are used, an equivalent detector radius R may be estimated by $R = \sqrt{\text{Detector area}/\pi}$. Also, slight adjustments may have to be made in some of the parameters for coaxial detectors, depending on the size and position of the dead region.

In summary, the model's predictions of the variation of total counting efficiency with geometry were confirmed by experiment. With this model it is possible to use a single intrinsic efficiency curve that is virtually independent of geometry. Our experience has been that we can usually describe the counting efficiency as a function of detector-to-source distance to within 1% over the usable range of distances (0.2 cm to 100 cm) as indicated in Table 2.

Measurement of the Intrinsic Efficiency Curve

The intrinsic efficiencies as defined in Eq. (14) are determined by counting absolute standards at relatively large distances and normalizing the efficiencies obtained at these distances to a 1-cm distance.

A fifth- or sixth-order polynomial equation of the following form is used to describe the intrinsic efficiency

$$\ln \epsilon_i = \sum_{j=1}^{N} a_j (\ln E_i)^{(j-1)} \qquad (25)$$

where

ϵ_i = efficiency at the ith energy

E_i = gamma energy

a_j = coefficients of the polynomial.

As more standards became available and measurements became more precise, we found that this single function could not describe the efficiency over the range of interest (generally 0.05 to 4.0 MeV) to the desired accuracy. Subsequently, we have used two polynomial equations, one for low energies (up to 100 to 200 keV) and one for higher energies. When the data are fitted by the supplemental program called EFFICIENCY,[5] an overlap region is specified. We examine the resulting fitted curves and choose a "crossover" energy which gives the same answer by both equations. The Type 5 input control cards[3] therefore contain a high-energy set of coefficients and a low-energy set together with a crossover energy value. In this way, the efficiency data are generally fitted to within ±1 to 2%.

Correcting for Sample Geometry

In the discussions thus far we have assumed that the sample activity resided at a point. In practice, most samples are extended in two or three dimensions. Not only must the change in geometry be considered but, for volume sources, self-attenuation in the sample must also be properly calculated.

Our basic approach again is to use approximate formulae to reduce the sample to an equivalent point in space. The location of this point will depend on the energy of the gamma ray, the physical dimensions of the sample, and its composition.

In order to avoid the extreme complexity of volume-volume geometry calculations, we will assume the detector to be adequately represented by an equivalent point (see Fig. 16).

Disk Sources

For disk sources placed on axis at distances that are large compared to the sample radius, it can be shown that the efficiency decreases by the ratio

$$G/G_p \approx \frac{a^2}{a^2 + R^2/2} \qquad (26)$$

where

G = the desired geometry term

G_p = the point-source geometry

a = the source-to-detector distance

R = the source radius.

We have evaluated this simplified approximation and find it to be generally adequate. In one experiment, an extended source of 4.5 cm radius was prepared and counted at a number of distances with respect to a 6-cm^3 planar detector. The normalized results for the various gamma-ray energies in the sample obtained by using geometries corrected by the above equation are shown in Fig. 17. These results show that even for rather large source areas, the correction formula applies rather well, especially for the higher energies. However, there is obviously some residual source of error that is energy dependent. This is apparently in addition to one such source already taken into account in the data shown in Fig. 17, which is related to

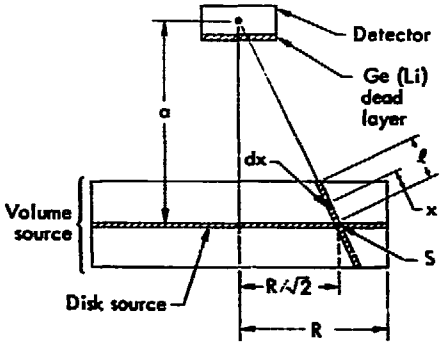

Fig. 16. Schematic illustration of a cylindrical (or disk) source and a detector.

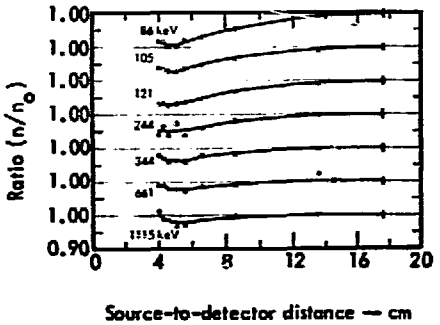

Fig. 17. Plots showing the small residual errors in the geometry calculation when measuring gamma rays from a 4.5 cm radius disk source.

the "dead" layer present on most larger Ge(Li) detectors. Although the efficiency curve takes into account the attenuation of gamma rays entering the detector in a direction normal to the detector surface, many of the gamma rays from large disk sources counted at close-in geometries enter the detector at a rather oblique angle. Low-energy gamma rays especially will then suffer attenuation greater than that indicated by the intrinsic efficiency curve. If there were no attenuation (i.e., no dead layer), a detector's intrinsic efficiency should be invariant with energy and its efficiency at low energies would then be determined solely by its area. Using this fact, the dead layer thickness can be estimated within GAMANAL by using the slope of the efficiency curve in such a low-energy region. Once this thickness has been calculated, a correction can be applied that will approximately account for the additional attenuation suffered by gamma rays entering the detector at oblique angles from large disks or volume sources. The angle we use in our calculations assumes the activity to be concentrated in a ring of radius $R/\sqrt{2}$, as in Fig. 16.

Cylindrical Sources

A volume source can be thought of as a multilayered disk source. The additional complication introduced is gamma-ray attenuation in passing through the upper layers. The effect on the counting rate (n/n_o) for a linear element of dimensions 2 ℓdx is expressed by

$$n/n_o = \left(e^{-\mu\ell}/2\ell\right) \int_{-\ell}^{\ell} e^{\mu x} \times (1 - x/a)^{-2}\, dx \qquad (27)$$

where

μ = absorption coefficient

a = distance from the detector to midpoint of source

See Ref. 10 for a more complete discussion.

When this integrand is expanded and integrated term by term, we obtain

$$n/n_o = e^{-\mu\ell}\left[1 + \frac{\mu^2\ell^2}{3!} + \frac{\mu^4\ell^4}{5!} + \frac{\mu^6\ell^6}{7!} + \ldots + \frac{2\ell}{a}\left(\frac{\mu\ell}{3(1!)} + \frac{\mu^3\ell^3}{5(3!)} + \frac{\mu^5\ell^5}{7(5!)} + \ldots\right) + \frac{\ell^2}{a^2}\left(1 + \frac{3\mu^2\ell^2}{5(2!)} + \frac{3\mu^4\ell^4}{7(4!)} + \ldots\right) + \ldots\right]. \qquad (28)$$

This may be rewritten as

$$n/n_o = e^{-\mu\ell}\left[\left(\frac{a^2}{a^2 - \ell^2}\right) + \frac{\mu^2\ell^2}{3!} + \frac{\mu^4\ell^4}{5!} + \ldots + \frac{2\ell}{a}\left(\frac{\mu\ell}{3(1!)} + \frac{\mu^3\ell^3}{5(3!)} + \ldots\right) + \ldots\right]. \qquad (29)$$

If either μ or ℓ/a are small compared with 1.0, the higher-order terms can be disregarded. The average sample thickness ℓ that gamma rays must penetrate in reaching the detector is calculated at the effective sample radius of $R/\sqrt{2}$ as illustrated in Fig. 16.

To test this correction formula, we first counted an active solution in the form of a very thin layer of 4.5 cm radius in three positions corresponding roughly to 6, 9, and 15 cm from the detector. We subsequently diluted the sample with water to achieve sample thicknesses of 1, 2, 3, and 4 cm, each time counting the sample

in the same three positions. The spectra were processed by GAMANAL and the results for various gamma rays were each normalized to the answer obtained for the disk source of the same area at that distance. These normalized results are shown in Fig. 18.

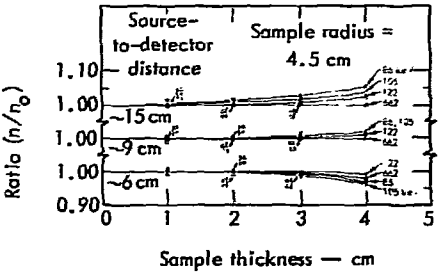

Fig. 18. Plots showing small residual errors in the geometry and attenuation calculations as a function of sample thickness. The measurements were made on a 4.5 cm radius cylindrical source containing a radioactive aqueous solution and were normalized to a disk sample of the same radius.

Corrections for External Absorption

It is obviously desirable to correct for gamma-ray attenuation by external absorbers. These absorbers may be an unavoidable part of the sample container or environment or they may be one or more materials used deliberately to attenuate the lower-energy gamma rays. Using input information on the composition of the absorbing materials,[3] absorption coefficients are calculated in CALCMU. Subroutine CALGPM then makes the necessary corrections for such external attenuation.

Calculation of Absorption Coefficients

To correct for the gamma-ray attenuation that occurs in the source or in external absorbers, the appropriate absorption coefficients must first be determined. Subroutine CALCMU computes and accumulates the coefficients for each of the materials that have been specified on the Materials and Absorber input cards.[3] The total absorption coefficient is returned to the calling subroutine CALGPM.

A seventh-order polynomial equation is used to describe the mass attenuation coefficient of a material as a function of energy. The auxiliary program EFFICIENCY[5] was used to determine the appropriate coefficients by fitting cross-sections vs energy values obtained from Ref. 9. A set of polynomial coefficients for each element or material of interest has been coded into the subroutine CALCMU.

A problem arises in that the absorption curve is discontinuous at the K-shell binding energy. We have found that the magnitude of the discontinuity can be represented empirically by

$$\mu_\ell/\mu_\mu = 0.1027 + 0.0068\sqrt{E_K} + 0.000654\ E_K \qquad (30)$$

where μ_ℓ and μ_μ are the mass absorption coefficients just below and above the absorption edge and E_K is the K-shell binding energy. Since the slope of the absorption curve is nearly the same just below and just above the absorption edge, Eq. (30) is used along with the general polynomial equation to describe the absorption coefficient below the absorption edge.

Spectral Interpretation

We have described the reduction of spectral data to gamma-ray energies and total intensities. In some uses of the program, such as for decay scheme studies, this is the only information desired. More typically, however, these energies and intensities must be interpreted in terms of disintegration rates (or atoms) of specific nuclides to provide a complete qualitative and quantitative analysis of the source. This we do with the aid of certain decay-scheme information read from a magnetic tape specially prepared for this purpose by the auxiliary program, LIBETP.[5] This preassembled information includes the half-life and parent-daughter relationships for each nuclide and the exact energy and branching intensity of its gamma rays. For each gamma ray we select and list up to four associative gamma rays that may be found in the same or in the parent or daughter decay scheme. The first two of these listed associative gamma rays that are within the energy bound of a spectrum are used in its identification scheme. All this information is organized and cross-indexed so that GAMANAL can easily find the required information without time-consuming searches through various arrays. It is quite important for the proper performance of GAMANAL that the information in the library be accurate and complete to avoid improper identifications and incorrect answers.

Complete interpretation of a spectrum involves, first, the determination of a set of nuclides that could be responsible for the observed spectral energies and intensities, and second, calculation of the amount of each nuclide in the source.

In our original approach, the observed peaks were essentially evaluated on an individual basis. Identification of the nuclides most likely to be responsible for each peak was based on the assignment of numerical weights to the results of several tests made on each candidate using information from the decay-scheme library. The best candidate was then assigned to each peak, and individual peak results were computed, reported, and summarized along with those for any other peaks identified as belonging to the same nuclide.

The principal drawback to this approach was that it could not cope with unresolved peak interferences. Consequently, the results for individual peaks frequently disagreed with each other and the average result for a nuclide tended to be high. The solution to this problem, which will be discussed in a later section, was to form a matrix of linear equations that would describe the spectral intensities. For this purpose each peak is assumed to be made up of a linear combination of gamma rays from one or more components. The contribution of a component to a particular peak is determined then by two factors—the branching intensity and the amount of the component present, which is what we wish to determine.

TENTATIVE IDENTIFICATION OF RADIONUCLIDES PRESENT

As mentioned, subroutine IDENTIFY has always been used to make peak-by-peak identification using the decay-scheme library. In our later version of GAMANAL, its function was changed so that it is now used simply to determine a set of probable

nuclides that qualitatively accounts for the observed spectrum and serves as input for subroutine EVAL. Although this set is generally over-determined, any impossible or implausible selections can be weeded out later in subroutine EVAL.

The evaluation of the individual peaks is shown schematically in Fig. 19. IDENTIFY first searches the energy library for those isotopes that emit gamma rays within some specified range of this peak energy. The energy window used is fixed by starting and ending energies for the peak as determined in FIT if this range does not exceed a maximum of ± 3 keV. Several nuclides may become candidates for a given peak. A selection must now be made of the one most likely to be the source of the peak in question. To do this, each candidate is subjected to a series of up to six tests. These tests, which are mathematically formulated, give rise to confidence indices ranging in value from 0 to 1.

The first question is one of energy evaluation, that is, how well does the candidate's gamma-ray energy agree with the energy of the peak in question? The test uses a Gaussian function, as shown in Fig. 20.

The second test makes a half-life vs decay time evaluation. This test, shown in Fig. 21, is quite subjective in character and is meant only to perform bulk screening of improbable choices. For example, we do not normally expect to see an isotope a month after zero time if it has a half-life of only one day. Therefore, the confidence index drops very rapidly for decay times of several half-lives, as shown by the right hand portion of the curve. For shorter decay times the test is even more subjective. The family of curves shown depends on the decay time and on the complexity of the spectrum and is described by the empirical relationship.

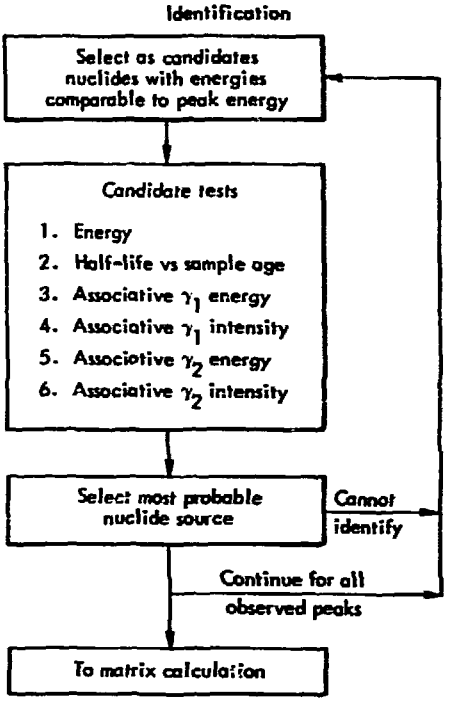

Fig. 19. Block diagram of the method used for isotope identification.

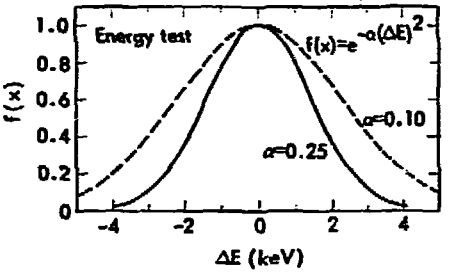

Fig. 20. Gaussian curves of the type used for photopeak energy evaluation in IDENTIFY.

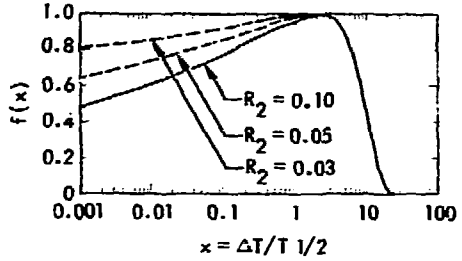

Fig. 21. Shape of curve used in making decay time vs half-life evaluations in IDENTIFY.

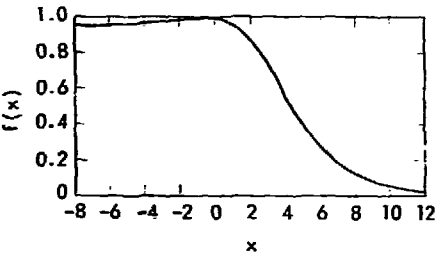

Fig. 22. Shape of curve used for evaluating the intensity of the photopeaks associated with the gamma ray choice being considered.

$$f(x) = \left(\sqrt{\frac{2R_3}{R_2}}\ x\right)^{R_2} \exp\left[-R_3 x^2 + 0.5\ R_2\right] \quad (31)$$

where x is the decay time divided by the half-life and R_2 and R_3 are inter-related parameters dependent on the number of peaks found in the spectrum.

For isotopes with only one gamma ray, such as ^{51}Cr, ^{54}Mn, and ^{203}Hg, the two tests mentioned thus far are the only tests that can be made. However, if the gamma ray of interest for a particular candidate has associative gamma rays as indicated by the library, additional tests will be made.

First, a search is made to see if the associative gamma peak was found in the spectrum. If it was, an energy test similar to the first test is made. This is followed by a mathematical test of the intensity relationship, as shown in Fig. 22 and given by the equation

$$f(x) = \left[C_1 + C_2\left(\frac{e^{\mu}}{1+e^{\mu}}\right)\right]\left[\frac{e^{-\mu}}{1+e^{-\mu}}\right] \quad (32)$$

where

$\mu = \alpha x \quad \beta$

x = (calculated intensity - observed intensity)/ $\left(\sigma_1^2 + \sigma_2^2\right)^{1/2}$

σ_1 and σ_2 = Errors associated with the peak intensities. C_1, C_2, α, β, are presently set at 0.95, 1.49, 0.5 and 1.2 respectively.

We should point out that if a candidate's associative gamma ray is in the decay scheme of a parent or a daughter nuclide, the effects of their respective half-li[illegible] are considered when making the intensity test. If the calculated intensity agrees with the observed intensity, a confidence value near 1.0 results. If the observed intensity is much less than that calculated, the candidate is discredited. However, a similar judgment cannot be made if the observed intensity of the [illegible]ociative peak is larger than the calcul[illegible] intensity, since one must allow for the possible interference of a gamma ray from some other nuclide.

An obvious possibility is that the program did not detect the associative gamma

ray of a particular candidate. Investigation is then made of the region in which the associative is expected to see if it should have been detected above the background of that region. This test, shown in Fig. 23, possesses some of the features of Fig. 22 and is given by the equation

$$f(x) = \frac{e^{-\mu}}{1 + e^{-\mu}} \qquad (33)$$

where x now = (calculated intensity - background intensity)/ $\left(\sigma_1^2 + \sigma_2^2\right)^{1/2}$

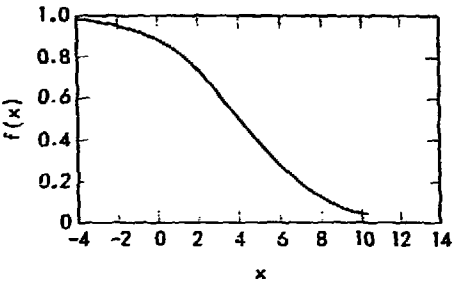

Fig. 23. Shape of curve used for comparing the computed intensity of unlocated associative photopeaks with the observed background intensity.

and μ is calculated as in Eq. (32) but with $\beta = 2.0$.

The foregoing two tests are repeated if a second associative gamma ray is specified by the library.

The individual results of the above tests are multiplied together to give what we term a final confidence-level index for the candidate. This means that even though a candidate may have scored high in five of the six tests but flunked one of them, it receives a low confidence level index. The choice now as to which isotope is responsible for the peak in question is simply made by choosing the one with the highest confidence level index. If there is a close runner-up, it will also be retained as a best-alternate candidate.

By using a Select card[3] as input, a bias may be placed upon the above selection criteria. This mode of operation is sometimes useful when certain information is already available to the experimenter. For example, he may have performed chemical separations and feels confident about the nuclides present. In other instances, he may want to aid in the identification, as in the choice between ^{203}Hg and ^{203}Pb, which cannot be made easily from spectral information alone. In these cases, IDENTIFY, instead of selecting the best candidate for a peak, will first search for an identity match between any of the various candidates and the nuclides or elements listed on the Select card. If no match can be made, the program reverts to its normal method of selecting the best candidate. Even if the Select card is used, "contaminants" will usually be included in the component set by virtue of some peaks belonging to them uniquely. The use of a negative sign with the nuclides listed on the Select card will inhibit their selection as candidates.

FORMATION OF MATRIX OF EQUATIONS AND THEIR LEAST-SQUARES SOLUTION

We now have a list of peaks that have been tentatively identified. Their disintegration rates must now be calculated and spurious assignments rejected. This process is performed by subroutine EVAL.

Each identified peak is considered to be composed of a linear combination of one or more components which may be written

$$Y_i = \sum_{j=1}^{J} A_j \cdot X_{ij} \qquad (34)$$

where

Y_i = the intensity of the ith peak in gammas/min

X_{ij} = the branching intensity of the jth component at the ith peak energy

A_j = the disintegration rate of the jth component (a number which is to be determined).

The calculational method is to set up the matrix of linear equations and to solve them by the method of least-squares. That is, we minimize

$$\sum_{n=1}^{N} (\omega_i R_i)^2 \qquad (35)$$

where

$$R_i = Y_i - \sum_{j=1}^{J} A_j \cdot X_{ij} \qquad (36)$$

and

ω_i = weighting factor

Since many of the coefficients X_{ij} will be zero, that is, the nuclide j cannot contribute to peak i, an equation or set of equations is sometimes independent of all the others. For this reason, a storage matrix (AMATRX) is initially constructed (in LDMATX) whose dimensions are determined by the number of nuclides to be considered and the number of identified peaks. Our present operating storage dimensions of 65 components by 150 peaks are usually adequate. The data corresponding to interference sets are then taken from the storage arrays into working arrays for analysis. The current maximum size of the working matrix (AMLR) is 55 components by 125 peaks.

Although the procedure is straightforward in principle, we will now consider in greater detail the many precautionary steps and evaluations that must be made in order to make the routines functional.

Assembling of Components (LDMATX)

First, the list of nuclides is assembled and ordered by number (atomic number and mass) into an array. Many of these nuclides have genetic relationships that should be considered. If this is indicated by the decay-scheme library, the appropriate growth and decay relations will be included in the calculations. An option is available[3] to negate this consideration for specific nuclides and even for all parent-daughter pairs. Also, if no zero time is specified, the relationship is automatically voided. Barring these exceptions, three rules are currently used. First, daughter-nuclide concentrations are assumed to be zero at time zero. Second, the production time of the isotopes is assumed to be short (instantaneous) compared to the half-lives involved. Third, if the parent nuclide has a longer half-life than the daughter, the pair will be combined and reported only in terms of the parent (e.g., ^{95}Zr-^{95}Nb, ^{132}Te-^{132}I, ^{140}Ba-^{140}La). If the daughter has a longer half-life than the parent, they will be reported separately (e.g., ^{105}Ru - ^{105}Rh). However, if the library indicates that the latter relationship exists and it has not been purposely voided, the amount of the daughter calculated will be based on the anticipated complete decay of the parent.

The appropriate growth factors are calculated and an abbreviated component list is made by combining the parent-daughter pairs according to the above rules.

Loading of Storage Matrix

An ordered storage matrix is now prepared with one column for each identified nuclide and one row for each identified peak. The entries in this matrix of coefficients are the appropriate gamma branching probabilities, expressed as photons/disintegration, obtained from the library arrays. In the case of genetically-related pairs, the entry for the daughter is first multiplied by the appropriate growth factor.

Recombination of Close-Lying Peaks

In some instances, the intensities of close-lying peaks tagged in subroutine FIT will be added together to form one peak, or equation. This is done before the matrix calculations because the uncertainty in the relative intensities of such peaks becomes too high as their spacing decreases. The apportionment of these intensities among the candidates is then handled much more effectively by subroutine EVAL.

Treatment of "Escape" Peaks Resulting from Pair Production

A complication occurs when an observed peak may be the result of a pair-production interaction in which one or both photons escape from the detector. The intensity of such a peak as interpreted by CALGPM does not have the same physical meaning as the intensity derived from a photopeak. To circumvent this difficulty, a scheme was devised that would allow for a reasonably good interpretation of escape peaks. In this scheme, the intensity for a double escape peak is tagged by entering it into the library as the full energy branching intensity multiplied by 10^{-10}; similarly the single-escape-peak intensity is multiplied by 10^{-20} (e.g., the 1596.2 keV ^{140}La peak with a branching probability of 0.965 is then said to produce peaks at 574.2 and 1085.2 keV with branching intensities of 9.65×10^{-11} and 9.65×10^{-21} respectively). The 10^{-10} and 10^{-20} factors serve only as flags, which are recognized and removed in LDMATX. The resulting value corresponds to the branching intensity of the full energy peak. This number cannot be used directly, but we have found a simple relationship that adequately converts this intensity to a usable pseudo-branching intensity.

$$\ln R = A + B \ln E \qquad (37)$$

where

> R is the ratio of the intensity (photons/min) assigned to the escape peak by CALGPM to that assigned to the full energy peak, and E is the energy of the escape peak in MeV.

The constants A and B are detector dependent for double escape peaks (see Fig. 24), and therefore must be characterized for each detector and their values placed on the appropriate efficiency input card.[3] The single escape peak relationship is nearly detector independent and can best be described by adding a C $(\ln E)^2$ term to Eq. (37) (see Fig. 25). The constants A, B, and C for single escape peaks have been written directly into the code.

The pseudo-branching probability now stored in the coefficients matrix is simply the full energy branching intensity multiplied by the value of R.

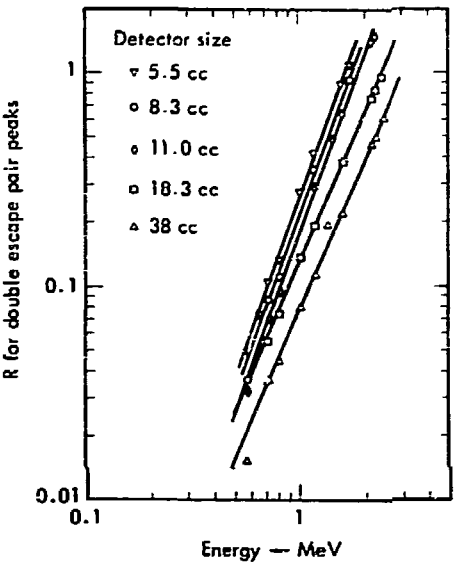

Fig. 24. Plots showing the relationship used to interpret the intensity of double escape peaks resulting from pair interaction. R is the gamma intensity of the double escape peak (as calculated in GAMANAL) divided by the full energy peak intensity.

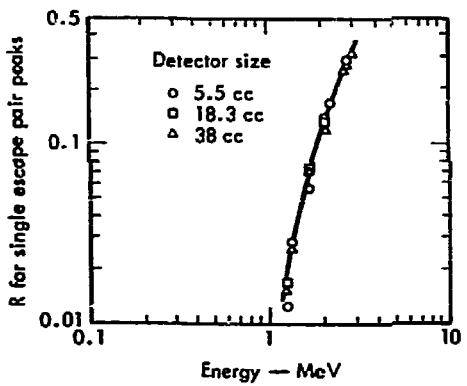

Fig. 25. Plot showing the relationship used to interpret the intensity of single escape peaks resulting from pair interaction.

Inclusion in the Matrix of Certain Associative Peaks not Found in the Spectrum

Frequently, the spectrum contains peaks that have been assigned, at least in part, to a nuclide having one or more associative gamma rays that could not be detected above the Compton background by PKSCH. The background intensity in the regions where these associative gamma rays should have been found can, however, be used to limit the amount assigned to the nuclide in question. In fact it may, under certain circumstances, be used to decide whether the peak intensity should be given completely to some other nuclide for which there may be no associative gamma rays.

To implement this logic, subroutine IDENTIFY stores background intensity data (interpreted as a gamma intensity) whenever the associative gamma rays for a prime candidate are not found. Although these background peaks are fictitious, they are nonetheless loaded into the matrix if space is available. Because they are given a 100% error, their inclusion will not affect the resulting least-squares answer unduly, but they may assist in discriminating between otherwise ambiguous identifications.

Modification of Peak Intensity Errors

In calculating the weighting factors for the equations, we have taken the liberty of adjusting slightly the statistical errors (SIGPCT) associated with the peak intensities (YARRAY) as determined by FIT.

A 0.7% error is added in quadrature to the errors of all peaks, because we believe that uncertainties in the efficiency curve and in the methods of determining

peak intensities do not warrant smaller errors, regardless of the number of counts in the peak.

Although the low-energy peaks in a spectrum are generally much more intense than higher-energy peaks, there are several factors that frequently decrease the precision with which their intensities are determined. Among these factors are the extreme complexity of some low-energy spectra, the large scattering humps that are sometimes present, and inaccuracies in the efficiency calibration at low energies. Some of these factors will be related to the resolution of the detector. For our purposes, we have chosen to add in quadrature an additional error

$$ERS = 200 \cdot SHAPC(1)/(EXPK)^2 \qquad (38)$$

where

ERS = additional error
SHAPC(1) = zero energy $(FWHM)^2$
EXPK = peak energy in keV.

The total error (ERROR) then becomes

$$ERROR = \left[(SIG)^2 + (0.007)^2 + (ERS)^2\right]^{1/2} \qquad (39)$$

and the weighting factor,

$$\omega = 1/(ERROR \cdot YARRAY)$$

Loading of Working Matrix (Subroutine EVAL)

After the loading of the storage matrix is accomplished, a search is made for the first interference set. Referring to Fig. 26, we see that nuclides A, B, C, and D constitute a set because of mutual interference and are transferred over to the working matrix shown in Fig. 27. Returning to Fig. 26 we find that the nuclides E and F form a second independent set and G, H, and I yet a third. It should be noted, however, that this last set cannot be solved since the coefficients for nuclides G and I are all zero except for one equation to which they both can contribute. This situation is detected and flagged before an analysis is attempted. In this case, nuclide H will be calculated on the basis of its remaining peaks. In the final printout for the example in Fig. 26, the contribution of H to peak number 8 will be subtracted out and the remaing peak strength assigned independently to both G and I, with an appropriate comment about the nuclide assignment being ambiguous.

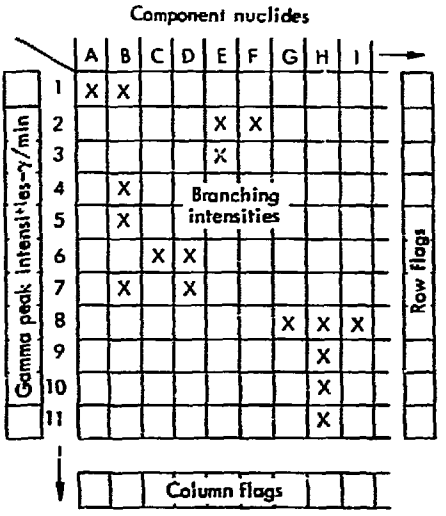

Fig. 26. An illustration of the storage matrix containing data and coefficients for a set of equations which describe the observed peak intensities. The three interference sets illustrated are found in sequence by EVAL and calculated separately as shown in Fig. 27.

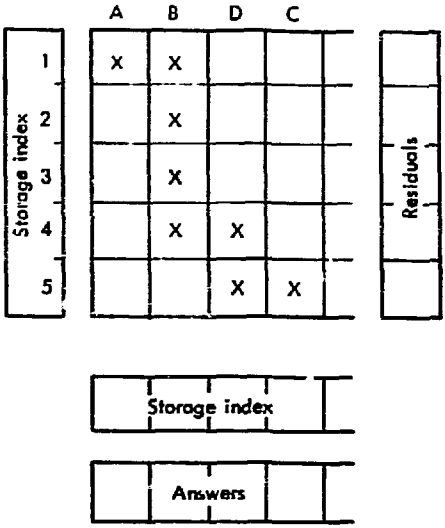

Fig. 27. An illustration of the working matrix containing data and coefficients of the first interference set found in Fig. 26.

The elements of the equations of each interference set are multiplied by the appropriate weighting factor as they are being transferred to the working matrix. An abbreviated flow diagram of the processing of an interference set is given in Fig. 28.

Matrix Calculations

If the working matrix appears to be well conditioned, a least-squares solution is attempted by the system subroutine MLR. After the calculation, several checks are made to see that the fit is good and the answers and their associated errors are reasonable.

First, the errors are calculated using the formula

$$\text{ERROR (j)} = \sqrt{\text{QFIT} \cdot \text{DMLR(j)}} \qquad (40)$$

where

$$\text{QFIT} = \left(\sum_{i=1}^{I} (\text{RMLR(i)})^2\right) \Big/ \text{DOF}$$

RMLR(i) = weighted residual

DOF = degrees of freedom (number of rows minus number of columns)

DMLR(j) = diagonal matrix element corresponding to jth component.

We next examine the residuals of the fit. Excessive residuals may arise from a number of sources. Some examples are a channel overflow or dropped channel, or a malfunction in subroutine BKGRD or

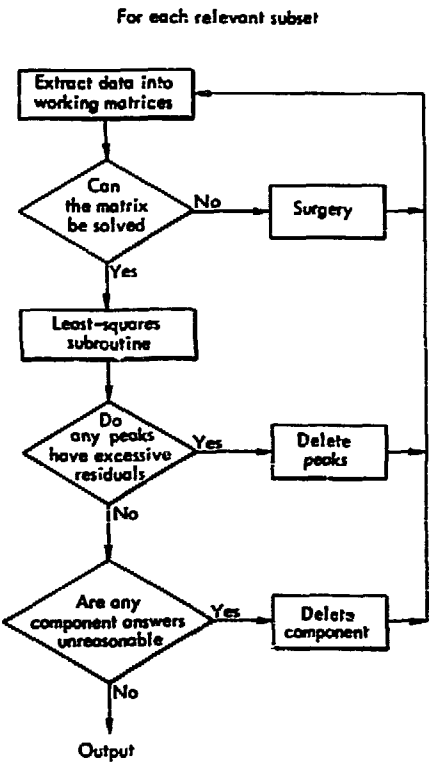

Fig. 28. Flow diagram of procedures used in the final calculations.

FIT resulting in an inaccurate peak area determination, or inaccurate or missing library decay-scheme information. If any of these conditions prevail, the answers for the components in that interference set will be affected somewhat. It is therefore important that the peak or peaks exhibiting large residuals be eliminated from the matrix and flagged as unidentified peaks. We have decided to remove peaks having residuals greater than +5 or -10 standard deviations. After this the remaining peaks are reanalyzed.

After the criteria for residuals are satisfied, the answers for each nuclide and the associated errors are checked. We have stated before that the set of component nuclides submitted by subroutine IDENTIFY for consideration will probably be over-determined. Those nuclides that indeed are not present in the spectrum will generally exhibit answers that are negative or have excessive errors. Therefore, components are appropriately flagged as not being present in the spectrum whenever their answers are negative or have errors in excess of 100%. Since elimination of components reduces interference, we then redetermine the current interference set. It will certainly be smaller by the number of components eliminated and may even have been split into a number of smaller interference sets.

If a set is to be recalculated because of the elimination of components, a further effort is first made to break the interference set into smaller groups. The approximate answers just obtained are used to calculate the contribution of each component to each peak. If the contribution to a given peak is less than one-tenth of the error associated with the peak intensity, the contribution is termed "trivial" and the corresponding matrix coefficient is tagged so that no contribution or interference is said to exist in the next calculation.

The above processes continue until all the nuclides have been considered.

FINAL CALCULATIONS AND PRINTOUTS

The answers for each nuclide, expressed in distintegrations/min at count time, can now be normalized, corrected for decay, converted to atoms, and calculated (subroutine OUTGO). The answers may be normalized by dividing by the sample weight and multiplying by the factor we call 100% weight. If these are not specified on the control card, they are set equal to 1.0.

The final printout for an analysis is in three sections (see Appendix A). The first identifies the sample, lists some of its pertinent parameters, and prints a condensed table of results which is confined to those components with less than 70% error and having an identification confidence greater than 0.1. This index is a qualitative value based upon the number of peaks the nuclide exhibits in the spectrum, upon its fractional contribution to them, and upon the tests performed in IDENTIFY. In addition to the values mentioned, this table gives the sequential set number and quality of fit for the interference set in which each of these nuclides was determined.

The second section lists in detail the contribution of each nuclide to each of the peaks with which it was identified. The label of the nuclide, atoms at zero time, and error are repeated in the first three

columns of this table and are followed by a peak-by-peak listing of some related quantities. Among these, the column headed ATOMS represents the least-squares answer for the nuclide adjusted algebraically on the basis of the residual for that peak. Rather than assign the entire residual to the one nuclide, we arbitrarily use the same fraction of it as the nuclide's contribution to the bulk of the peak.

A related quantity, under the column heading FRACTION OF PEAK, indicates the ratio of the nuclide's contribution to the peak's actual total intensity. The sum of the individual contributions to a peak plus the residual must equal unity.

The PEAK ERROR column lists the modified statistical error of the peak intensity as used in LDMATX. Any peaks showing exactly 100% error should be recognized as the "fictitious" peaks whose intensities represent maximum values relative to the observed background counts in the peak region.

The peak residuals, expressed in standard deviation units, are tabulated in the next column. A good fit is indicated by residual values less than 1 or 2 standard deviations. As discussed earlier, peaks having residuals greater in magnitude than +5 or -10 standard deviations will be removed from the fitting operation and tagged as unidentified. They are nonetheless listed in this section of the printout with an appropriate comment. However, the corresponding ATOMS reported for such a peak is incorrect.

The final column is a guide to all the interferences that were considered in the analytical process. The interferences are separated into three categories, first, those that are believed to be present, second, those that are present to a negligible extent and therefore ignored, and third, those that were at one time considered but were subsequently rejected because of negative answers or excessive error.

The final table in the printout (see Appendix A) simply lists the unidentified peaks. It may contain some peaks rejected in the course of the matrix calculations, but it consists primarily of peaks that are not in the decay-scheme library or that had large errors and may well be spurious.

Acknowledgments

The authors thank H. B. Levy for his participation in the early development of GAMANAL and for his helpful discussions on some of the mathematical aspects of the program.

References

1. R. Gunnink, H. B. Levy, and J. B. Niday, Identification and Determination of Gamma Emitters by Computer Analysis of Ge(Li) Spectra, Lawrence Livermore Laboratory, Rept. UCID-15140 (1967).
2. R. Gunnink and J. B. Niday, "Quantitative Analysis of Unknown Mixtures by Computer Reduction of Ge(Li) Spectra," in Modern Trends in Activation Analysis, J. R. DeVoe, Ed. (National Bureau of Standards, Washington, D. C., 1969), Vol. II, p. 1244.
3. J. B. Niday and R. Gunnink, Computerized Quantitative Analysis by Gamma-Ray Spectrometry. Vol. III, A User's Guide to GAMANAL, Lawrence Livermore Laboratory, Rept. UCRL-51061, Vol. III (1971).
4. R. Gunnink and J. B. Niday, Computerized Quantitative Analysis by Gamma-Ray Spectrometry. Vol. II, Source Listing of the GAMANAL Program, Lawrence Livermore Laboratory, Rept. UCRL-51061, Vol. II (1971).
5. R. Gunnink and J. B. Niday, Computerized Quantitative Analysis by Gamma-Ray Spectrometry. Vol. IV, Auxiliary Programs for GAMANAL, Lawrence Livermore Laboratory, Rept. UCRL-51061, Vol. IV (to be published).
6. H. R. Ralston and G. E. Wilcox, "A Computer Method of Peak Area Determinations from Ge(Li) Spectra," in Modern Trends in Activation Analysis, J. R. DeVoe, Ed. (National Bureau of Standards, Washington, D. C., 1969), Vol. II, p. 1238.
7. W. M. Sanders and D. M. Holm, An Analytical Method for Unfolding Gamma-Ray Spectra, Los Alamos Scientific Laboratory, Los Alamos, N. Mex., Rept. LA-4030 (1969).
8. D. C. Camp, Applications and Optimization of the Lithium-Drifted Germanium Detector System, Lawrence Livermore Laboratory, Rept. UCRL-50156 (1967).
9. E. Storm and H. I. Israel, Nucl. Data Tables U. S. Atomic Energy Comm. A7, 565 (1970).
10. R. D. Evans and R. O. Evans, Rev. Mod. Phys. 20, 305 (1948).

Appendix A

A Typical Printout from an Analysis by GAMANAL

The following printout of the analysis of a fission- and activation-product sample is typical of the results reported by GAMANAL, although several other options are available. The first two pages show the library of cards containing data on the efficiency, linearity, and peak shape parameters for the various detectors and systems in use. After the spectrum requested has been read in, the control parameters are checked and summarized along with the spectral data. When the spectrum has been reduced and interpreted in terms of peak energies and intensities, this information and related quantities are tabulated in an intermediate printout. A continuation of the analysis of the spectrum results in the identification of the radioactive materials in the sample and a quantitative assessment of the amounts present. An initial summary of the results for each identified nuclide is followed by a more detailed listing showing how the intensity of each peak was evaluated. A final table reports peaks that have remained unidentified for any of several reasons.

```
PROGRAM ENTERING  INPUT    ROUTINE AFTER   0.199 SECS.  (CPU#1/CPSYS =  00096033)  CLOCK READS 01.033 002/08 1972
INPUT CARD READS  7    1.5        9.         3.        1.8        1.6        4.         4.              1
INPUT CARD READS  ABSORBER ACC1.362E+0
INPUT CARD READS  ABSORBER BHO.344E+00CD.447E+00CU.745E+00
INPUT CARD READS  ABSORBER CCC1.362E+0AL0.16E+00
INPUT CARD READS  ABSORBER IAL  .15
INPUT CARD READS  PKSHAPE  E 2.618    .00122    -3.276    .003536   1.408     .400
INPUT CARD READS  PKSHAPE  F 1.06     .002212   -2.979     .0020    1.192     .40
INPUT CARD READS  PKSHAPE  L+1.05     +.002     -2.78     +.0049    +1.574    .4
INPUT CARD READS  PKSHAPE  M+2.465    +.002139  -1.631    +.000617  +1.066    +.4
INPUT CARD READS  PKSHAPE  N 3.567    .002158   -4.384    0.00009939 0.401    0.400
INPUT CARD READS  PKSHAPE  P .205     .001838   -2.816    .006      2.283     .400
INPUT CARD READS  4-438579E-01 /53842E-02-783385E-08 196621E-11                                  X4
INPUT CARD READS  4-805652E-01+504026E-01-398373E-06+185468E-09-423752E-13+409763E-17            L2
INPUT CARD READS  4+491592E+00+603756E-01-427438E-06+137638E-09-243670E-13+191263E-17            M1
INPUT CARD READS  4+556605E-01+602398E-01-314472E-06+693836E-10-403558E-14+340525E-19            SM1
INPUT CARD READS  4+491592E+00+603756E-01-427438E-06+137638E-09-243670E-13+191263E-17            M3
INPUT CARD READS  4+5566G5E-01+602398E-01-314472E-06+693836E-10-403558E-14+340525E-19            SM3
INPUT CARD READS  4-873997E-01+500969E-01-170268E-06+879836E-10-248098E-13+275899E-17            F1
INPUT CARD READS  4-873997E-01+50C969E-01-17G268E-06+879836E-10-248098E-13+275899E-17            F2
INPUT CARD READS  4-759732E-01+151028E-01-879C72E-07+376306E-10-918631E-14+941722E-18            P3
INPUT CARD READS  4-759732E-01+151C28E-01-879C72E-07+376306E-10-918631E-14+941722E-18            P4
INPUT CARD READS  4-201635E-01+561750E-01+276C91E-06-145167E-09+384517E-13-319414E-17            L5
INPUT CARD READS  4-762733E-01+5635564E-01-275822E-06+138768E-09-342493E-13+365321E-17           SL2
INPUT CARD READS  4-143185E-01+502180E-01-224567E-06+750432E-10-140432E-13+114365E-17           4L4
INPUT CARD READS  4-143185E-01+502180E-01-224567E-06+750432E-10-140432E-13+114365E-17            L4
INPUT CARD READS  4-821018E+0C+573363E-01+106289E-06-139689E-09+423729E-13-376225E-17            R5
```

```
INPUT CARD READS  4+143915E+00+142019E-01+188878E-04-105282E-09+256434E-13-223018E-17           P2
INPUT CARD READS  4-120035E+01+517035E-01-657255E-04+357537E-09-104088E-12+118468E-16           E4
INPUT CARD READS  4+193350E-01+358713E-01+356732E-05-531983E-08+392119E-11-149902E-14          3E4
INPUT CARD READS  4+281920E-18-205818E-22         E          E          E          E          13E4
INPUT CARD READS  4-120035E+01+517035E-01-657255E-04+357537E-09-104088E-12+118468E-16          4E4
INPUT CARD READS  4-832149E+00+663663E-01-484748E-05+599636E-08-422744E-11+155254E-14          5E4
INPUT CARD READS  5-3653168E+0-1311903E+0+5346700E-2-1396810E-1+1395000E-2+3522800E-2   1430.   E
INPUT CARD READS  5-1688835E+1-2488766E+1-1476297E+1-4061978E+0-4356480E-1           6013155 1 E
INPUT CARD READS  5-2886752E+0-1017625E+0+4249263E-3-9666160E-2+3065552E-3+2660775E-2    30 80   M
INPUT CARD READS  5-1216074E+2-2078643E+2-1343424E+2-3868456E+1-4192399E+0-2.6062.369  8540141 1 M
INPUT CARD READS  5-3803715E+0-1222386E+0+4524111E-2-5808513E-2-3329120E-3+1660820E-2    14130   M
INPUT CARD READS  5-3384371E+1-4971316E+1-2847533E+1-7340782E+0-7307726E-1-2.08 2.375  5031231 1 M
INPUT CARD READS  5-5363497E+0-1485524E+0+1079...E-1-1318840E-1+1263385E-4+2781769E-2    19195   F
INPUT CARD READS  5+9243067E+0+2077372E+1+1203194E+1+2313368E+0+5560108E-2-1.4042.775  5010130 1 F
INPUT CARD READS  5-8536411E+0-1483544E+0+1344176E+0+1096970E+0+4853530E-1+8565337E-2    .3.82   F
INPUT CARD READS  5-3521664E+1-3494413E+1-1390939E+1-2429201E+0-1583945E-1           30.5 80 1 F
INPUT CARD READS  5-4659439E+0-1420150E+0+1110033E-1-1200893E-1-3420023E-3+2225860E-2    25 95   L
INPUT CARD READS  5-3440538E+1-4317834E+1-2051351E+1-4619576E+0-4033728E-1-1.5852.775  40 9130 1 L
INPUT CARD READS  7    1.5       9.        6.        1.8       1.6       4.      10.              1
INPUT CARD READS  TAPE      GESTGTP-27 STORAGE TAPE STARTED 8/3/70            FLS02UNIT27
INPUT CARD READS  UNITS     STORAGE 27    LIB 16    DATA 7    AMPX 5

1

TYPE 2 CARD READ  2FISS. +ACT. PRODS.F2 30  1C 3064642C0 300383    10  E              7  441 462201

FOUND LIBRARY FILE LABELLED GELIBE1015  LENGTH=  64C2
PROGRAM ENTERING  READ      ROUTINE AFTER   C.537 SECS.  (CPU01/C0SYS =  04492+01)  CLOCK READS 01.066 602/08 1972


   DATA FOR EXPERIMENT  FISS. +ACT. PRODS.  FOUND AS FILE GEF2462201, NO 106 ON STORAGE TAPE NO -27
  DATA ORIGINATED 1970, ON SHELF C5, CHANGER C2, AT GEOMETRY CF    31.95, WITH   0 OVERFLOWS CORRECTED

INPUT CARD READS  3 280.   140.42 465.   228.2 1545.   772.7 1692.   846.782475.  1238.29
INPUT CARD READS  33192.  1596.20                                                          1
INPUT CARD READS  BOUNDS              BEGMID  90
INPUT CARD READS  MATERIALS HG 85.     U 15.
INPUT CARD READS  9

TERMINAL INPUT CARD READ - END OF CARD DECK


DATA ON ENERGY/CHANNEL, SYSTEM LINEARITY, AND DETECTOR EFFICIENCY TO BE USED IN THE ANALYSIS
   CL    280.00    465.00   1545.00   1692.C0   2475.00   3192.00   INTERNAL
   EN   140.420   228.200   772.7C0   846.78C  1238.290  1596.200   PEAKS

LINEARITY COEFFS  -8.739970E-CL 5.009690E-C1-1.702680E-06 8.798360E-10-2.480980E-13 2.758990E-17        SYSTEM-2
                        0.          0.            C.           0.           0.          0.

EFFICIENCY COEFFS -5.363497E+00-1.485524E+00 1.079516E-01-1.318840E-01 1.263385E-04 2.781769E-02       DETECTOR-F
                     FOR CALCULATIONS BEGINNING AT     50. KEV WITH CROSSOVER AT   130. KEV TC
                    9.243067E+C0 2.077372E+C1 1.203194E+01 2.313368E+00 5.560108E-02 0.
                PAIR-PEAK EFFICIENCY COEFFS ARE  -1.406    2.775

DETECTOR F4 HEIGHT = 1.00, RADIUS SQUARED =  1.9, RESOLUTION AT ZERO ENERGY =   1.05
          DISTANCE FROM DETECTOR SURFACE TO WINDOW=  1.95   TOTAL (TO PIG POINT OF SOURCE) =  31.95 CM

SAMPLE AREA (CM SQ)=10.00, DEPTH =  1.00, COMPOSITION= HG 85.     U 15.

COMPOSITION OF ABSORBER  1 = AL  1.500E-01     0.          0.          0.          0.          0.
```

PEAK ANALYSIS TO BE BASED ON APPROXIMATE GAIN OF 0.500 KEV/CHANNEL AND PEAK SHAPE PARAMETERS ARE

1.10260E+00 2.1170E-03-2.4440E+00 1.4420E-03 1.0800E+00 4.0000E-01

PROGRAM ENTERING REPORT ROUTINE AFTER 0.100 SECS. (CPU01/COSYS = 20174100) CLOCK READS 01.066 002/08 1972

1 SAMPLE FISS. FACT. PROCS.. DELTAT= 6.150 DAYS. 200 MIN COUNT BEGAN 105.486 (1970) ON GE(LI) CTR-F2

21989.0	34502.0	135769.0	254778.0	334552.0	355250.0	348209.0	317584.0	273316.0	252496.0	10
248897.0	239753.0	229641.0	220083.0	210659.0	203623.0	196216.0	190026.0	183910.0	178345.0	20
174976.0	171371.0	169857.0	166403.0	162881.0	160262.0	157688.0	155213.0	153466.0	150383.0	30
148475.0	146576.0	143712.0	142835.0	142008.0	139892.0	138760.0	137162.0	136291.0	134694.0	40
133970.0	132610.0	131225.0	130928.0	130785.0	129564.0	129718.0	129826.0	131428.0	129545.0	50
124623.0	122556.0	120943.0	121165.0	120591.0	120236.0	119118.0	118463.0	117324.0	118644.0	60
117226.0	114929.0	113770.0	112251.0	110990.0	110466.0	110261.0	110991.0	110434.0	110052.0	70
110701.0	110894.0	110270.0	108650.0	107327.0	108440.0	107632.0	107581.0	108924.0	112129.0	80
111270.0	107141.0	103515.0	102494.0	103538.0	103344.0	102364.0	101322.0	100968.0	101765.0	90
103225.0	107084.0	99808.0	98763.0	97726.0	96589.0	96886.0	98412.0	105281.0	110804.0	100
103205.0	95026.0	93278.0	92969.0	92802.0	92803.0	92677.0	92384.0	92522.0	93384.0	110
95425.0	93310.0	94842.0	100578.0	106555.0	104515.0	97650.0	94725.0	95605.0	96265.0	120
96265.0	97664.0	99014.0	100782.0	102064.0	103625.0	103225.0	103187.0	104210.0	106095.0	130
106654.0	106041.0	107793.0	110249.0	109324.0	106179.0	106685.0	101093.0	108060.0	108903.0	140
109412.0	109964.0	112886.0	115810.0	127096.0	137831.0	132567.0	124182.0	134518.0	156467.0	150
157001.0	134107.0	120573.0	119370.0	121533.0	122565.0	122587.0	122760.0	126842.0	152007.0	160
264292.0	473269.0	468227.0	245899.0	122317.0	101514.0	101999.0	105924.0	114725.0	121410.0	170
117768.0	109780.0	106405.0	109233.0	113167.0	112168.0	109344.0	109292.0	110231.0	113772.0	180
130154.0	170771.0	183777.0	145183.0	122485.0	117495.0	124157.0	155196.0	228039.0	259769.0	190
193591.0	129473.0	111774.0	112443.0	132850.0	215834.0	331794.0	304913.0	177412.0	112354.0	200
97602.0	95659.0	94827.0	95406.0	95588.0	96139.0	97295.0	96377.0	93707.0	91951.0	210
92173.0	93008.0	92417.0	91378.0	89655.0	89266.0	88383.0	89766.0	93617.0	105320.0	220
124985.0	145119.0	155917.0	137501.0	107446.0	90387.0	87516.0	94033.0	104382.0	106394.0	230
97053.0	93492.0	93510.0	90779.0	85682.0	84165.0	83072.0	[illegible]	83881.0	84532.0	240
86477.0	97208.0	125428.0	149997.0	127828.0	96289.0	85881.0	84594.0	84268.0	84118.0	250
83205.0	83125.0	83131.0	82642.0	83175.0	82338.0	82448.0	82540.0	83160.0	83133.0	260
84332.0	85800.0	85971.0	85146.0	84271.0	84731.0	84666.0	84140.0	81073.0	79905.0	270
79967.0	78140.0	78583.0	77809.0	77430.0	77917.0	78858.0	83222.0	128745.0	278772.0	280
523138.0	494692.0	233632.0	92114.0	65889.0	64385.0	64640.0	65246.0	73461.0	138836.0	290
150992.0	135049.0	86467.0	64425.0	60555.0	60605.0	60532.0	59816.0	61321.0	61765.0	300
60162.0	58993.0	58502.0	58114.0	57533.0	57423.0	57621.0	57121.0	56937.0	56561.0	310
54907.0	55569.0	55639.0	55625.0	55020.0	54760.0	54016.0	53927.0	54146.0	51962.0	320
54233.0	53381.0	54354.0	59689.0	76491.0	74630.0	62951.0	54416.0	51695.0	51679.0	330
51167.0	51518.0	51079.0	51825.0	51211.0	51681.0	50920.0	50812.0	50419.0	50529.0	340
50681.0	49981.0	50441.0	50669.0	50527.0	50663.0	50581.0	50677.0	50115.0	50015.0	350
49894.0	50163.0	50084.0	50255.0	49840.0	49399.0	46763.0	49086.0	48781.0	50247.0	360
57368.0	88316.0	88603.0	56329.0	48824.0	47249.0	46524.0	46763.0	46611.0	46219.0	370
46348.0	46180.0	45763.0	45118.0	45081.0	45218.0	45363.0	45179.0	44833.0	44659.0	380
46624.0	44394.0	44447.0	44046.0	44137.0	44140.0	43510.0	43784.0	44005.0	43476.0	390
43634.0	43697.0	43252.0	43148.0	42855.0	43133.0	42579.0	42380.0	42442.0	42286.0	400
42522.0	42356.0	41824.0	41860.0	41558.0	41334.0	40870.0	40800.0	40338.0	40234.0	410
39889.0	39879.0	39380.0	39301.0	38566.0	38664.0	38410.0	38335.0	37651.0	37911.0	420
37684.0	37373.0	37069.0	36796.0	36725.0	36078.0	36129.0	35482.0	35550.0	34764.0	430
34666.0	34579.0	34394.0	34094.0	33751.0	33529.0	33303.0	33531.0	33381.0	33070.0	440
32852.0	32689.0	32910.0	33222.0	32577.0	32769.0	32812.0	32239.0	32403.0	32315.0	450
32801.0	34945.0	33662.0	41509.0	78605.0	159530.0	194108.0	125510.0	54190.0	31860.0	460
29220.0	29471.0	30342.0	29920.0	29248.0	28850.0	28853.0	28229.0	27971.0	27529.0	470
27216.0	27393.0	26873.0	26893.0	27144.0	26710.0	26527.0	26836.0	26731.0	26739.0	480
26349.0	26877.0	26462.0	26781.0	26245.0	25905.0	25864.0	27302.0	29430.0	29829.0	490
27043.0	25764.0	25029.0	24649.0	24561.0	24821.0	24378.0	24406.0	24710.0	24482.0	500
24185.0	24428.0	23970.0	24322.0	23878.0	24044.0	23649.0	23827.0	23848.0	24006.0	510
23675.0	23348.0	23049.0	23016.0	23015.0	22788.0	22854.0	22694.0	22469.0	22596.0	520
22461.0	22353.0	22722.0	22991.0	24032.0	23999.0	21250.0	22257.0	22069.0	21714.0	530
22031.0	22244.0	22464.0	22024.0	21534.0	21237.0	21321.0	21222.0	20973.0	21022.0	540
21184.0	21291.0	21095.0	20976.0	20810.0	20891.0	20363.0	20879.0	20887.0	21005.0	550
20918.0	20676.0	20680.0	20563.0	20340.0	20344.0	20185.0	20150.0	20351.0	20029.0	560
20049.0	19849.0	19950.0	19694.0	19810.0	20250.0	21535.0	23174.0	24943.0	22948.0	570
20675.0	20334.0	19584.0	19114.0	19113.0	19272.0	19084.0	19206.0	18999.0	19153.0	580
19257.0	19159.0	19408.0	21758.0	29045.0	39951.0	40449.0	29374.0	21223.0	18736.0	590
18693.0	18480.0	18596.0	18494.0	18445.0	18303.0	18269.0	18238.0	18250.0	18517.0	600
18177.0	18019.0	18287.0	18137.0	18426.0	18161.0	18272.0	18722.0	21870.0	22540.0	610
20854.0	19232.0	18507.0	18331.0	17792.0	17967.0	17619.0	17701.0	17748.0	17494.0	620
17935.0	17742.0	17650.0	17485.0	17566.0	17901.0	17449.0	17429.0	17458.0	17292.0	630
17277.0	17532.0	17399.0	17129.0	17470.0	17186.0	18270.0	19199.0	19354.0	18219.0	640
17001.0	16812.0	16744.0	16392.0	16673.0	16539.0	16456.0	16755.0	16376.0	16372.0	650
16573.0	16477.0	16684.0	16777.0	16640.0	25466.0	34567.0	34312.0	24424.0	17792.0	660
15998.0	15558.0	15610.0	15326.0	15452.0	15642.0	15625.0	15615.0	15624.0	15633.0	670
15208.0	15017.0	15400.0	15210.0	15035.0	14866.0	15014.0	14950.0	15012.0	15118.0	680
14812.0	14497.0	14383.0	14416.0	14257.0	14985.0	17804.0	21248.0	21123.0	17272.0	690
14608.0	13759.0	13490.0	13459.0	13424.0	13355.0	13444.0	13290.0	13451.0	14053.0	700
14395.0	14165.0	13503.0	12920.0	13030.0	13028.0	12932.0	12966.0	13045.0	12820.0	710
12800.0	12972.0	12749.0	12635.0	12599.0	12662.0	12509.0	12596.0	12608.0	12510.0	720
12504.0	12682.0	12505.0	12732.0	13076.0	15464.0	25076.0	42159.0	48573.0	34890.0	730
19304.0	13741.0	12805.0	12364.0	11921.0	11659.0	11447.0	11519.0	11456.0	11282.0	740
11220.0	11257.0	11136.0	11163.0	11147.0	11236.0	11275.0	10973.0	10899.0	11146.0	750
10880.0	11111.0	11198.0	11058.0	10903.0	10951.0	10894.0	10813.0	10968.0	11010.0	760
10961.0	11014.0	11003.0	10864.0	10913.0	10646.0	10776.0	10809.0	10709.0	10838.0	770
10777.0	10763.0	10733.0	10657.0	10985.0	10864.0	10728.0	10546.0	10340.0	10469.0	780
10481.0	10446.0	10516.0	10452.0	10258.0	10505.0	10472.0	10483.0	10400.0	10167.0	790
10357.0	10169.0	10304.0	10249.0	10437.0	10426.0	10543.0	10326.0	10264.0	10175.0	800
10267.0	10159.0	10278.0	10003.0	10132.0	10140.0	10208.0	9922.0	10311.0	10237.0	810
9952.0	9922.0	10013.0	10089.0	10179.0	10009.0	10057.0	9969.0	9168.0	10091.0	820
10542.0	10375.0	10268.0	10101.0	10055.0	9865.0	9868.0	9126.0	9809.0	9907.0	830
9895.0	9881.0	10181.0	10233.0	9919.0	9781.0	9923.0	9150.0	9916.0	9640.0	840
9814.0	9735.0	9619.0	9797.0	9860.0	10574.0	11216.0	10920.0	10122.0	9490.0	850

9204.0	9159.0	9316.0	9312.0	9381.0	9522.0	9315.0	9174.0	8771.0	9026.0	860
9000.0	9304.0	9796.0	10393.0	10746.0	10128.0	9316.0	8953.0	8792.0	8939.0	870
8790.0	9038.0	9116.0	9599.0	9880.0	9702.0	9025.0	8854.0	9274.0	9036.0	880
9147.0	8894.0	8856.0	8619.0	8835.0	8999.0	9254.0	9400.0	9128.0	9080.0	890
8951.0	9191.0	9095.0	8724.0	8674.0	8906.0	8649.0	8476.0	8721.0	8724.0	900
8704.0	8715.0	8604.0	8631.0	8581.0	8481.0	8494.0	8565.0	8606.0	8587.0	910
8571.0	8504.0	8670.0	8525.0	8664.0	8550.0	8458.0	8464.0	8546.0	8594.0	920
8660.0	8484.0	8420.0	8755.0	8743.0	8524.0	8636.0	8667.0	8580.0	8653.0	930
8508.0	8578.0	8619.0	8442.0	8418.0	8602.0	8503.0	8509.0	8469.0	8576.0	940
8535.0	8581.0	8511.0	8549.0	8564.0	8817.0	8876.0	8555.0	8642.0	8478.0	950
8715.0	8323.0	8321.0	8203.0	8265.0	8357.0	8238.0	8027.0	8167.0	7798.0	960
7997.0	8112.0	8028.0	7985.0	7970.0	7743.0	7600.0	7828.0	7922.0	8147.0	970
10071.0	15711.0	24385.0	26879.0	19607.0	11418.0	8115.0	7405.0	7534.0	7566.0	980
7541.0	7361.0	7200.0	6920.0	7118.0	7244.0	7073.0	7237.0	7051.0	7189.0	990
7914.0	9899.0	12858.0	14102.0	11778.0	8612.0	7227.0	6916.0	6872.0	7037.0	1000
7040.0	6832.0	6918.0	6582.0	7015.0	7253.0	7005.0	7208.0	7319.0	7975.0	1010
9025.0	8837.0	8324.0	7831.0	8142.0	9123.0	10834.0	14576.0	20368.0	26352.0	1020
30992.0	31505.0	27454.0	21260.0	14915.0	10783.0	8532.0	7428.0	6932.0	6549.0	1030
6622.0	6501.0	6420.0	6458.0	6583.0	6502.0	6540.0	6510.0	6565.0	6698.0	1040
6638.0	7118.0	8367.0	10986.0	12357.0	10458.0	8123.0	6844.0	6474.0	6546.0	1050
6428.0	6495.0	6274.0	6426.0	6612.0	6757.0	7174.0	8851.0	10092.0	10599.0	1060
9748.0	8665.0	7487.0	6693.0	6402.0	6364.0	6563.0	6593.0	6470.0	6470.0	1070
7136.0	6530.0	11611.0	14728.0	13031.0	9605.0	6945.0	6347.0	6315.0	6300.0	1080
6133.0	6152.0	6219.0	6134.0	6245.0	6061.0	6020.0	6016.0	6191.0	6174.0	1090
6240.0	6171.0	6334.0	6279.0	6193.0	6083.0	6044.0	6043.0	6031.0	6001.0	1100
5981.0	6039.0	6033.0	5980.0	5967.0	5962.0	5970.0	5917.0	5977.0	5872.0	1110
5875.0	6066.0	5931.0	6052.0	5817.0	5928.0	5973.0	5937.0	5983.0	5852.0	1120
5712.0	5992.0	6028.0	6316.0	6678.0	7024.0	6883.0	6297.0	6061.0	5829.0	1130
5849.0	5864.0	5903.0	5896.0	6032.0	6326.0	7184.0	7966.0	7736.0	6607.0	1140
5905.0	5770.0	5776.0	5785.0	5837.0	6265.0	6623.0	7023.0	6663.0	6274.0	1150
5627.0	5705.0	5607.0	5623.0	5612.0	5648.0	5636.0	5537.0	5568.0	5455.0	1160
5410.0	5266.0	5270.0	5297.0	5197.0	5342.0	5387.0	5216.0	5166.0	5184.0	1170
5238.0	5303.0	5324.0	5198.0	5244.0	5130.0	5211.0	5235.0	5120.0	5109.0	1180
5048.0	5161.0	5152.0	4993.0	5023.0	5120.0	5054.0	5088.0	5139.0	5147.0	1190
5105.0	4914.0	5016.0	5100.0	5035.0	5026.0	5139.0	5185.0	5110.0	5148.0	1200
5184.0	5599.0	6831.0	8981.0	10238.0	10699.0	10849.0	14545.0	16957.0	13832.0	1210
8791.0	5814.0	4764.0	4579.0	4721.0	4716.0	4658.0	4775.0	4853.0	5088.0	1220
4838.0	4657.0	4608.0	4587.0	4578.0	4517.0	4503.0	4488.0	4575.0	4570.0	1230
4581.0	4559.0	4621.0	4662.0	4544.0	4554.0	4469.0	4501.0	4637.0	4732.0	1240
5033.0	4885.0	4776.0	4527.0	4542.0	4445.0	4464.0	4557.0	4532.0	4451.0	1250
4827.0	4219.0	4196.0	4315.0	4291.0	4475.0	4699.0	5448.0	6969.0	7305.0	1260
6890.0	5538.0	4401.0	4355.0	4239.0	4144.0	4262.0	4332.0	4215.0	4364.0	1270
4525.0	4803.0	5158.0	5169.0	4801.0	4455.0	4172.0	4100.0	4129.0	4215.0	1280
4211.0	4198.0	4076.0	4166.0	4112.0	4102.0	4047.0	4034.0	4043.0	4206.0	1290
4304.0	4293.0	4244.0	4653.0	3783.0	3704.0	3855.0	3886.0	4069.0	4209.0	1300
4148.0	3900.0	3697.0	3540.0	3535.0	3559.0	3321.0	3511.0	3407.0	3387.0	1310
3311.0	3317.0	3426.0	3712.0	3749.0	4165.0	4141.0	3653.0	3560.0	4330.0	1320
6353.0	9121.0	10560.0	8623.0	5456.0	3855.0	3606.0	3866.0	3572.0	3790.0	1330
4133.0	5660.0	11169.0	19514.0	24545.0	19787.0	16087.0	5816.0	4372.0	4012.0	1340
3773.0	3723.0	3715.0	3470.0	3015.0	2791.0	2735.0	2736.0	2660.0	2658.0	1350
2777.0	2546.0	2746.0	2688.0	2693.0	2735.0	2598.0	2684.0	2601.0	2725.0	1360
2621.0	2613.0	2684.0	2534.0	2613.0	2617.0	2591.0	2670.0	2766.0	2807.0	1370
2750.0	2699.0	2728.0	2622.0	2581.0	2626.0	2634.0	2513.0	2550.0	2535.0	1380
2512.0	2578.0	2500.0	2551.0	2488.0	2562.0	2534.0	2514.0	2515.0	2502.0	1390
2499.0	2444.0	2489.0	2536.0	2412.0	2514.0	2505.0	2475.0	2430.0	2394.0	1400
2326.0	2350.0	2386.0	2352.0	2317.0	2407.0	2459.0	2353.0	2332.0	2375.0	1410
2294.0	2389.0	2371.0	2352.0	2422.0	2340.0	2375.0	2425.0	2357.0	2342.0	1420
2184.0	2257.0	2344.0	2323.0	2367.0	2341.0	2424.0	2272.0	2367.0	2218.0	1430
2294.0	2320.0	2253.0	2297.0	2243.0	2317.0	2759.0	2366.0	2293.0	2257.0	1440
2377.0	2575.0	2964.0	3147.0	3340.0	3803.0	4472.0	4457.0	4016.0	3038.0	1450
2666.0	2649.0	3131.0	3189.0	2849.0	2525.0	2448.0	2282.0	2263.0	2118.0	1460
2050.0	2118.0	2066.0	2129.0	2054.0	2075.0	2089.0	2131.0	2081.0	2048.0	1470
2112.0	2140.0	2143.0	2199.0	2265.0	2668.0	3641.0	4677.0	4756.0	3105.0	1480
2807.0	2230.0	2111.0	2193.0	2440.0	2630.0	2625.0	2342.0	2195.0	2098.0	1490
1985.0	1980.0	2047.0	1990.0	2058.0	2167.0	2225.0	2267.0	2310.0	2313.0	1500
2454.0	2659.0	2757.0	2606.0	2260.0	2031.0	1945.0	1978.0	1930.0	2327.0	1510
2996.0	3962.0	4516.0	4181.0	2886.0	2271.0	1937.0	1872.0	1967.0	1779.0	1520
1829.0	1834.0	1832.0	1980.0	1829.0	1633.0	1777.0	1906.0	2023.0	2207.0	1530
2507.0	2274.0	2110.0	1940.0	1964.0	1937.0	1881.0	1973.0	1945.0	1943.0	1540
2352.0	3673.0	7650.0	12213.0	14375.0	11267.0	6265.0	3116.0	2098.0	1884.0	1550
1765.0	1735.0	1900.0	2612.0	2825.0	3030.0	2904.0	2669.0	2211.0	2098.0	1560
1839.0	1803.0	1747.0	1854.0	1655.0	1771.0	1758.0	1723.0	1726.0	1656.0	1570
1792.0	1705.0	1726.0	1741.0	1718.0	1775.0	1748.0	1743.0	1733.0	2716.0	1580
1739.0	1731.0	1749.0	1755.0	1763.0	1764.0	1952.0	2392.0	3765.0	5983.0	1590
2954.0	7265.0	4907.0	2758.0	1860.0	1597.0	1642.0	1685.0	1613.0	1324.0	1600
1778.0	2030.0	2254.0	2219.0	1924.0	1837.0	2755.0	1611.0	1663.0	1667.0	1610
1640.0	1647.0	1617.0	1626.0	1682.0	1766.0	1844.0	1938.0	2112.0	2037.0	1620
1968.0	2087.0	2346.0	2563.0	2528.0	2259.0	2250.0	2581.0	3353.0	4573.0	1630
5408.0	4742.0	3174.0	2209.0	1699.0	1635.0	1592.0	1578.0	1563.0	1574.0	1640
1647.0	1637.0	1646.0	1630.0	1651.0	1792.0	1620.0	1612.0	1628.0	1665.0	1650
1609.0	1644.0	1597.0	1651.0	1630.0	1649.0	1696.0	1662.0	1591.0	1625.0	1660
1554.0	1696.0	1667.0	1612.0	1775.0	1954.0	2591.0	3557.0	4154.0	4067.0	1670
2968.0	2056.0	1656.0	1647.0	1527.0	1621.0	1584.0	1594.0	1620.0	1571.0	1680
1610.0	1700.0	1648.0	1647.0	1657.0	1682.0	1776.0	1817.0	2373.0	4056.0	1690
8138.0	14167.0	18559.0	15835.0	9300.0	4649.0	2152.0	1446.0	1518.0	1427.0	1700
1484.0	1537.0	1535.0	1507.0	1492.0	1516.0	1479.0	1536.0	1401.0	1419.0	1710
1635.0	1456.0	1456.0	1617.0	1434.0	1464.0	1388.0	1367.0	1416.0	1420.0	1720
1470.0	1437.0	1477.0	1411.0	1500.0	1526.0	1475.0	1474.0	1455.0	1449.0	1730
1421.0	1463.0	1881.0	2693.0	2445.0	2225.0	1872.0	1621.0	1394.0	1438.0	1740
1599.0	1413.0	1516.0	1381.0	1463.0	1465.0	1495.0	1513.0	1465.0	1543.0	1750
1587.0	1540.0	1511.0	1559.0	1544.0	1401.0	1505.0	1425.0	1364.0	1424.0	1760
1482.0	1505.0	1356.0	1369.0	1434.0	1492.0	1467.0	1414.0	1422.0	1437.0	1770
1414.0	1418.0	1428.0	1402.0	1434.0	1426.0	1494.0	1415.0	1418.0	1488.0	1780
1449.0	1492.0	1411.0	1422.0	1319.0	1433.0	1445.0	1451.0	1519.0	1479.0	1790
1528.0	1636.0	1959.0	2594.0	3452.0	3669.0	2988.0	2042.0	1659.0	1394.0	1800

1452.0	1374.0	1487.0	1447.C	1428.0	1428.C	1390.0	1451.0	1443.0	1434.0	1810
1371.0	1412.C	1473.0	1454.0	1452.0	1379.C	1410.0	1444.0	1516.0	1563.0	1820
1547.0	1444.0	1419.0	1427.0	1375.0	1425.C	1430.0	1448.0	1390.0	1460.0	1830
1475.0	1459.0	1389.0	1476.0	1425.0	1463.C	1663.0	1805.0	1700.0	1632.0	1840
1528.0	1495.0	1435.0	1456.C	1485.0	1448.C	1561.0	1881.C	2120.0	2219.0	1850
2227.0	1807.0	1611.0	1506.C	1458.0	1445.C	1459.0	1456.0	1483.0	1407.0	1860
1452.0	1393.0	1433.0	1392.0	1411.0	1476.C	1428.C	1377.0	1448.0	1347.0	1870
1434.0	1408.0	1423.0	1461.C	1182.0	1460.C	1458.0	1456.0	1411.0	1474.0	1880
1475.0	1438.0	1515.0	1454.C	1457.0	1483.C	1510.0	1440.C	1428.0	1401.0	1890
1469.0	1442.0	1497.0	1465.C	1475.0	1475.C	1485.0	1439.C	1506.0	1572.0	1900
1581.0	1585.0	1517.0	1492.0	1642.0	1923.C	2412.0	3122.0	3346.0	2938.0	1910
2161.0	1674.0	1495.0	1473.0	1466.0	1445.C	1393.0	1442.0	1400.0	1366.0	1920
1449.0	1437.0	1483.0	1441.C	1525.0	1775.C	1954.0	1965.C	1732.C	1540.0	1930
1382.0	1334.C	1325.0	1328.C	1168.0	1371.C	1342.0	1321.C	1281.0	1292.0	1940
1339.0	1330.0	1324.0	1270.C	1331.0	1296.C	1284.0	1210.0	1338.0	1291.0	1950
1328.0	1368.0	1444.0	1472.C	1458.0	1433.C	1364.0	1302.C	1322.0	1334.0	1960
1270.0	1340.0	1296.0	1367.0	1311.C	1298.C	1366.0	1319.C	1335.0	1343.0	1970
1330.0	1352.0	1294.0	1303.0	1245.0	1321.0	1360.0	1347.0	1358.0	1289.0	1980
1349.0	1351.0	1406.0	1371.0	1356.0	1447.0	1360.0	1300.0	1329.0	1327.0	1990
1392.0	1311.0	1359.0	1382.C	1254.0	1334.0	1352.0	1445.C	1313.0	1338.0	2000
1259.0	1357.0	1361.0	1405.0	1373.0	1413.C	1374.0	1357.C	1330.0	1414.0	2010
1397.0	1401.0	1333.0	1347.9	1250.0	1366.C	1344.0	1303.0	1417.0	1422.0	2020
1309.0	1353.0	1437.0	1412.C	1400.0	1578.C	1450.0	1382.0	1306.0	1313.0	2030
1374.0	1298.0	1292.0	1399.0	1363.0	1347.C	1345.0	1375.0	1318.0	1386.0	2040
1318.0	1359.0	1330.0	1345.0	1264.C	1363.C	1313.0	1263.C	1217.0	1176.0	2050
1273.0	1242.0	1185.0	1174.0	1159.0	1163.C	1114.0	1060.0	1140.0	1096.0	2060
1152.0	1064.0	1098.0	1035.0	1076.0	1000.C	1080.0	1113.0	1091.0	1165.0	2070
1199.0	1152.0	1665.0	2299.C	2634.0	2571.0	1920.0	1642.0	1045.0	1039.0	2080
970.0	965.0	995.0	955.0	930.0	1010.C	1064.0	1062.C	1021.0	1045.0	2090
1005.0	981.0	1071.0	1023.0	1011.0	983.C	939.0	1004.C	1002.0	982.C	2100
989.0	994.0	1003.0	984.0	1062.9	976.C	970.0	983.0	1035.0	990.0	2110
923.0	960.C	918.0	994.0	973.0	926.0	977.0	998.0	1020.0	977.0	2120
1013.0	955.0	939.0	992.0	965.0	957.C	952.0	1010.C	995.0	988.0	2130
983.0	979.0	972.C	892.0	972.0	954.C	1043.0	973.0	1004.0	933.0	2140
982.0	965.0	931.0	935.0	974.0	952.C	952.0	969.0	971.0	966.0	2150
958.0	940.0	951.0	917.C	911.0	979.C	933.0	970.0	920.0	908.0	2160
967.0	987.0	914.0	953.0	978.0	969.C	1011.0	1654.0	1154.0	1331.0	2170
1307.0	1318.0	1161.0	1034.C	858.0	1089.C	986.0	1695.0	1962.0	979.0	2180
938.0	1021.0	984.0	910.0	938.0	948.C	944.0	952.0	988.0	925.0	2190
948.0	913.0	916.0	834.0	916.0	900.0	864.0	890.0	941.0	966.0	2200
927.0	897.0	943.0	881.0	925.0	919.C	905.0	926.C	907.0	952.0	2210
908.0	890.0	936.0	927.0	942.0	950.C	871.0	903.0	934.0	938.0	2220
1349.0	1199.0	1283.0	1295.0	1199.0	1011.C	939.0	905.0	872.0	908.0	2230
870.0	877.0	837.0	869.0	951.0	861.0	819.0	813.C	823.0	819.0	2240
715.0	752.0	791.0	792.C	864.0	784.C	799.0	730.C	790.0	791.0	2250
862.0	808.C	785.0	797.C	751.0	717.C	754.0	752.C	727.0	744.0	2260
760.0	815.0	769.0	713.0	745.0	749.C	743.0	718.0	834.0	917.0	2270
972.0	978.0	946.0	835.0	795.0	739.C	804.0	730.0	794.0	722.0	2280
785.0	746.0	752.0	716.C	864.0	803.C	790.0	782.C	783.0	749.0	2290
753.3	710.0	771.0	751.C	735.0	816.C	775.0	716.C	763.0	742.0	2300
738.C	710.0	712.0	693.C	695.0	734.C	704.C	744.0	681.0	748.0	2310
713.0	695.0	672.0	667.C	674.0	699.C	699.0	722.0	715.0	774.0	2320
732.0	712.0	674.0	772.C	682.0	724.C	698.0	695.C	710.0	726.0	2330
683.0	721.0	710.0	810.0	750.0	738.C	709.0	754.C	731.0	726.0	2340
793.0	966.0	1666.0	2261.C	3095.0	3480.C	2779.0	2051.0	1316.0	1001.0	2350
832.0	738.0	696.0	672.0	643.0	611.C	665.0	664.0	733.0	629.0	2360
649.0	669.0	653.0	679.C	675.C	616.C	667.0	661.C	634.0	631.0	2370
663.0	596.0	610.0	643.C	582.C	617.C	639.0	625.0	645.0	640.0	2380
634.0	672.0	632.0	568.0	616.0	589.0	557.0	621.0	591.0	625.0	2390
601.0	618.0	604.0	619.C	635.0	620.0	585.0	662.0	650.0	609.0	2400
575.0	609.0	596.0	589.0	610.0	530.0	614.0	672.0	649.0	622.0	2410
611.0	637.0	621.0	681.C	582.0	621.C	568.0	616.0	605.0	593.0	2420
602.0	614.0	653.0	620.C	595.0	655.0	664.0	584.C	649.0	591.0	2430
602.0	598.0	503.0	590.0	581.0	578.0	587.0	564.0	598.0	632.0	2440
589.0	585.0	592.0	623.0	638.0	613.0	609.0	635.0	591.0	590.0	2450
606.0	552.0	634.0	638.0	612.0	618.5	609.0	652.0	594.0	606.0	2460
647.0	595.0	641.0	644.0	644.0	669.C	679.0	664.0	659.0	753.0	2470
769.0	1242.0	3980.0	3531.C	5247.0	6066.C	5341.0	3427.0	1810.0	980.0	2480
631.0	562.0	596.0	560.0	623.0	544.0	578.0	548.0	562.0	560.0	2490
595.0	556.0	624.0	578.C	558.0	593.C	571.0	583.0	576.0	570.0	2500
630.0	566.0	568.0	567.C	567.0	585.C	570.0	623.0	[illegible]	[illegible]	2510
537.0	584.0	549.0	612.C	586.0	568.C	569.0	605.0	600.0	532.0	2520
538.0	638.0	614.0	555.0	586.0	573.C	600.0	538.0	547.0	592.0	2530
581.0	595.2	628.0	574.C	559.0	594.C	617.0	566.0	580.0	582.0	2540
566.0	625.0	642.0	562.C	567.0	594.0	618.0	538.0	570.0	583.0	2550
689.0	588.0	572.0	571.0	587.0	622.0	634.0	655.0	629.0	592.0	2560
641.0	633.0	581.0	592.0	583.0	621.C	681.0	606.0	611.0	630.0	2570
630.0	662.0	589.0	620.C	620.C	616.C	622.0	597.0	638.0	702.0	2580
699.0	760.0	636.0	643.0	588.0	625.0	619.0	621.0	681.0	729.0	2590
745.0	653.0	682.0	647.C	687.0	645.0	694.0	714.0	654.0	634.0	2600
630.0	665.0	611.0	661.0	613.0	697.C	635.0	630.0	634.0	661.0	2610
590.0	608.C	579.0	630.0	648.C	657.C	614.0	647.0	644.0	641.0	2620
696.0	661.0	646.0	635.0	655.C	675.C	628.0	625.0	648.0	641.0	2630
679.0	656.0	630.0	667.C	697.0	699.C	714.0	649.0	698.0	690.0	2640
693.0	673.0	657.C	672.0	623.0	695.C	686.0	670.C	712.0	731.0	2650
614.0	736.C	736.0	751.0	658.0	761.C	692.0	711.C	741.0	847.0	2660
1082.0	1523.0	2156.0	2690.0	2294.0	2196.0	1503.0	1029.0	765.0	734.0	2670
770.0	665.0	734.0	760.C	744.0	739.C	718.0	726.0	741.0	718.0	2680
726.0	690.0	706.0	715.0	723.C	674.C	675.0	734.0	731.0	723.0	2690
721.0	[illegible]	674.0	684.C	727.C	722.C	671.0	725.0	719.0	727.0	2700
713.0	[illegible]	745.0	737.C	738.0	763.C	728.0	765.0	728.0	744.0	2710
718.0	773.0	663.0	724.C	782.0	681.C	790.0	908.0	1002.0	978.0	2720
1019.0	663.C	693.0	745.C	772.0	729.C	769.0	793.C	814.0	830.0	2730
851.0	791.C	774.0	750.C	757.C	756.C	735.0	735.C	710.0	726.0	2740
744.0	784.C	828.0	648.C	784.0	762.C	668.0	652.0	644.0	620.0	2750
595.0	567.0	551.0	568.C	511.0	532.C	585.C	668.0	497.0	476.0	2760

499.0	492.0	478.0	479.0	425.0	433.0	451.0	448.0	459.0	456.0	2770
435.0	419.0	454.0	424.0	411.0	461.0	468.0	459.0	442.0	429.0	2780
449.0	408.0	435.0	374.0	350.0	386.0	421.0	401.0	444.0	439.0	2790
427.0	442.0	483.0	543.0	465.0	357.0	322.0	322.0	422.0	472.0	2800
411.0	392.0	367.0	403.0	385.0	468.0	420.0	384.0	440.0	377.0	2810
429.0	499.0	557.0	711.0	767.0	776.0	718.0	537.0	470.0	381.0	2620
393.0	344.0	373.0	369.0	413.0	386.0	387.0	342.0	381.0	381.0	2830
362.0	351.0	393.0	337.0	361.0	361.0	377.0	372.0	343.0	365.0	2840
403.0	360.0	348.0	386.0	348.0	358.0	368.0	360.0	367.0	362.0	2850
380.0	351.0	388.0	378.0	360.0	353.0	351.0	350.0	372.0	368.0	2860
348.0	346.0	362.0	355.0	378.0	379.0	361.0	352.0	356.0	346.0	2870
368.0	359.0	378.0	346.0	345.0	360.0	354.0	303.0	358.0	361.0	2887
391.0	365.0	405.0	399.0	358.0	468.0	377.0	345.0	340.0	337.0	2890
299.0	336.0	329.0	349.0	342.0	346.0	334.0	325.0	310.0	348.0	2900
349.0	343.0	328.0	345.0	333.0	349.0	365.0	330.0	332.0	347.0	2910
311.0	357.0	353.0	331.0	326.0	370.0	330.0	315.0	321.0	303.0	2920
316.0	325.0	308.0	326.0	335.0	342.0	325.0	316.0	303.0	343.0	2930
321.0	340.0	296.0	327.0	295.0	288.0	291.0	295.0	328.0	287.0	2940
282.0	318.0	293.0	326.0	310.0	264.0	309.0	310.0	287.0	285.0	2950
296.0	297.0	324.0	271.0	272.0	260.0	312.0	324.0	284.0	283.0	2960
260.0	281.0	275.0	269.0	265.0	290.0	296.0	243.0	262.0	289.0	2970
305.0	265.0	273.0	289.0	261.0	264.0	244.0	216.0	265.0	254.0	2980
291.0	307.0	284.0	272.0	278.0	254.0	261.0	252.0	263.0	235.0	2990
242.0	272.0	293.0	265.0	264.0	328.0	264.0	383.0	383.0	348.0	3000
324.0	327.0	290.0	275.0	230.0	259.0	276.0	286.0	295.0	264.0	3010
276.0	261.0	266.0	250.0	288.0	255.0	274.0	290.0	289.0	300.0	3020
278.0	252.0	269.0	280.0	255.0	287.0	241.0	290.0	263.0	230.0	3030
241.0	276.0	258.0	250.0	264.0	274.0	260.0	263.0	270.0	243.0	3040
261.0	272.0	287.0	262.0	269.0	270.0	268.0	233.0	309.0	315.0	3050
275.0	268.0	250.0	281.0	264.0	271.0	307.0	264.0	283.0	258.0	3060
277.0	260.0	241.0	277.0	244.0	281.0	251.0	257.0	254.0	266.0	3070
287.0	268.0	302.0	253.0	283.0	268.0	281.0	286.0	282.0	261.0	3080
243.0	287.0	285.0	248.0	285.0	268.0	302.0	269.0	233.0	220.0	3090
276.0	238.0	310.0	265.0	235.0	285.0	241.0	232.0	225.0	208.0	3100
225.0	208.0	238.0	226.0	238.0	9.0	227.0	227.0	225.0	226.0	3110
241.0	247.0	215.0	251.0	219.0	231.0	193.0	242.0	218.0	258.0	3120
222.0	226.0	218.0	231.0	265.0	219.0	214.0	229.0	229.0	239.0	3130
225.0	242.0	239.0	204.0	193.0	233.0	242.0	231.0	242.0	242.0	3140
238.0	245.0	213.0	227.0	228.0	219.0	244.0	327.0	380.0	338.0	3150
745.0	993.0	1001.0	878.0	614.0	417.0	315.0	251.0	224.0	246.0	3160
257.0	288.0	229.0	243.0	230.0	270.0	230.0	237.0	246.0	249.0	3170
238.0	199.0	241.0	260.0	271.0	251.0	277.0	253.0	237.0	281.0	3180
271.0	255.0	264.0	268.0	344.0	383.0	575.0	927.0	1008.0	2874.0	3190
4030.0	4704.0	4104.0	2746.0	1923.0	713.0	332.0	235.0	189.0	195.0	3200
197.0	204.0	222.0	208.0	180.0	192.0	221.0	192.0	187.0	159.0	3210
205.0	210.0	158.0	214.0	182.0	197.0	186.0	168.0	206.0	179.0	3220
186.0	167.0	167.0	164.0	174.0	171.0	175.0	149.0	160.0	145.0	3230
130.0	144.0	124.0	153.0	162.0	170.0	160.0	167.0	148.0	155.0	3240
155.0	153.0	153.0	163.0	141.0	155.0	135.0	138.0	159.0	153.0	3250
141.0	156.0	146.0	150.0	145.0	170.0	117.0	126.0	144.0	144.0	3260
150.0	120.0	138.0	133.0	155.0	128.0	154.0	128.0	123.0	139.0	3270
124.0	140.0	145.0	135.0	147.0	132.0	141.0	143.0	135.0	140.0	3280
145.0	152.0	142.0	139.0	123.0	130.0	148.0	139.0	157.0	148.0	3290
152.0	153.0	129.0	134.0	145.0	144.0	162.0	140.0	139.0	133.0	3300
116.0	127.0	137.0	115.0	138.0	125.0	129.0	131.0	126.0	139.0	3310
133.0	133.0	144.0	148.0	131.0	127.0	115.0	121.0	130.0	123.0	3320
127.0	122.0	140.0	122.0	151.0	136.0	134.0	143.0	135.0	122.0	3330
128.0	132.0	140.0	141.0	135.0	140.0	148.0	121.0	132.0	141.0	3340
116.0	120.0	131.0	118.0	123.0	140.0	158.0	123.0	118.0	130.0	3350
119.0	121.0	124.0	125.0	130.0	122.0	131.0	108.0	115.0	113.0	3360
107.0	111.0	126.0	140.0	132.0	150.0	128.0	128.0	144.0	131.0	3370
117.0	147.0	140.0	145.0	130.0	121.0	169.0	269.0	296.0	405.0	3380
542.0	498.0	391.0	278.0	204.0	181.0	126.0	118.0	113.0	123.0	3390
131.0	131.0	132.0	119.0	114.0	127.0	116.0	116.0	136.0	136.0	3400
128.0	119.0	130.0	123.0	118.0	120.0	143.0	119.0	123.0	105.0	3410
101.0	124.0	122.0	117.0	121.0	127.0	110.0	112.0	110.0	125.0	3420
102.0	123.0	114.0	130.0	115.0	109.0	110.0	129.0	115.0	121.0	3430
126.0	114.0	101.0	111.0	107.0	105.0	118.0	101.0	117.0	112.0	3440
116.0	121.0	121.0	138.0	130.0	127.0	95.0	126.0	126.0	126.0	3450
116.0	115.0	124.0	118.0	98.0	120.0	118.0	102.0	101.0	121.0	3460
123.0	115.0	123.0	121.0	111.0	111.0	125.0	116.0	102.0	131.0	3470
107.0	130.0	107.0	116.0	114.0	127.0	123.0	119.0	128.0	130.0	3480
95.0	127.0	109.0	113.0	107.0	124.0	118.0	133.0	120.0	111.0	3490
118.0	115.0	125.0	104.0	108.0	124.0	121.0	115.0	114.0	101.0	3500
107.0	123.0	132.0	116.0	139.0	110.0	113.0	121.0	109.0	123.0	3510
113.0	112.0	116.0	147.0	125.0	119.0	121.0	111.0	103.0	119.0	3520
128.0	126.0	119.0	122.0	136.0	128.0	126.0	121.0	115.0	142.0	3530
138.0	133.0	137.0	124.0	126.0	134.0	202.0	243.0	305.0	369.0	3540
330.0	285.0	221.0	515.0	348.0	196.0	134.0	129.0	118.0	114.0	3550
104.0	114.0	130.0	119.0	120.0	110.0	126.0	123.0	122.0	100.0	3560
85.0	108.0	106.0	107.0	100.0	117.0	112.0	125.0	123.0	110.0	3570
118.0	113.0	128.0	119.0	101.0	113.0	115.0	106.0	99.0	105.0	3580
117.0	113.0	125.0	107.0	119.0	107.0	107.0	110.0	106.0	99.0	3590
102.0	108.0	101.0	92.0	128.0	99.0	78.0	102.0	106.0	113.0	3600
103.0	98.0	125.0	99.0	114.0	141.0	106.0	110.0	106.0	100.0	3610
97.0	93.0	86.0	82.0	100.0	90.0	105.0	119.0	97.0	123.0	3620
124.0	104.0	103.0	106.0	95.0	88.0	84.0	101.0	84.0	93.0	3630
81.0	84.0	84.0	97.0	89.0	101.0	95.0	96.0	76.0	83.0	3640
86.0	93.0	98.0	90.0	85.0	79.0	94.0	109.0	84.0	101.0	3650
84.0	71.0	84.0	84.0	88.0	77.0	81.0	96.0	85.0	93.0	3660
84.0	101.0	97.0	97.0	111.0	121.0	195.0	243.0	426.0	558.0	3670
655.0	635.0	494.0	341.0	182.0	109.0	72.0	97.0	78.0	89.0	3680
89.0	75.0	88.0	89.0	75.0	79.0	72.0	81.0	89.0	86.0	3690
91.0	78.0	71.0	67.0	92.0	84.0	78.0	84.0	91.0	74.0	3700
94.0	72.0	82.0	80.0	80.0	86.0	85.0	79.0	80.0	95.0	3710

72.0	83.0	77.0	73.0	83.0	79.0	74.0	80.0	81.0	91.0	3720
90.0	63.0	66.0	84.0	71.0	61.0	81.0	81.0	65.0	77.0	3730
79.0	70.0	82.0	64.0	66.0	77.0	78.0	60.0	86.0	73.0	3740
75.0	78.0	90.0	65.0	61.0	69.0	68.0	68.0	67.0	64.0	3750
87.0	73.0	72.0	75.0	67.0	76.0	72.0	68.0	79.0	71.0	3760
68.0	57.0	70.0	61.0	70.0	73.0	65.0	80.0	74.0	92.0	3770
68.0	91.0	65.0	74.0	72.0	80.0	57.0	72.0	76.0	71.0	3780
71.0	71.0	76.0	67.0	55.0	76.0	68.0	72.0	76.0	73.0	3790
76.0	85.0	73.0	68.0	72.0	72.0	69.0	69.0	71.0	82.0	3800
55.0	80.0	78.0	67.0	75.0	76.0	70.0	70.0	69.0	74.0	3810
77.0	60.0	59.0	70.0	72.0	66.0	73.0	84.0	54.0	68.0	3820
67.0	61.0	74.0	63.0	65.0	61.0	71.0	64.0	65.0	80.0	3830
65.0	69.0	82.0	59.0	53.0	53.0	76.0	72.0	82.0	98.0	3840
98.0	91.0	94.0	68.0	68.0	82.0	57.0	52.0	55.0	59.0	3850
61.0	61.0	72.0	61.0	53.0	71.0	71.0	65.0	64.0	47.0	3860
55.0	68.0	58.0	55.0	65.0	72.0	72.0	67.0	61.0	70.0	3870
66.0	54.0	67.0	67.0	66.0	53.0	63.0	49.0	47.0	62.0	3880
61.0	61.0	63.0	46.0	65.0	58.0	71.0	73.0	60.0	73.0	3890
70.0	66.0	44.0	48.0	65.0	52.0	73.0	64.0	51.0	69.0	3900
59.0	61.0	56.0	47.0	68.0	57.0	74.0	72.0	51.0	58.0	3910
61.0	67.0	78.0	65.0	59.0	57.0	59.0	69.0	60.0	53.0	3920
56.0	69.0	68.0	67.0	74.0	81.0	81.0	88.0	46.0	69.0	3930
54.0	61.0	53.0	60.0	58.0	62.0	60.0	61.0	58.0	67.0	3940
55.0	76.0	42.0	59.0	64.0	70.0	55.0	65.0	57.0	54.0	3950
49.0	54.0	64.0	55.0	52.0	49.0	60.0	76.0	68.0	59.0	3960
50.0	74.0	61.0	62.0	73.0	54.0	55.0	61.0	78.0	91.0	3970
77.0	88.0	101.0	105.0	84.0	97.0	82.0	72.0	60.0	71.0	3980
63.0	65.0	53.0	67.0	70.0	63.0	58.0	70.0	62.0	49.0	3990
65.0	50.0	61.0	71.0	58.0	64.0	43.0	72.0	50.0	84.0	4000
73.0	94.0	102.0	87.0	87.0	81.0	61.0	73.0	61.0	60.0	4010
62.0	51.0	63.0	62.0	58.0	65.0	68.0	62.0	72.0	87.0	4020
57.0	54.0	69.0	79.0	52.0	103.0	112.0	143.0	163.0	164.0	4030
131.0	98.0	82.0	80.0	68.0	60.0	65.0	51.0	64.0	61.0	4040
62.0	69.0	59.0	56.0	49.0	61.0	53.0	58.0	64.0	62.0	4050
64.0	58.0	52.0	67.0	60.0	58.0	57.0	75.0	67.0	72.0	4060
59.0	56.0	93.0	119.0	154.0	229.0	287.0	299.0	324.0	246.0	4070
145.0	95.0	70.0	65.0	64.0	52.0	68.0	63.0	51.0	59.0	4080
58.0	52.0	65.0	56.0	77.0	53.0	72.0	54.0	76.0	42.0	4090
70.0	56.0	61.0	50.0	37.0	0.	0.0				

PROGRAM ENTERING BKGRD ROUTINE AFTER 2.211 SECS. CPU01/C05YS = 55644001 CLOCK READS 01.086 G02/08 1972

PROGRAM ENTERING SEARCH ROUTINE AFTER 2.921 SECS. CPU01/C05YS = 99000001 CLOCK READS 01.086 G02/08 1972
WARNING** ANALYSIS OF PEAK GROUPING STARTING AT 165 MAY BE INCORRECT.
NUMBER OF PEAKS FOUND EXCEEDS CAPACITY.

PROGRAM ENTERING MAIN ROUTINE AFTER 28.085 SECS. CPU01/C05YS = 94005001 CLOCK READS 01.074 G02/08 1972

1 SAMPLE FISS. #ACT. PRODS.. CELTAT= 6.15C DAYS. 2C0 MIN COUNT BEGAN 306.464 (1970) ON GE(LI) CTR-F2

LIVE-TIME DURATION OF COUNT = 200 MINUTES

SUMMARY OF ENERGY CALIBRATION

(INPUT)	CHANNEL	STD ENERGY	CALCC ENERGY	DELTA E	(BASED ON INTERNAL PEAKS)
280.00	281.432	140.420	140.358	-0.062	
465.00	456.813	228.200	228.229	0.029	
1545.00	1544.920	772.700	772.719	0.019	
1692.00	1693.128	846.780	846.839	0.059	
2475.00	2476.040	1238.290	1238.263	-0.027	
3192.00	3192.069	1596.200	1596.181	-0.019	

GAIN = APPROX. 0.500 KEV/CHANNEL AVG. DEVN.= 0.036

SUMMARY OF PEAKS WITH SIGNIFICANT NET TOTALS IN SPECTRUM NO. 482201

INDEX	CHANNEL	KEV	(+/-)	- PEAK - START	END	CALC. COUNTS	PROP. COUNTS	PHOTONS/MIN	PCT ERROR	QFIT	FWHM USED	PCT DIFF	INDEX
1	80.425	39.564	0.034	76.0	84.C	23447.	25515.	0.	8.54	1.3	1.275	11.8	1
2	86.112	42.417	0.146	84.0	88.4	4094.	4191.	0.	31.41	1.0	1.250	9.3	2
3	91.316	45.023	0.066	88.4	95.C	10144.	10352.	0.	12.79	1.0	-		3
4	99.957	49.363	0.015	96.0	103.C	39657.	39002.	0.	3.89	1.C	1.225	-2.2	4
5	115.261	57.040	0.019	112.0	118.C	31727.	30931.	2.503E+06	4.59	1.C	1.158	0.1	5
6	125.621	62.237	0.117	122.0	129.7	12659.	13403.	1.414E+06	16.50	4.2	1.298	11.8	6
7	130.131	64.499	0.082	129.7	131.9	10725.	11386.	5.596E+05	13.25	1.3	-		7
8	133.991	66.434	0.057	131.9	138.C	14173.	14985.	8.693E+05	9.77	1.1	-		8
9	146.181	72.549	0.028	142.0	148.1	71911.	72567.	2.864E+06	4.26	7.8	1.215	1.8	9
10	150.442	74.680	0.023	148.1		133382.	134265.	4.864E+06	3.00	9.6	-		10
11	153.123	76.030	0.168		153.5	18651.	18753.	6.320E+05	19.03	8.5	-		11
12	156.161	77.553	0.094	153.5	157.8	30183.	30294.	9.931E+05	11.63	10.C	-		12
13	159.524	79.240	0.079	157.8		34319.	34414.	1.092E+06	9.74	8.0	-		13
14	162.486	80.725	0.009		166.C	1091464.	1093490.	3.394E+07	0.51	6.8	-		14
15	170.026	84.507	0.021	166.0		54520.	55052.	1.627E+06	4.29	1.0	1.321	11.8	15
16	172.148	85.571	0.198		172.5	8882.	8567.	2.625E+05	24.34	1.C	-		16
17	175.376	87.189	0.035	172.5	177.3	31548.	31764.	9.197E+05	5.46	1.1	-		17

18	178.945	89.979	0.011	177.3	179.3	19904.	20010.	5.737E+05	11.53	2.4	-		18
19	182.740	90.685	0.005	179.3	186.0	246578.	243499.	6.872E+05	1.03	1.9	-		19
20	186.403	92.719	0.045	186.0	187.0	40722.	40826.	1.157E+06	7.29	1.5	-		20
21	189.796	94.421	0.009	187.0		467149.	467750.	1.323E+07	0.52	1.1	-		21
22	193.361	96.377	0.027		193.7	23309.	23314.	6.541E+05	14.94	5.0	-		22
23	197.358	98.212	0.007	193.7	202.2	705266.	704369.	1.996E+07	1.37	28.4	-		23
24	202.632	100.856	0.442	202.2	204.6	3723.	3711.	1.058E+05	91.19	5.8	-		24
25	207.155	103.124	0.677	204.6	210.0	14540.	14472.	4.101E+05	14.46	2.3	-		25
26	212.666	105.888	0.093	210.0	216.0	7795.	7742.	2.294E+05	18.78	1.0	-		26
27	221.323	110.227	0.023	217.0	221.7	87612.	88095.	2.481E+06	3.44	1.4	1.346	11.8	27
28	223.293	111.215	0.014	221.7	226.7	176786.	177620.	5.297E+06	2.26	2.4	-		28
29	229.843	114.398	0.012	226.7	231.7	65809.	65887.	2.004E+06	2.12	1.0	-		29
30	233.055	116.109	0.024	231.7	237.0	27682.	27874.	1.086E+06	4.40	1.0	-		30
31	244.031	121.611	0.008	237.0	254.0	187778.	134228.	7.649E+06	2.42	1.9	1.298	7.1	31
32	262.855	131.046	0.084	258.0	264.5	14725.	16392.	6.512E+05	12.89	2.9	1.366	1.8	32
33	266.926	133.082	0.086	264.9	271.0	14765.	16409.	6.607E+05	12.92	1.0	-		33
34	281.432	140.358	0.002	275.0	285.0	1535768.	1524179.	5.468E+07	0.82	9.5	1.244	1.2	34
35	291.286	145.297	0.005	287.0	295.0	247689.	244279.	1.121E+07	1.08	5.2	1.242	0.7	35
36	299.958	149.643	0.087	298.0	303.0	5029.	4865.	2.278E+05	26.19	1.0	1.131	-8.7	36
37	325.336	162.561	0.058	322.0	331.0	60420.	59874.	3.113E+06	2.13	1.0	1.239	-0.8	37
38	362.505	180.985	0.006	359.0	367.0	62990.	62166.	3.283E+06	2.02	1.0	1.278	1.1	38
39	456.813	228.729	0.002	448.0	461.0	476219.	473662.	4.272E+07	0.51	2.7	1.305	0.3	39
40	463.649	231.653	0.145	462.0	468.0	1972.	1364.	1.519E+05	42.18	1.0	1.193	-8.7	40
41	489.864	244.683	0.026	487.0	494.0	12402.	12634.	1.262E+06	6.34	1.0	1.202	-8.7	41
42	525.680	262.720	0.063	522.0	530.0	6467.	6547.	7.676E+05	12.50	1.0	1.465	10.1	42
43	532.893	266.332	0.133	530.0	538.0	2342.	2315.	7.601E+05	26.31	1.0	1.244	-6.7	43
44	550.305	275.051	0.228	547.0	553.0	1554.	2013.	2.283E+05	47.60	1.6	1.499	11.8	44
45	568.898	284.361	0.026	564.0	574.0	17597.	18354.	2.453E+06	5.55	1.2	1.507	11.8	45
46	586.540	293.194	0.006	579.0	592.0	70409.	70120.	1.037E+07	1.55	1.0	1.371	1.3	46
47	609.936	304.874	0.029	604.0	617.0	15588.	16837.	2.531E+06	7.63	1.3	1.524	11.8	47
48	620.216	310.055	0.309	617.0	624.0	1127.	1111.	1.804E+05	59.29	1.0	1.448	5.8	48
49	638.652	319.285	0.042	634.0	644.0	8348.	8862.	1.451E+06	9.80	1.0	1.451	5.5	49
50	657.495	328.719	0.006	649.0	664.0	61626.	62367.	1.1[illegible]E+07	1.59	1.0	1.334	0.3	50
51	679.784	339.676	0.229	676.0	682.0	1066.	988.	1.974E+05	55.94	1.0	1.270	-8.7	51
52	688.503	344.241	0.013	683.0	693.0	13864.	23675.	4.688E+06	3.10	1.0	1.371	-1.6	52
53	701.194	350.394	0.072	698.0	704.0	3534.	3465.	7.144E+05	14.89	1.0	1.277	-8.7	53
54	728.811	364.418	0.003	721.0		116179.	116496.	2.555E+07	1.04	1.0	1.424	1.1	54
55	733.075	366.552	0.081		740.0	3785.	3791.	8.415E+05	10.14	1.0	-		55
56	775.631	387.853	0.242	770.0	779.0	981.	950.	2.385E+05	64.24	1.0	1.302	-8.7	56
57	821.875	410.997	0.154	818.0	[illegible]	1815.	1922.	5.141E+05	29.49	1.0	1.480	2.5	57
58	833.572	416.851	0.227	829.0	836.0	979.	897.	2.650E+05	51.72	1.0	1.322	-8.7	58
59	847.305	423.724	0.047	843.0	851.0	5712.	5706.	1.661E+05	9.35	1.0	1.450	-0.2	59
60	864.791	432.474	0.047	861.0	869.0	5946.	5864.	1.784E+06	8.80	1.0	1.529	4.7	60
61	875.043	437.605	0.015	871.0	877.1	5180.	5231.	9.859E+05	13.66	1.0	1.314	-6.1	61
62	879.790	439.980	0.208	877.7	884.0	1147.	1163.	3.549E+05	37.54	1.0	-		62
63	887.762	443.970	0.171	885.0	890.1	1262.	1206.	3.909E+05	29.28	1.0	1.340	-8.7	63
64	892.080	446.121	0.298	890.1	894.0	590.	563.	1.842E+05	61.36	1.0	-		64
65	947.180	473.702	0.267	945.0	952.0	1698.	1605.	4.449E+05	43.64	1.0	1.360	-8.7	65
66	973.741	486.993	0.005	967.0	978.0	65278.	65880.	2.462E+07	0.80	1.0	1.505	0.5	66
67	980.291	490.270	0.137	978.0	983.0	1641.	1659.	6.277E+05	27.08	1.0	-		67
68	993.822	497.045	0.011	989.0	998.0	23671.	23279.	9.064E+06	2.53	1.0	1.504	-0.1	68
69	1011.430	505.851	0.038	1007.0	1013.6	6150.	11349.	8.494E+06	30.68	1.0	1.380	-8.7	69
70	1015.307	507.791	0.116	1013.8	1015.7	2136.	3935.	1.221E+06	37.07	1.0	-		70
71	1021.614	510.947	0.006	1019.7	1033.0	145972.	139942.	9.811E+07	2.18	1.0	-		71
72	1046.943	522.619	0.013	1040.0	1053.0	19329.	19532.	8.213E+06	3.30	1.0	1.510	-0.9	72
73	1059.512	529.908	0.102	1053.0		11603.	12953.	5.616E+06	21.80	1.0	1.708	11.8	73
74	1061.527	530.916	0.284		1065.0	5133.	5112.	2.225E+06	55.27	1.0	-		74
75	1074.223	537.260	0.013	1069.0	1081.0	27560.	27495.	1.219E+07	2.41	1.9	1.510	-1.5	75
76	1093.408	546.867	0.292	1088.0	1098.0	650.	866.	3.809E+05	60.05	1.0	1.547	0.5	76
77	1126.095	563.219	0.059	1121.0	1130.0	4676.	4554.	2.168E+06	10.30	1.0	1.702	9.7	77
78	1138.268	569.309	0.010	1130.0	1142.5	7321.	7446.	3.611E+06	6.66	1.0	1.469	-5.5	78
79	1148.016	574.165	0.048	1142.5	1151.0	4360.	4425.	2.179E+06	11.01	1.0	-		79
80	1205.014	602.700	0.017	1196.0	1206.5	17328.	17424.	9.344E+06	2.53	1.0	1.591	0.9	80
81	1209.004	604.696	0.006	1206.5	1214.0	42122.	42320.	2.203E+07	1.14	1.0	-		81
82	1219.870	610.132	0.147	1214.0	1220.0	1298.	1463.	7.577E+05	38.10	1.0	1.445	-8.7	82
83	1241.518	620.961	0.118	1238.0	1247.0	1660.	1735.	9.64[illegible]E+05	23.40	1.0	1.524	-3.5	83
84	1260.043	630.228	0.018	1255.0	1266.0	12419.	12520.	7.2[illegible]E+06	3.71	1.0	1.591	-0.3	84
85	1273.463	636.941	0.058	1266.0	1277.0	3914.	4131.	2.369E+06	11.54	1.0	1.714	7.2	85
86	1291.970	646.199	0.146	1287.0	1296.0	1648.	1784.	1.036E+06	25.19	1.0	1.796	11.8	86
87	1300.430	650.431	0.097	1296.0	1307.0	2375.	2564.	1.510E+06	17.45	1.0	1.800	11.8	87
88	1316.082	658.261	0.058	1312.0	1318.5	3279.	3298.	2.642E+06	9.58	1.0	1.632	1.0	88
89	1322.893	661.667	0.009	1318.5	1326.6	26593.	26684.	1.667E+07	1.33	1.0	-		89
90	1328.713	664.578	0.074	1326.6	1329.1	2816.	2620.	1.651E+06	11.97	1.0	-		90
91	1335.013	667.727	0.004	1329.1		77410.	77428.	4.918E+07	0.56	1.0	-		91
92	1339.333	669.891	0.074		1361.2	4058.	4056.	2.590E+06	8.28	1.0	-		92
93	1342.882	671.666	0.076	1341.2	1347.0	3187.	3183.	2.042E+06	10.46	1.0	-		93
94	1370.493	685.480	0.251	1367.0	1375.0	756.	744.	5.151E+05	31.52	1.0	1.826	11.8	94
95	1406.300	703.387	0.269	1400.0	1408.0	328.	239.	1.452E+05	74.73	1.0	1.501	-8.7	95
96	1444.046	722.267	0.085	1440.0	1445.1	2907.	2975.	2.115E+06	11.45	1.0	1.781	1.5	96
97	1447.797	724.145	0.028	1445.1	1451.1	9492.	9703.	6.932E+06	3.76	1.0	-		97
98	1453.904	727.198	0.056	1451.1	1461.0	4087.	4169.	3.001E+06	8.14	1.5	-		98
99	1478.593	739.546	0.017	1470.0	1482.5	10413.	10553.	7.824E+06	3.04	1.0	1.685	1.2	99
100	1486.51[illegible]	743.505	0.066	1482.9	1491.0	2436.	2465.	1.845E+06	12.03	1.0	-		100
101	1498.401	749.453	0.154	1494.0	1500.1	1179.	1187.	9.014E+05	28.42	1.0	1.735	3.7	101
102	1502.863	751.684	0.060	1500.1	1506.7	3089.	3104.	2.370E+06	10.95	1.0	-		102
103	1513.058	756.784	0.018	1506.7	1526.0	10160.	10169.	7.869E+06	3.40	1.0	-		103
104	1531.151	765.833	0.070	1527.0	1537.0	1765.	1896.	1.481E+06	14.86	1.0	1.537	-8.7	104
105	1544.920	772.719	0.005	1537.0	1552.0	41029.	40781.	3.147E+07	0.96	1.0	1.702	0.9	105
106	1556.381	778.451	0.064	1552.0	1565.0	5937.	6603.	5.066E+06	4.08	4.3	1.891	11.8	106
107	1591.297	795.913	0.008	1582.0	1596.0	23743.	23695.	1.945E+07	1.59	1.0	1.699	-0.1	107
108	1603.533	802.933	0.065	1599.0	1608.0	2356.	2388.	2.008E+06	10.56	1.0	1.750	2.5	108
109	1619.241	809.889	0.106	1614.0	1621.3	1725.	1730.	1.463E+06	12.79	1.0	1.890	10.5	109
110	1624.462	812.500	0.050	1621.3	1627.0	3890.	3891.	3.357E+06	5.83	1.0	-		110
111	1631.022	815.781	0.017	1627.0	1637.0	15412.	15403.	1.337E+07	1.89	1.6	-		111
112	1669.263	834.905	0.011	1664.0	1675.0	10275.	10185.	9.196E+06	2.93	1.0	1.740	0.8	112

113	1693.126	846.659	0.006	1684.0	1698.0	64925.	64819.	5.959E+07	0.64	2.3	1.737	0.3	113
114	1735.140	867.849	0.043	1731.0	1739.0	3659.	3640.	3.471E+06	6.36	1.2	1.731	-0.4	114
115	1751.631	876.098	0.460	1747.0	1756.0	467.	519.	4.475E+05	54.32	1.0	1.958	11.0	115
116	1761.336	880.950	0.323	1759.0	1763.0	326.	213.	2.621E+05	60.95	1.0	1.602	-8.7	116
117	1766.530	883.546	0.319	1764.0	1771.0	329.	272.	2.942E+05	67.28	1.0	1.604	-8.7	117
118	1795.701	898.135	0.019	1788.0	1800.0	8168.	8416.	8.411E+06	3.52	1.0	1.701	-3.6	118
119	1820.154	910.361	0.226	1816.0	1825.0	564.	502.	9.556E+05	43.38	1.0	1.618	-8.7	119
120	1838.599	919.584	0.037	1835.0	1843.0	1323.	1289.	1.331E+06	17.84	1.0	1.623	-8.7	120
121	1850.083	925.327	0.046	1843.0	1856.0	3492.	3480.	3.658E+06	8.66	1.0	1.849	3.5	121
122	1908.865	954.729	0.022	1904.0	1917.0	7416.	7413.	8.141E+06	4.21	1.0	1.773	-1.4	122
123	1927.563	964.069	0.059	1920.0	1932.0	2275.	2248.	2.547E+06	12.12	1.0	1.674	-7.2	123
124	1954.263	977.419	0.191	1948.0	1958.0	808.	836.	9.343E+05	29.10	1.0	1.994	10.1	124
125	2025.154	1012.864	0.126	2022.0	2029.0	964.	913.	1.124E+06	20.52	1.0	1.673	-8.7	125
126	2075.269	1037.919	0.022	2065.0	2081.0	7101.	7332.	8.955E+06	4.57	1.0	1.905	3.2	126
127	2170.558	1085.758	0.079	2163.0	2175.0	1737.	1774.	2.376E+06	13.33	1.0	1.953	4.2	127
128	2178.297	1089.428	0.275	2175.0	2181.0	360.	282.	4.269E+05	49.61	1.0	1.713	-8.7	128
129	2223.575	1112.063	0.079	2218.0	2229.0	1796.	1782.	2.453E+06	11.89	1.0	1.934	2.4	129
130	2271.642	1136.092	0.112	2264.0	2276.0	1146.	1141.	1.618E+06	17.99	1.0	2.039	7.2	130
131	2346.004	1173.264	0.016	2337.0	2356.0	12735.	12906.	1.900E+07	2.49	1.7	2.110	9.8	131
132	2397.105	1199.207	0.341	2397.0	2401.0	209.	119.	2.483E+05	68.68	1.0	1.769	-8.7	132
133	2476.040	1238.263	0.005	2465.0	2482.0	24710.	24714.	3.958E+07	1.17	1.0	2.016	3.0	133
134	2581.254	1290.852	0.248	2578.0	2585.0	376.	317.	5.887E+05	40.83	1.0	1.814	-8.7	134
135	2590.743	1295.595	0.226	2588.0	2593.0	354.	261.	5.601E+05	41.24	1.0	1.816	-8.7	135
136	2651.595	1326.010	0.258	2648.0	2659.0	425.	473.	7.935E+05	41.65	1.0	1.937	-3.4	136
137	2664.587	1332.504	0.017	2658.0	2672.0	9725.	9734.	1.731E+07	2.51	1.0	2.058	2.5	137
138	2720.177	1360.288	0.102	2716.0	2726.0	1293.	1289.	2.360E+06	14.22	1.0	2.065	2.1	138
139	2730.320	1365.358	0.283	2726.0	2734.0	400.	402.	7.386E+05	39.17	1.0	1.903	-6.1	139
140	2744.105	1372.248	0.158	2739.0	2752.0	905.	971.	1.741E+06	22.25	1.0	2.269	11.8	140
141	2796.925	1398.648	0.065	2788.0	2802.0	1727.	1767.	3.393E+06	10.10	1.0	2.164	6.0	141
142	2815.538	1407.552	0.056	2810.0	2820.0	1949.	1939.	3.744E+06	7.15	1.0	2.116	3.3	142
143	2884.460	1442.411	0.287	2878.0	2890.0	367.	396.	7.548E+05	37.62	1.0	2.309	11.8	143
144	2958.470	1479.395	0.422	2956.0	2960.0	174.	88.	2.718E+05	63.50	1.0	1.903	-8.7	144
145	2998.979	1499.345	0.335	2991.0	3005.0	678.	904.	1.668E+06	24.73	1.0	2.361	11.8	145
146	3050.476	1525.386	0.367	3048.0	3053.0	176.	103.	3.011E+05	59.64	1.0	1.925	-8.7	146
147	3152.796	1576.544	0.028	3145.0	3159.0	3861.	3838.	8.728E+06	3.78	1.0	2.183	2.4	147
148	3192.069	1596.181	0.008	3182.0	3199.0	21995.	21941.	5.071E+07	0.96	1.0	2.199	2.7	148
149	3381.528	1690.941	0.040	3375.0	3387.0	1889.	1890.	4.741E+06	5.12	1.0	2.094	-4.3	149
150	3542.055	1771.278	0.027	3535.0	3549.0	3485.	3445.	9.301E+06	3.29	1.0	2.282	2.5	150
151	3620.744	1810.684	0.497	3616.0	3626.0	114.	119.	3.228E+05	57.63	1.0	2.310	2.8	151
152	3671.423	1836.068	0.027	3661.0	3677.0	5098.	5112.	8.788E+06	3.31	1.0	2.277	0.9	152
153	3841.314	1921.234	0.241	3836.0	3846.0	184.	183.	5.550E+05	29.89	1.0	2.100	-8.6	153
154	3927.511	1964.489	0.304	3921.0	3931.0	134.	140.	4.209E+05	39.52	1.0	2.115	-8.7	154
155	3973.820	1987.742	0.233	3968.0	3979.0	220.	245.	7.531E+05	25.84	1.0	2.603	11.8	155
156	4003.560	2002.481	0.236	3999.0	4012.0	217.	229.	7.156E+05	28.87	1.0	2.436	4.3	156
157	4029.298	2015.614	0.104	4022.0	4036.0	593.	619.	1.960E+06	11.90	1.0	2.551	9.0	157
158	4068.259	2035.198	0.046	4062.0	4076.0	1427.	1426.	4.702E+05	5.34	1.0	2.283	-2.8	158

```
PROGRAM ENTERING IDENTIFY   ROUTINE AFTER   4.377 SECS.  (CPU+I/C+SYS =  78+21+00)  CLOCK READS 01.077 G02/08 1972

PROGRAM ENTERING  EVAL      ROUTINE AFTER   3.021 SECS.  (CPU+I/C+SYS =  99+00+00)  CLOCK READS 01.077 G02/08 1972

PROGRAM ENTERING  MLR       ROUTINE AFTER   0.623 SECS.  (CPU+I/C+SYS =  99+00+00)  CLOCK READS 01.077 G02/08 1972

PROGRAM ENTERING  OUT       ROUTINE AFTER   0.447 SECS.  (CPU+I/C+SYS =  99+00+00)  CLOCK READS 01.077 G02/08 1972

         MATRIX FOR SET  1 HAD 37 COLUMNS AND125 ROWS.  CFIT =  23.3
THE PEAK AT  510.95 KEV IS BEING LABELED AS UNIDENTIFIED BECAUSE OF LARGE RESIDUAL
THE PEAK AT   94.42 KEV IS BEING LABELED AS UNIDENTIFIED BECAUSE OF LARGE RESIDUAL

PROGRAM ENTERING  MLR       ROUTINE AFTER   0.266 SECS.  (CPU+I/C+SYS =  99+00+00)  CLOCK READS 01.077 G02/08 1972

PROGRAM ENTERING  OUT       ROUTINE AFTER   0.410 SECS.  (CPU+I/C+SYS =  99+00+00)  CLOCK READS 01.077 G02/08 1972

         MATRIX FOR SET  1 HAD 37 COLUMNS AND123 ROWS.  CFIT =   2.3
     SE 344 WAS DELETED. IT HAD A CI OF  0.881 POSITION NO. 3
     ZR  89 WAS DELETED. IT HAD A CI OF  0.880 POSITION NO. 3
     XE 133 WAS DELETED. IT HAD A CI OF  0.469 POSITION NO. 3
     SB 122 WAS DELETED. IT HAD A CI OF  0.353 POSITION NO. 3
     HF 181 WAS DELETED. IT HAD A CI OF  0.445 POSITION NO. 3
     RE 183 WAS DELETED. IT HAD A CI OF  0.456 POSITION NO. 3
     TL 202 WAS DELETED. IT HAD A CI OF  0.453 POSITION NO. 3

PROGRAM ENTERING  MLR       ROUTINE AFTER   0.221 SECS.  (CPU+I/C+SYS =  99+00+00)  CLOCK READS 01.077 G02/08 1972

PROGRAM ENTERING  OUT       ROUTINE AFTER   0.195 SECS.  (CPU+I/C+SYS =  98+00+01)  CLOCK READS 01.077 G02/08 1972

         MATRIX FOR SET  1 HAD 24 COLUMNS AND116 ROWS.  CFIT =   2.5
THE PEAK AT  116.11 KEV IS BEING LABELED AS UNIDENTIFIED BECAUSE OF LARGE RESIDUAL

PROGRAM ENTERING  MLR       ROUTINE AFTER   0.148 SECS.  (CPU+I/C+SYS =  98+00+01)  CLOCK READS 01.077 G02/08 1972

PROGRAM ENTERING  OUT       ROUTINE AFTER   0.194 SECS.  (CPU+I/C+SYS =  98+00+01)  CLOCK READS 01.080 G02/08 1972

         MATRIX FOR SET  1 HAD 24 COLUMNS AND115 ROWS.  CFIT =   2.0

PROGRAM ENTERING  NEWSET    ROUTINE AFTER   0.016 SECS.  (CPU+I/C+SYS =  87+00+12)  CLOCK READS 01.080 G02/08 1972

         MATRIX FOR SET  2 HAD  1 COLUMNS AND  1 ROWS.  CFIT =   1.0

PROGRAM ENTERING  NEWSET    ROUTINE AFTER   0.035 SECS.  (CPU+I/C+SYS =  94+00+05)  CLOCK READS 01.080 G02/08 1972

         MATRIX FOR SET  3 HAD  1 COLUMNS AND  1 ROWS.  CFIT =   1.0
```

PROGRAM ENTERING NEWSET ROUTINE AFTER 0.035 SECS. (CPU11/C0SYS = 94400405) CLOCK READS 01.080 002/08 1972

MATRIX FOR SET 4 HAD 1 COLUMNS AND 1 ROWS. GFIT = 1.0

PROGRAM ENTERING NEWSET ROUTINE AFTER 0.100 SECS. (CPU11/C0SYS = 32465402) CLOCK READS 01.080 002/08 1972

GE GAMMA ANALYSIS OF FISS. +ACT. PRODS. DATE OF CALCULATION 01.080 002/08

EXPERIMENT NO.
SAMPLE NUMBER ZERO TIME 300.3P3

SAMPLE WEIGHT =1.000E+01 MIDTIME OF COUNT 300.533 SPECTRUM NO. 462201
NORMALIZATION WT = 1.000E+00
NORMALIZATION FACTOR = 1.000E-01 DECAY TIME IS 6.190 DAYS DETECTOR F SYSTEM 2

GEOMETRY IS 31.95 CM LIVE-TIME DURATION OF COUNT = 200 MINUTES 12/BY46/125HY3T

** MLR LEAST-SQUARES RESULTS **

NUCLIDE	CPM AT COUNT TIME	DPM AT ZERO TIME	ATOMS AT ZERO TIME	PCT ERROR	SET NO.	GFIT	IDENTIFICATION CONFIDENCE VALUE
CR 51	9.802E+05	1.143E+06	6.581E+10	21.3	1	2.0	0.30
MN 54	9.196E+05	9.322E+05	6.046E+11	3.0	2	1.0	0.62
CO 56	5.909E+06	6.244E+06	1.002E+12	1.1	1	2.0	1.00
CO 60	1.720E+06	1.724E+06	6.882E+12	2.1	1	2.0	0.86
Y 88	8.898E+05	9.361E+05	2.050E+11	1.5	1	2.0	0.93
ZR 95	1.449E+06	1.547E+06	2.089E+11	1.1	1	2.0	0.99
ZR 97	1.917E+05	8.407E+07	1.224E+11	10.1	1	2.0	0.16
MO 99	6.548E+06	3.083E+07	1.762E+11	1.6	1	2.0	1.00
RU 103	1.010E+06	1.125E+06	9.251E+10	3.4	1	2.0	0.88
SB 124	9.688E+05	1.040E+06	1.302E+11	3.3	1	2.0	1.00
TE 132	4.934E+06	1.039E+07	1.238E+11	0.8	1	2.0	1.00
TE 131	9.197E+04	2.785E+06	7.230E+09	27.3	1	2.0	0.41
I 131	3.226E+06	5.475E+06	9.165E+10	1.3	1	2.0	1.00
I 133	9.119E+05	6.086E+07	1.215E+11	5.5	1	2.0	0.43
CS 134	2.282E+06	2.295E+06	3.551E+12	1.5	1	2.0	1.00
CS 137	1.961E+06	1.962E+06	4.466E+13	1.5	3	1.0	0.54
BA 140	5.096E+06	7.110E+06	1.890E+11	0.9	1	2.0	1.00
CE 141	2.273E+06	2.553E+06	1.744E+11	1.7	4	1.0	0.71
CE 143	2.314E+06	5.054E+07	1.459E+11	2.4	1	2.0	1.00
CE 144	5.106E+05	5.164E+05	3.064E+11	21.6	1	2.0	0.37
ND 147	2.505E+06	3.686E+06	8.452E+10	4.2	1	2.0	0.98
EU 152	1.714E+06	1.716E+06	1.824E+13	3.5	1	2.0	1.00
PT 495	1.504E+06	4.254E+06	3.622E+10	24.9	1	2.0	0.24
U 0	1.797E+06	1.823E+06	1.136E+12	2.4	1	2.0	1.00
NP 239	1.076E+05	6.586E+05	3.219E+09	19.3	1	2.0	0.95

1 ** MLR RESULTS ** / EVALUATION OF INDIVIDUAL CONTRIBUTIONS FOR PEAKS 90.0 KEV

NUCLIDE	ATOMS	ERROR	GAMMA ENERGY	ATOMS	FRACTION OF PEAK	PEAK ERROR	RESIDUAL (STD DEVS)	INTERFERENCES PRESENT (AND OTHERS CONSIDERED)
CR 51	6.581E+10	21.3	319.3	6.581E+10	0.662	9.9	0.	PLUS0 I131 NC147 (REJECTED0 AM165)
MN 54	6.046E+11	5.0	834.9	6.046E+11	1.000	3.0	0.0	PLUS0
CO 56	1.002E+12	1.1	846.8	1.011E+12	0.992	1.1	0.8	PLUS0
			1037.9	1.003E+12	0.944	4.6	0.0	PLUS0 TE132 CS134
			1173.3	9.954E+11	0.672	2.6	-0.3	PLUS0 CO 60 TE132
			1238.3	9.913E+11	1.009	1.4	-0.8	PLUS0 I133
			1360.3	9.227E+11	1.006	14.2	-0.6	PLUS0 (TRIVIAL0 ZR 97)
			1576.5	9.929E+11	1.010	3.8	-0.2	PLUS0
			1771.3	9.999E+11	1.003	3.4	-0.1	PLUS0 (TRIVIAL0 EU152)
			2015.6	1.074E+12	0.933	11.9	0.6	PLUS0
			2035.2	1.003E+12	0.999	5.4	0.0	PLUS0 (REJECTED0 I124)
CD 57	1.423E+11	15.7	121.6	1.467E+11	0.279	2.9	1.0	PLUS0 NC147 EU152 NP239
			136.5	3.859E+10	3.036	100.0	-2.7	PLUS0
CO 60	6.882E+12	2.1	1173.3	6.833E+12	0.905	2.6	-0.3	PLUS0 CO 56 TE132
			1332.5	6.927E+12	0.993	2.6	0.3	PLUS0
Y 88	2.050E+11	3.5	815.8	1.992E+11	0.092	2.0	-1.4	PLUS0 BA140 (TRIVIAL0 SB127)
			898.1	2.081E+11	0.985	3.6	0.4	PLUS0
			1326.0	3.488E+11	0.395	41.7	1.0	PLUS0 SB124 (REJECTED0 I124)
			1836.1	2.037E+11	1.006	3.4	-0.2	PLUS0
ZR 95	2.089E+11	3.7	724.1	2.136E+11	0.899	3.8	0.6	PLUS0 I131
			756.8	2.078E+11	1.005	3.5	-0.2	PLUS0
			765.8	1.776E+11	1.144	14.9	-1.2	PLUS0 I133 EU152
ZR 97	1.224E+11	10.7	402.7	1.201E+11	0.001	2.6	-0.7	PLUS0 SB124 (REJECTED0 I124)
			658.3	1.206E+11	1.003	9.6	-0.2	PLUS0 EU152
			743.5	1.252E+11	0.977	12.1	0.2	PLUS0 (TRIVIAL0 SB127)
			1148.0	5.587E+11	0.219	100.0	0.8	PLUS0
MO 99	1.762E+11	1.6	140.4	1.772E+11	0.994	1.5	0.4	PLUS0
			181.0	1.746E+11	1.004	2.2	-0.4	PLUS0 TE431 (TRIVIAL0 NP239)
			366.4	1.761E+11	0.029	1.0	-0.1	PLUS0 I131 EU152
			739.5	1.754E+11	1.004	3.1	-0.1	PLUS0
			778.5	1.646E+11	0.995	9.1	-0.8	PLUS0 SB127 TE431 EU152
RU 103	9.251E+10	3.4	444.0	6.161E+10	0.698	29.3	-1.7	PLUS0 EU152
			497.0	9.245E+10	1.001	2.4	-0.0	PLUS0 (TRIVIAL0 NP239)(REJECTED0 AM105)
			610.1	1.235E+11	0.746	38.1	0.7	PLUS0
			557.1	2.374E+11	0.390	100.0	0.6	PLUS0
SB 124	1.302E+11	3.3	602.7	1.278E+11	1.016	2.8	-0.7	PLUS0 ZR 97 (REJECTED0 I124)
			646.2	1.958E+11	0.665	25.2	1.3	PLUS0 (REJECTED0 I124)
			667.7	1.343E+11	0.007	0.6	3.7	PLUS0 TE132 (TRIVIAL0 SB127 TE431)
			722.3	1.210E+11	0.485	11.9	-0.7	PLUS0 CE143 (TRIVIAL0 SB127)(REJECTED0 I124)
			1326.0	2.219E+11	0.193	41.7	1.0	PLUS0 Y 88 (REJECTED0 I124)
			1690.9	1.395E+11	0.934	5.2	1.3	PLUS0 (REJECTED0 I124)
SB 122	1.788E+09	82.4	411.0	2.162E+09	0.050	29.5	0.5	PLUS0 NC147 EU152
			473.7	1.488E+09	0.412	43.6	-0.5	PLUS0 CS134
			604.7	1.823E+09	0.001	1.3	1.4	PLUS0 CS134
			685.5	1.992E+09	0.528	37.9	0.3	PLUS0 NC147
			718.5	1.671E+09	0.022	9.1	-0.8	PLUS0 MO 99 TE431 EU152

TE 132	1.238E+11	0.8						
			111.2	1.391E+11	0.162	3.0	3.7	PLUS* L D
			THE FOLLOWING PEAK WAS NOT USED IN THE ANALYSIS BECAUSE OF LARGE RESIDUAL					
			116.1	1.967E+11	0.545	5.3	7.0	PLUS* NP239
			228.2	1.214E+11	1.017	1.0	-2.0	PLUS* NP239
			262.7	1.388E+11	0.867	12.5	0.9	PLUS* I133
			284.4	1.290E+11	0.211	5.6	0.2	PLUS* I131 NP239
			332.5	1.231E+11	0.123	8.9	-0.1	PLUS* BA140 CE143
			505.9	1.810E+11	0.664	30.7	1.0	PLUS*
			522.6	1.282E+11	0.966	3.4	1.0	PLUS*
								(REJECTED* TL202)
			621.0	1.128E+11	1.097	23.4	-0.4	PLUS*
			636.2	1.301E+11	0.951	3.8	1.3	PLUS*
			650.4	1.671E+11	0.761	17.5	1.5	PLUS*
								(TRIVIAL* SB127)
			667.7	1.277E+11	0.962	0.6	3.7	PLUS* SB124
								(TRIVIAL* SB127 TE431)
			671.7	8.286E+10	1.494	10.5	-4.7	PLUS*
			721.2	1.074E+11	1.152	8.2	-1.9	PLUS*
			772.7	1.203E+11	1.018	1.2	-2.4	PLUS* TE431
								(TRIVIAL* EU152)
			809.9	1.242E+11	0.960	12.8	0.0	PLUS* EU152
			812.5	1.362E+11	0.959	5.9	1.6	PLUS*
			876.1	7.234E+10	1.204	54.3	-1.3	PLUS* I133
			910.4	1.439E+11	0.860	43.4	0.3	PLUS*
								(REJECTED* ZR 89)
			925.3	1.212E+11	0.965	8.7	-0.2	PLUS* BA140
								(TRIVIAL* SB127)
			954.7	1.187E+11	1.043	4.3	-1.0	PLUS*
			1037.9	1.234E+11	0.929	4.6	0.0	PLUS* CE 96 CS134
			1136.1	1.349E+11	0.918	18.0	0.5	PLUS*
			1173.3	1.229E+11	0.930	2.6	-0.3	PLUS* CE 96 CO 60
			1290.9	1.102E+11	1.123	40.8	-0.3	PLUS*
								(TRIVIAL* SB127 EU152)
			1295.6	7.411E+10	1.670	41.2	-1.6	PLUS*
			1372.2	1.859E+11	0.666	22.3	1.5	PLUS*
								(REJECTED* I124)
			1398.5	1.193E+11	1.037	10.1	-0.4	PLUS*
								(TRIVIAL* CS136)
			1442.4	1.368E+11	0.905	37.6	0.3	PLUS*
			1521.2	1.185E+11	1.044	29.9	-0.1	PLUS*
								(REJECTED* I124)
			2002.7	1.395E+11	0.853	28.9	0.4	PLUS* TE431
TE 431	7.230E+09	27.3						
			103.1	1.075E+10	0.166	14.0	2.2	PLUS* NP239
								(REJECTED* SN153)
			149.6	7.396E+09	0.978	20.2	0.1	PLUS*
			161.0	7.166E+09	0.009	2.2	-0.4	PLUS* NL 99
								(TRIVIAL* NP239)
			772.7	7.027E+09	0.011	1.2	-2.4	PLUS* TE132
								(TRIVIAL* EU152)
			778.5	6.757E+09	0.014	9.1	-0.8	PLUS* MC 99 SB127 EU152
			795.9	7.017E+09	0.007	1.7	-1.7	PLUS* CS134
			2002.7	8.149E+09	0.035	28.9	0.4	PLUS* TE132
			1125.5	1.220E+10	0.593	100.0	0.4	PLUS*
			852.3	6.518E+09	1.169	100.0	-0.1	PLUS*
I 131	9.165E+10	1.3						
			284.4	9.253E+10	0.776	5.0	0.2	PLUS* TE132 NP239
			319.3	9.169E+10	0.622	9.9	0.	PLUS* CR 51 MO147
								(REJECTED* RH105)
			328.7	8.991E+10	0.608	2.0	-1.0	PLUS* BA140 EU152
			364.4	9.160E+10	0.966	1.0	-0.1	PLUS* NL 99 EU152
			636.9	9.810E+10	0.934	11.6	0.6	PLUS*
								(TRIVIAL* SB127)
			724.1	9.372E+10	0.079	3.8	0.6	PLUS* ZR 95
I 133	1.215E+11	5.2						
			262.7	1.363E+11	1.025	12.5	0.9	PLUS* TE132
			THE FOLLOWING PEAK WAS NOT USED IN THE ANALYSIS BECAUSE OF LARGE RESIDUAL					
			510.9	3.003E+12	0.002	2.3	46.8	PLUS*
								(REJECTED* SC344 ZR 89)
			529.9	1.216E+11	0.581	21.8	0.0	PLUS* MO147
			765.8	1.033E+11	0.016	10.9	-1.2	PLUS* ZR 95 EU152
			876.1	7.102E+10	0.507	54.3	-1.3	PLUS* TE132
			1238.3	1.202E+11	0.002	1.4	-0.8	PLUS* CO 56
			1296.4	2.759E+11	0.440	100.0	0.6	PLUS*
CS 134	3.551E+12	1.5						
			473.7	2.955E+12	0.290	43.6	-0.5	PLUS* SB127
			563.2	3.825E+12	0.928	10.3	0.7	PLUS*
								(TRIVIAL* EU152)(REJECTED* SB122)
			569.3	3.556E+12	0.998	6.7	0.0	PLUS*
								(TRIVIAL* EU152)
			604.7	3.620E+12	0.940	1.3	1.4	PLUS* SB127
			795.9	3.446E+12	1.023	1.7	-1.7	PLUS* TE431
			802.0	3.287E+12	1.080	10.6	-0.8	PLUS*
			1023.9	3.554E+12	0.027	4.6	0.0	PLUS* CO 56 TE132
			1365.4	3.832E+12	0.927	39.2	0.2	PLUS*
CS 137	4.466E+13	1.5						
			661.7	4.466E+13	1.000	1.5	0.0	PLUS*
								(REJECTED* I124)

BA 140	1.890E+11	0.9						
			110.2	2.043E+11	C.044	4.0	1.9	PLUS* U 0
								(REJECTED* RE183)
			131.0	1.875E+11	0.364	13.0	-0.1	PLUS* PT495
								(REJECTED* AU195)
			133.1	1.862E+11	0.154	13.0	-0.0	PLUS* CE144
								(REJECTED* HF181)
			162.6	1.878E+11	1.007	2.0	-0.3	PLUS*
								(REJECTED* RE183)
			266.3	1.988E+11	C.951	28.3	0.2	PLUS*
			304.9	2.290E+11	C.825	7.7	2.3	PLUS*
								(REJECTED* RH105 AE133)
			328.7	1.854E+11	1.008	2.0	-1.0	PLUS* I131 EU152
			423.7	1.926E+11	C.981	9.4	0.2	PLUS*
								(TRIVIAL* I133)
			432.5	1.880E+11	0.863	8.9	-0.1	PLUS* TE132 CE143
			437.6	1.835E+11	1.030	13.7	-0.2	PLUS*
			487.0	1.912E+11	C.986	1.1	1.0	PLUS* EU152
			537.3	1.884E+11	1.003	2.5	-0.1	PLUS*
			574.2	1.555E+11	1.216	11.0	-2.0	PLUS*
			751.7	1.907E+11	C.991	11.0	0.1	PLUS*
			815.8	1.837E+11	C.937	2.0	-1.4	PLUS* Y 88
								(TRIVIAL* SB127)
			867.8	1.770E+11	0.857	6.4	-1.1	PLUS* EU152
			919.6	1.831E+11	0.981	17.9	-0.2	PLUS* EU152
			925.3	1.850E+11	C.956	8.7	-0.2	PLUS* TE132
								(TRIVIAL* SB127)
			1085.8	1.907E+11	0.236	13.4	0.1	PLUS* EU152
			1499.3	2.462E+11	0.768	24.7	0.9	PLUS*
								(REJECTED* SC344)
			1596.2	1.902E+11	0.994	1.2	0.5	PLUS*
CE 141	1.744E+11	1.7						
			145.3	1.744E+11	1.000	1.7	0.0	PLUS*
CE 143	1.459E+11	2.4						
			231.7	4.559E+10	3.200	42.2	-2.2	PLUS*
			293.2	1.474E+11	0.990	1.7	0.6	PLUS*
								(TRIVIAL* SB127)(REJECTED* RE183)
			350.6	1.348E+11	1.082	14.9	-0.6	PLUS*
			432.5	1.451E+11	0.819	8.9	-0.1	PLUS* TE132 BA140
			490.3	1.726E+11	0.782	27.1	0.6	PLUS* ND147
			664.6	1.832E+11	0.796	11.9	1.7	PLUS*
			722.3	1.356E+11	C.591	11.5	-0.7	PLUS* SE124
								(TRIVIAL* SB127)(REJECTED* I124)
CE 144	3.784E+11	21.6						
			133.1	3.051E+11	0.850	13.0	-0.0	PLUS* BA140
								(REJECTED* HF181)
			696.5	9.115E+11	C.336	100.0	0.7	PLUS*
ND 147	8.452E+10	4.2						
			90.9	8.431E+10	1.002	2.9	-0.1	PLUS*
			121.6	8.716E+10	C.011	2.9	1.0	PLUS* CD 57 EU152 NP239
			319.3	8.452E+10	0.316	9.9	0.	PLUS* CR 51 I131
								(REJECTED* RH105)
			411.0	9.935E+10	0.043	29.5	0.5	PLUS* SB127 EU152
			440.0	1.075E+11	C.786	37.6	0.6	PLUS*
								(TRIVIAL* SB127)(REJECTED* TL202)
			490.3	9.996E+10	0.004	27.1	0.6	PLUS* CE143
			529.9	8.457E+10	0.418	21.8	0.0	PLUS* I133
			685.5	9.414E+10	C.370	37.5	0.3	PLUS* SE127
EU 152	1.824E+13	3.5						
			121.6	1.881E+13	0.676	2.9	1.0	PLUS* CD 57 ND147 NP239
			244.7	1.761E+13	1.035	6.4	-0.6	PLUS*
								(REJECTED* RE183)
			328.7	1.789E+13	0.004	2.0	-1.0	PLUS* I131 BA140
			344.2	1.811E+13	1.007	3.4	-0.2	PLUS*
								(REJECTED* HF181)
			364.4	1.822E+13	0.006	1.0	-0.1	PLUS* ND 99 I131
			411.0	2.144E+13	0.757	29.5	0.5	PLUS* SB127 ND147
			444.0	1.214E+13	1.403	29.1	-1.7	PLUS* RU103
			487.0	1.844E+13	0.003	1.1	1.0	PLUS* BA140
			658.3	1.796E+13	0.012	5.6	-0.2	PLUS* ZR 97
			765.8	1.551E+13	0.016	14.9	-1.2	PLUS* ZR 95 I133
			778.5	1.704E+13	0.440	9.1	-0.8	PLUS* MO 99 SB127 TE431
			809.9	1.830E+13	0.036	12.8	0.0	PLUS* TE132
			867.8	1.708E+13	0.210	6.4	-1.1	PLUS* BA140
			919.6	1.766E+13	0.052	17.9	-0.2	PLUS* BA140
			964.1	1.831E+13	0.996	12.1	0.0	PLUS*
			1085.8	1.840E+13	0.755	13.4	0.1	PLUS* BA140
			1112.1	1.864E+13	0.978	11.9	0.2	PLUS*
			1408.0	1.852E+13	0.984	7.2	0.2	PLUS*
PT 495	3.622E+10	24.9						
			98.2	3.632E+10	C.C90	2.8	0.1	PLUS* U 0 NP239
								(REJECTED* SM153 RE183 AU195)
			131.0	3.592E+10	0.645	13.0	-0.1	PLUS* BA140
								(REJECTED* AU195)

U 0	1.136E+12	2.4					
		THE FOLLOWING PEAK WAS NOT USED IN THE ANALYSIS BECAUSE OF LARGE RESIDUAL					
		94.4	1.321E+12	0.8G8	0.5	5.6	PLUS0
		98.2	1.139E+12	0.9C0	2.6	0.1	PLUS0 PI495 NP239 (REJECTED SM153 RE183 AU195)
		110.2	1.228E+12	C.881	4.0	1.9	PLUS0 BA140 (REJECTED RE183)
		111.2	1.277E+12	C.787	3.0	1.7	PLUS0 TE132
		114.4	1.C3CE+12	1.103	2.8	-3.7	PLUS0
NP 239	3.219E+09	19.3					
		98.2	3.227E+C9	C.CC7	2.8	0.1	PLUS0 PI495 U 0 (REJECTED SM153 RE183 AU195)
		103.1	4.725E+C9	C.5C7	14.6	2.2	PLUS0 TE431 (REJECTED SM153)
		105.9	2.676E+C9	1.2C3	18.9	-1.1	PLUS0 (REJECTED EU155)
		THE FOLLOWING PEAK WAS NOT USED IN THE ANALYSIS BECAUSE OF LARGE RESIDUAL					
		116.1	5.117E+C9	C.CFC	5.3	7.C	PLUS0 TE132
		121.6	3.329E+C9	C.CC3	2.9	1.0	PLUS0 CL 57 NC147 EU152
		228.2	3.15..E+C9	C.CC3	1.0	-2.0	PLUS0 TE132
		264.4	3.25CE+C9	C.CC3	5.6	0.2	PLUS0 TE132 I131
		277.6	2.38CE+C9	1.392	100.0	-0.4	PLUS0

1 THE FOLLOWING PHOTOPEAKS ARE UNIDENTIFIED.

CHANNEL	ENERGY	PHOTONS PER MIN	PCT ERROR	
80.4	39.6	C.	8.5	
86.1	42.4	0.	31.4	
91.3	45.0	0.	12.8	
100.0	49.4	C.	3.9	
115.3	57.0	2.56E+06	4.8	
125.6	62.2	7.41E+C5	16.5	
130.1	64.5	5.5EE+C5	13.2	
134.0	66.4	6.69E+05	9.8	
146.2	72.5	2.66E+C6	4.3	
150.4	74.7	4.6EE+C6	3.C	
153.1	76.0	6.32E+05	19.C	
156.2	77.6	9.9CE+05	11.6	
159.5	79.2	1.09E+C6	9.7	
162.5	80.7	3.35E+07	0.5	
170.0	84.5	1.63E+06	4.3	
172.1	85.6	2.62E+C5	24.3	
175.4	87.2	9.26E+C5	5.5	
178.9	89.0	5.74E+05	11.5	
186.4	92.7	1.1EE+C6	7.3	
189.8	94.4	1.32E+C7	0.5	THIS PEAK REJECTED BECAUSE OF LARGE ERRORS
202.6	100.9	1.0EE+05	91.2	
223.1	110.1	1.09E+C6	5.3	THIS PEAK REJECTED BECAUSE OF LARGE ERRORS
550.3	275.1	2.26E+C5	47.6	
620.2	310.1	1.8CE+05	59.3	
679.8	339.9	1.97E+05	55.9	
775.6	387.9	2.39E+C5	64.2	
833.6	416.9	2.65E+05	51.7	
892.1	446.1	1.84E+C5	61.4	
1015.3	507.8	1.22E+06	37.1	
1021.6	510.9	5.81E+07	2.3	THIS PEAK REJECTED BECAUSE OF LARGE ERRORS
1093.4	546.9	3.81E+C5	60.1	
1406.3	703.4	1.85E+05	74.7	
1498.4	749.5	9.01E+05	28.4	

```
 1761.3    880.9   2.83E+05      40.5
 1766.5    883.5   2.94E+05      67.3
 1954.3    977.4   9.34E+05      24.1
 2025.2   1012.9   1.12E+04      20.5
 2178.3   1089.4   4.27E+05      49.0
 2399.1   1199.8   2.48E+05      68.7
 2458.5   1479.4   2.72E+05      63.5
 3050.5   1525.4   3.01E+05      59.4
 3420.7   1810.7   3.23E+05      57.8
 3927.5   1964.5   4.27E+05      39.5
 3973.8   1987.7   7.53E+05      25.8

PROGRAM ENTERING   MAIN      ROUTINE AFTER   1.992 SECS.  (CPU01/CASYS =  4A032000)  CLOCK READS 01.080 002/08 1972



1          END OF INPUT DATA
PROGRAM ENTERING  QUIT      ROUTINE AFTER   C.C75 SECS.  (CPU01/CASYS =  09087002)  CLOCK READS 01.080 002/08 1972
ELAPSED TIME FOR NO.  1 WAS  46.2977 SECONDS.

          TIME USED FOR  1 PROBLEMS WAS  46.26 SECS
```

Appendix B

Cathode Ray Tube Pictures of the Spectrum Described in Appendix A

Subroutine GRAPH can be called to make use of the facilities available at the Laboratory to produce hard copies of CRT display pictures. The following series of CRT plots (Fig. B-1) show the same spectral data presented in Appendix A and also show the "background" that was determined by GAMANAL and the peaks that were found.

Another option of the program provides CRT plots showing the fit of the individual peaks to the net counts. Figures B-2, B-3, and B-4 are examples showing in greater detail some of the fitting results for the spectrum shown in Fig. B-1.

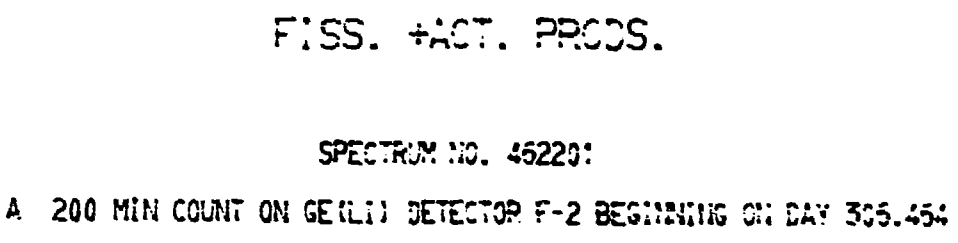

Fig. B-1.

FISS. +ACT. PROBS.

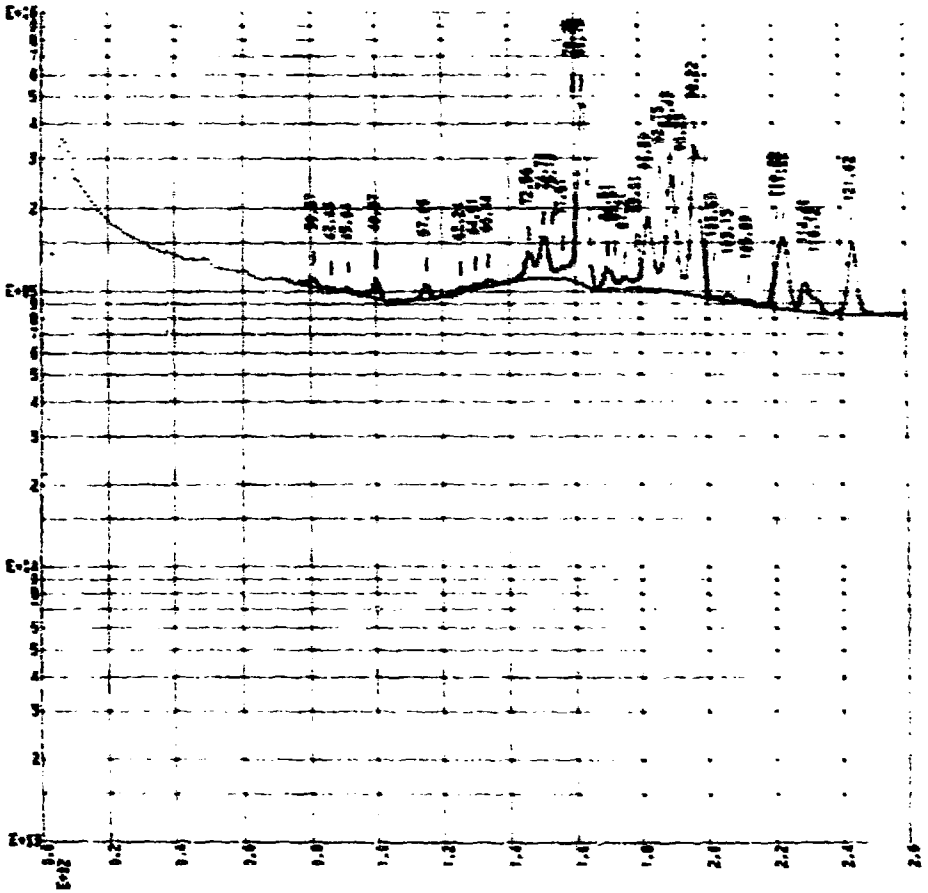

FISS. +ACT. PRODS. DETECTOR F-2 SPECTRUM 45220

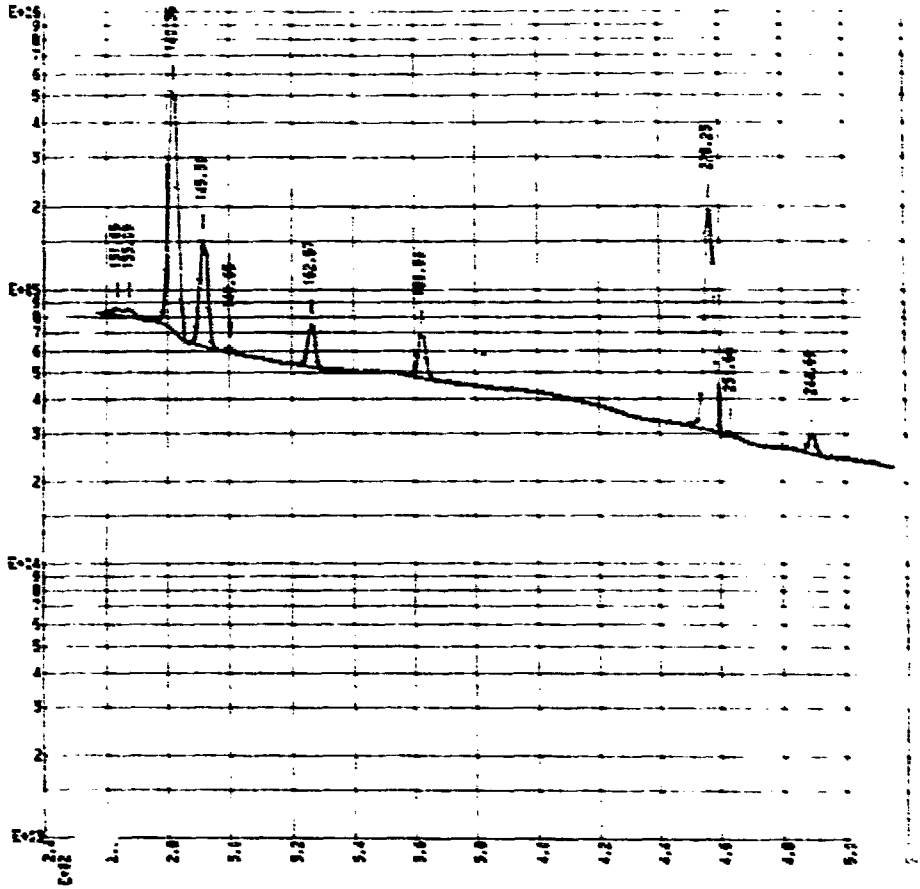

FISS. +ACT. PRODS. DETECTOR F-2 SPECTRUM 462201

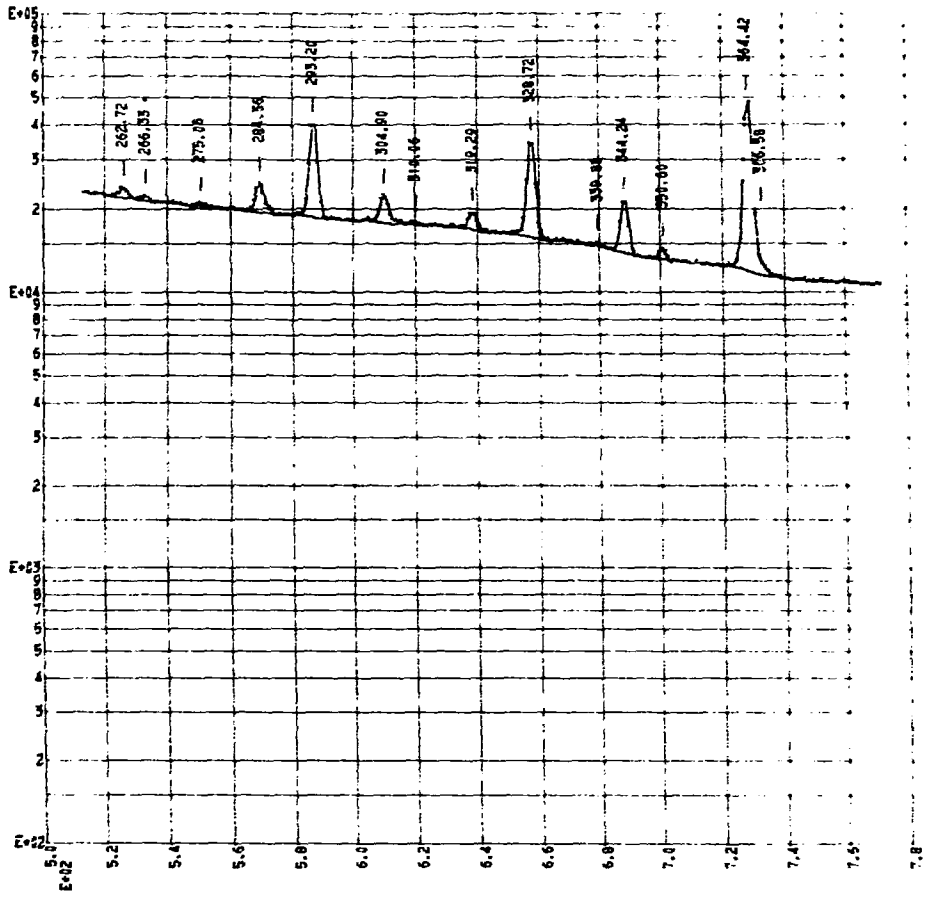

FISS. +ACT. PRODS. DETECTOR F-2 SPECTRUM 45220

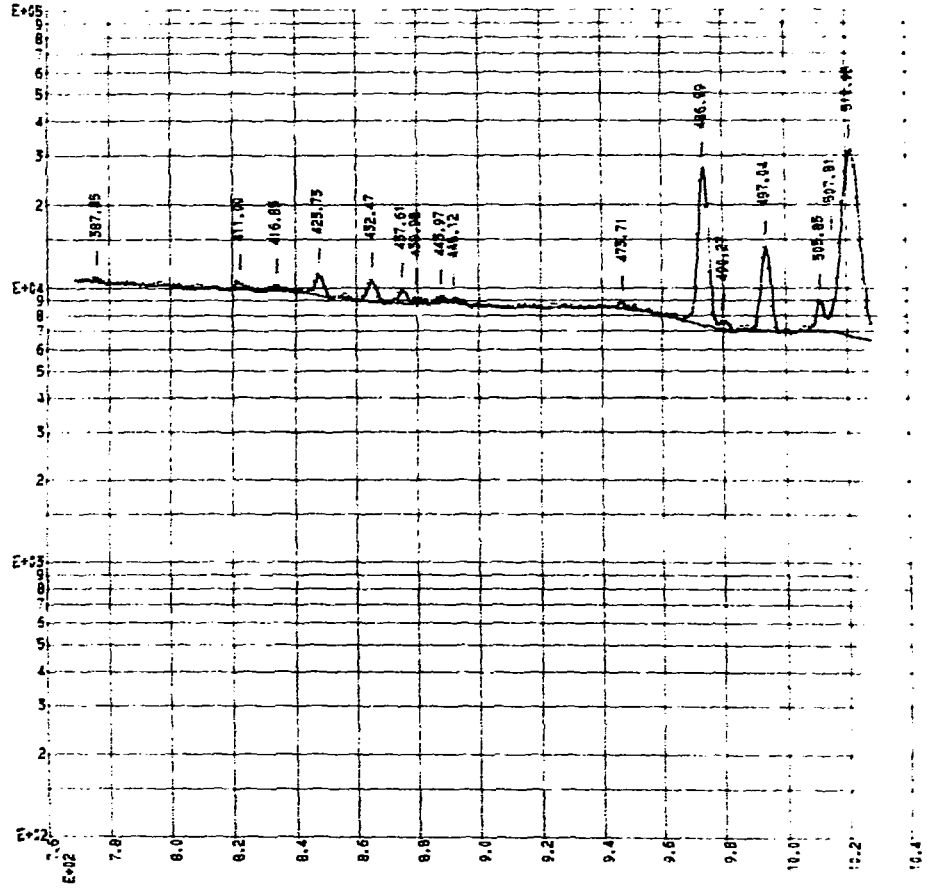

FISS. +ACT. PRODS. DETECTOR F-2 SPECTRUM 46220

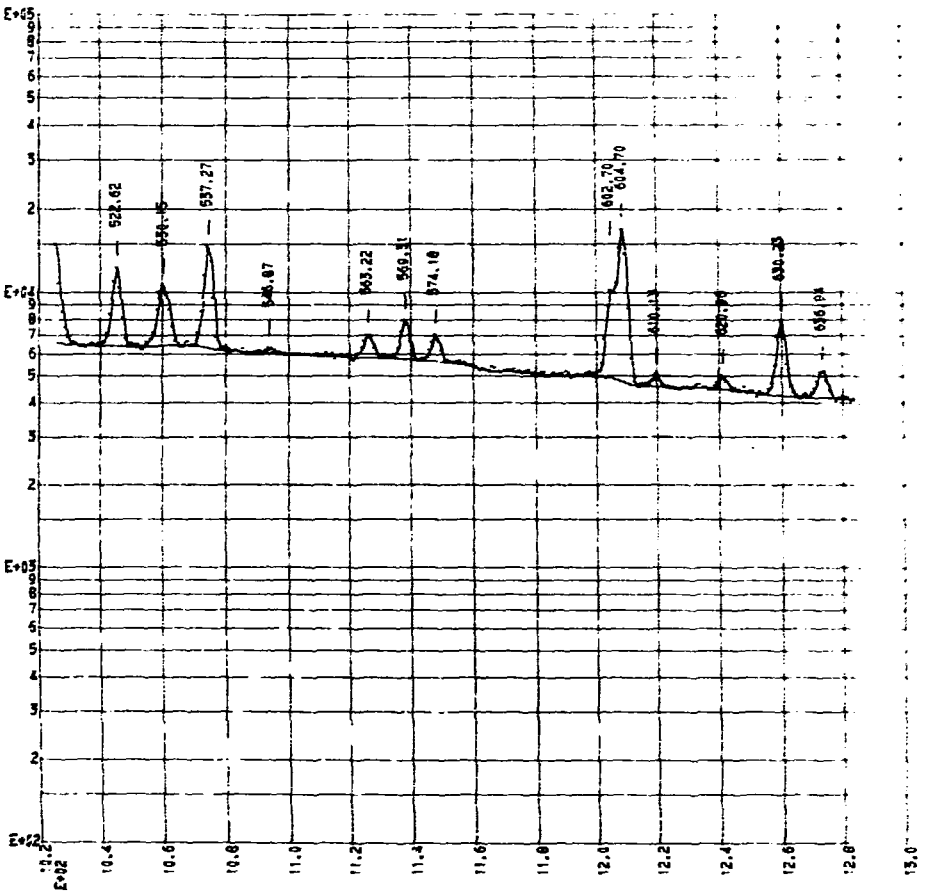

FISS. +ACT. PRODS. DETECTOR F-2 SPECTRUM 46220:

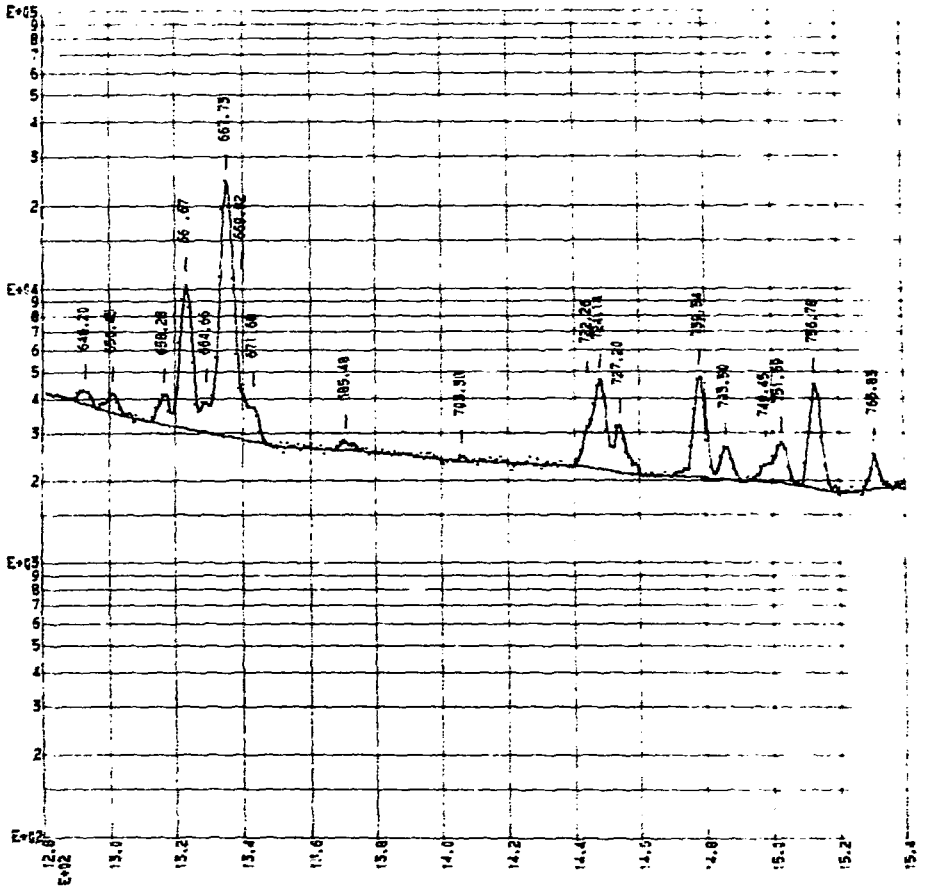

FISS. +ACT. PRODS. DETECTOR F-2 SPECTRUM 46220

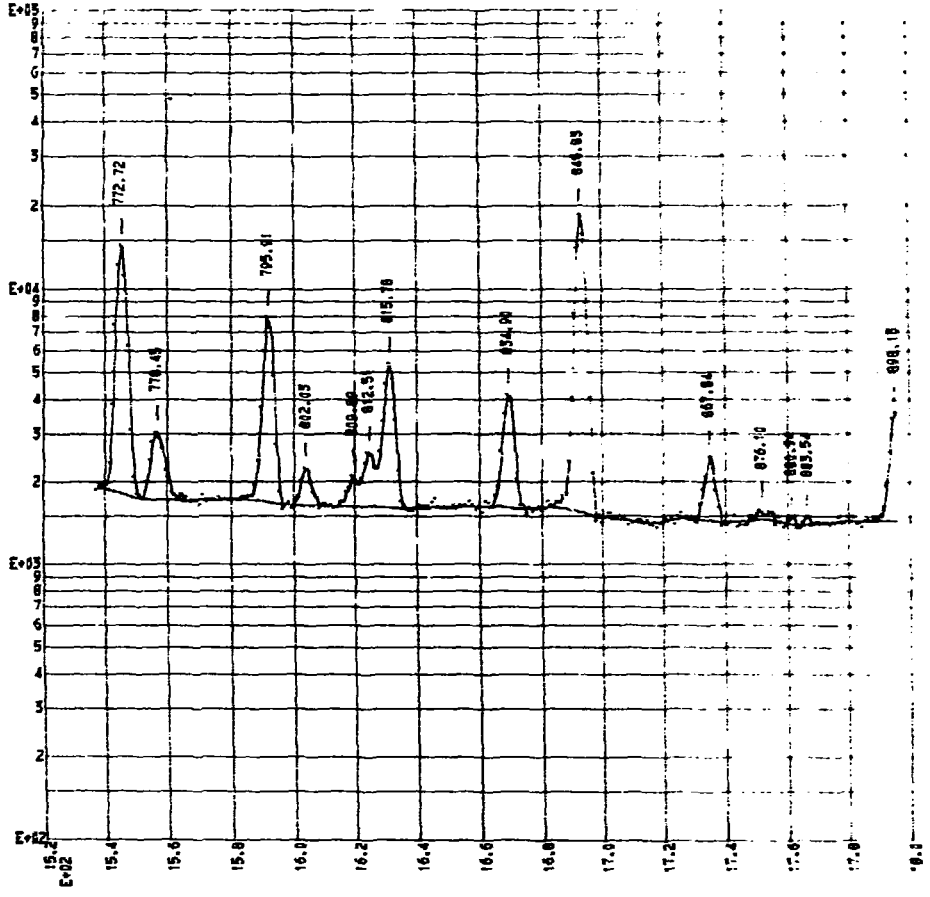

FISS. +ACT. PRODS. DETECTOR F-2 SPECTRUM 46220

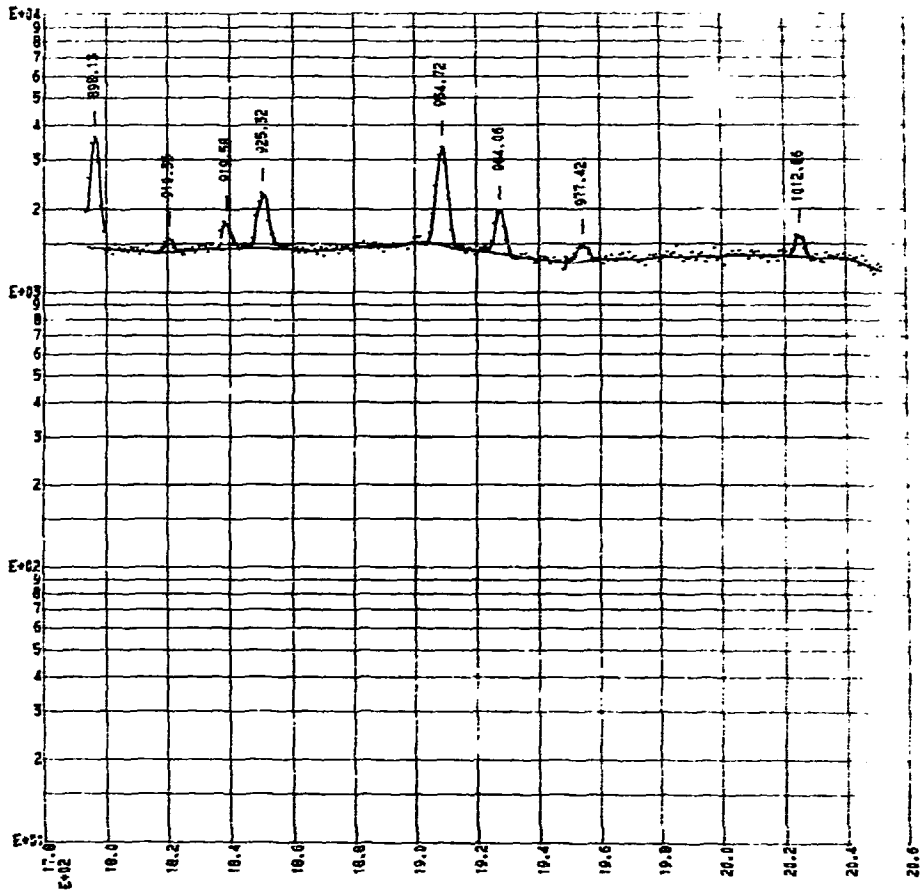

FISS. +ACT. PRODS. DETECTOR F-2 SPECTRUM 46220

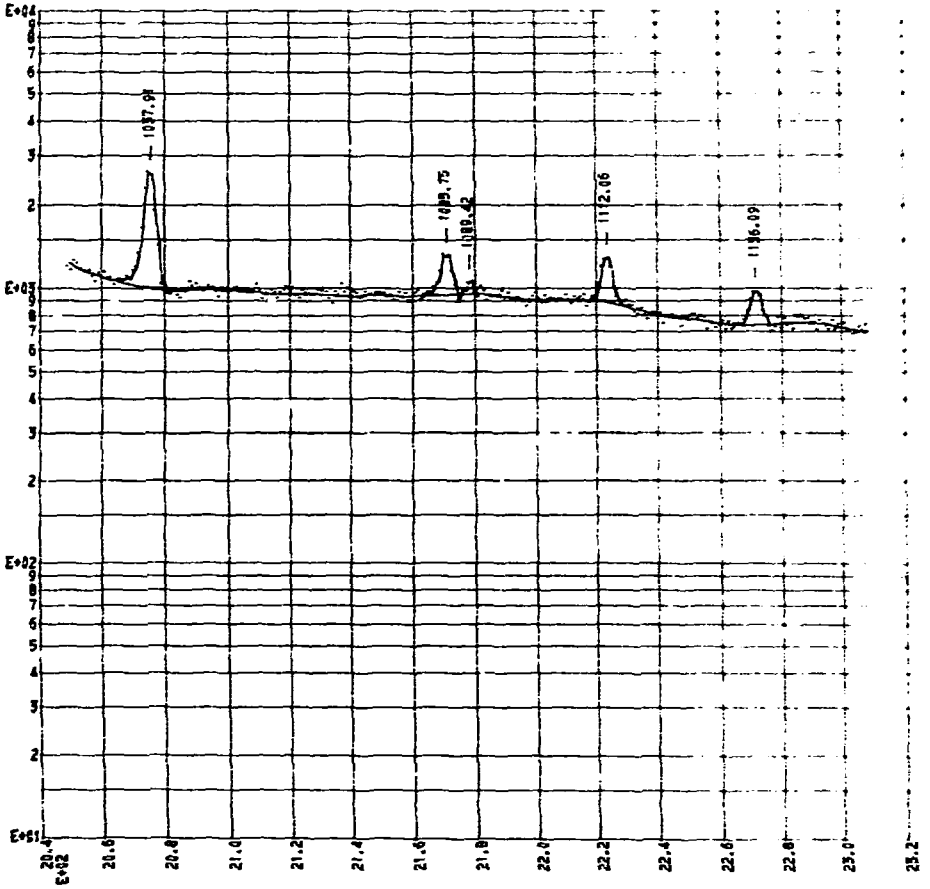

FISS. +ACT. PRODS. DETECTOR F-2 SPECTRUM 46220

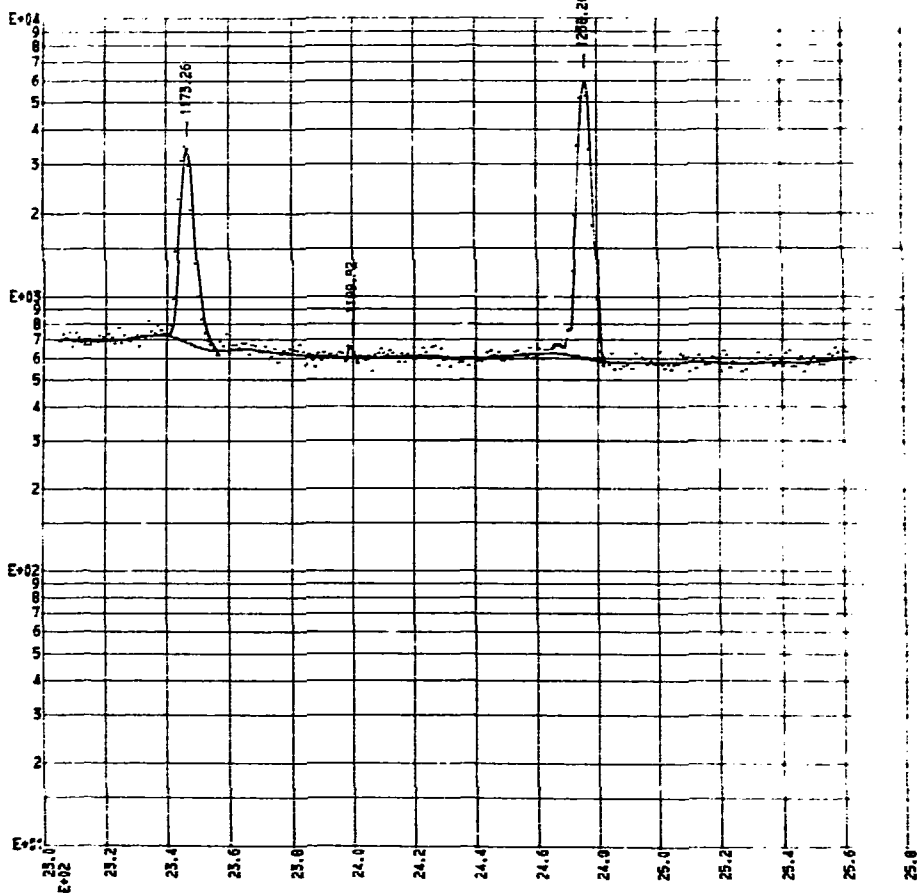

FISS. +ACT. PRODS. DETECTOR F-2 SPECTRUM 45220

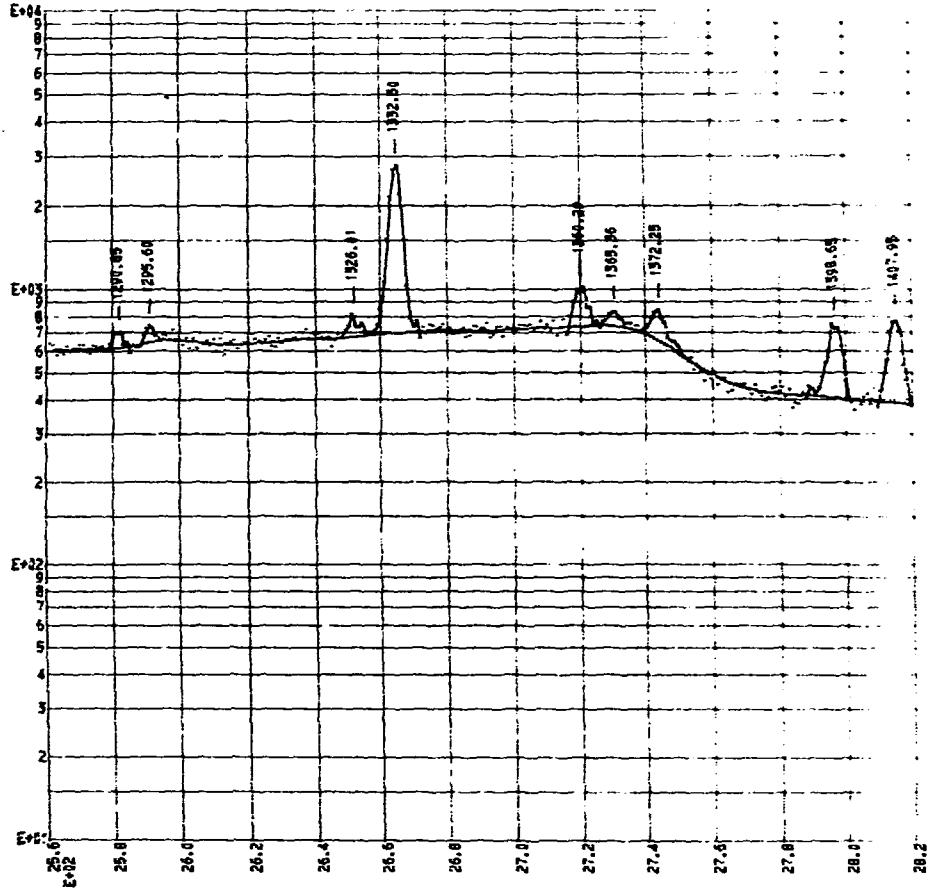

FISS. +ACT. PRODS. DETECTOR F-2 SPECTRUM 462201

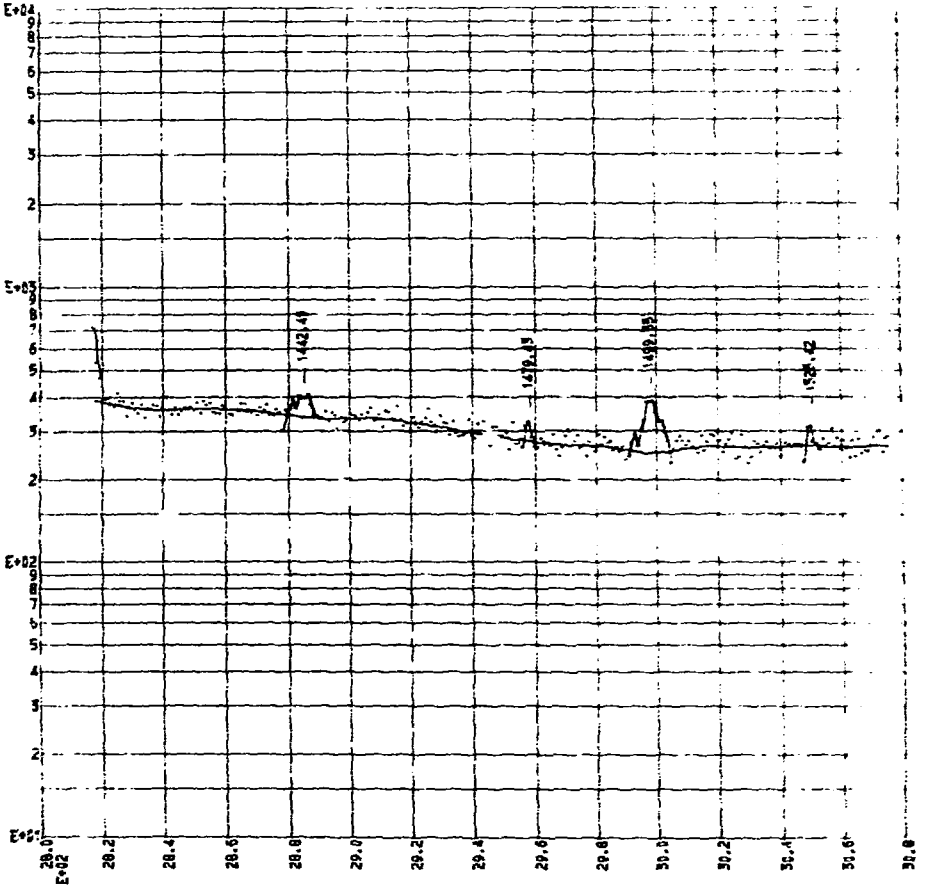

FISS. +ACT. PRODS. DETECTOR F-2 SPECTRUM 46220

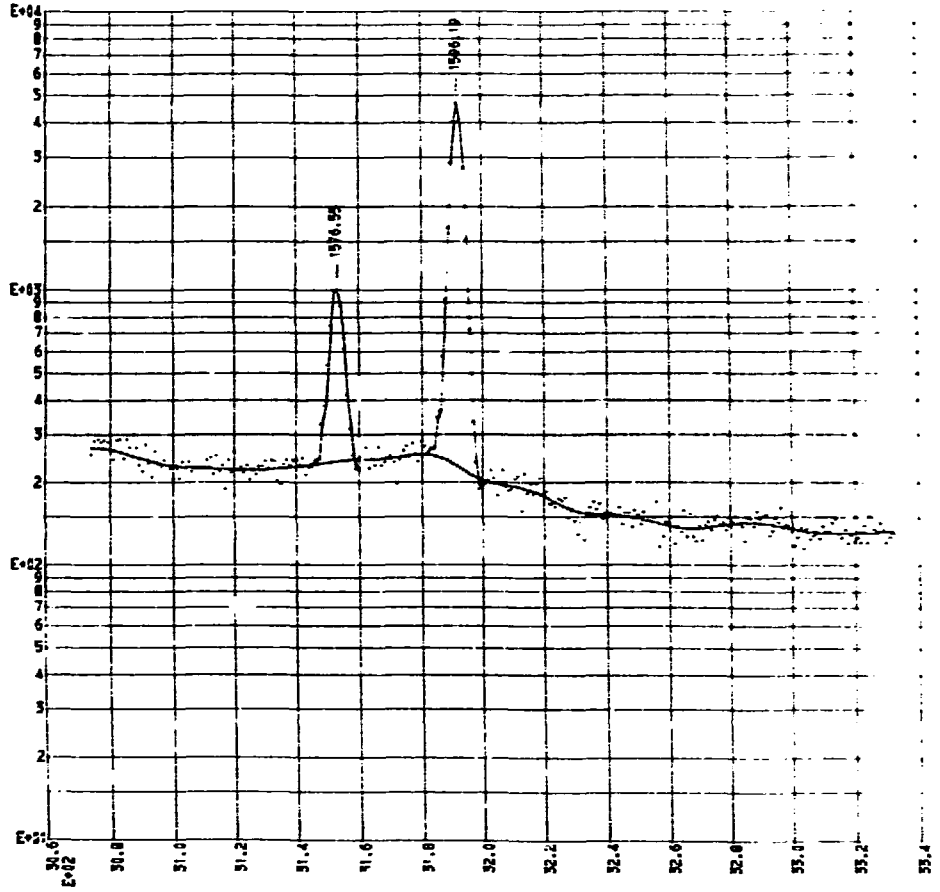

FISS. +ACT. PRODS. DETECTOR F-2 SPECTRUM 46220

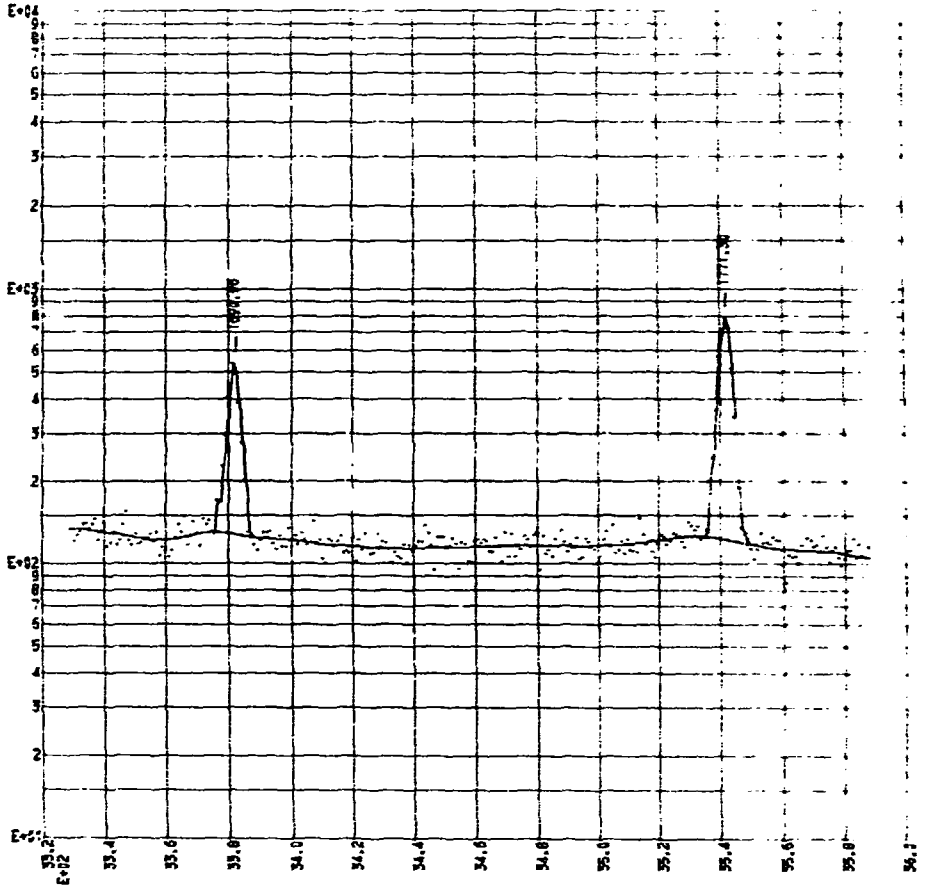

FISS. +ACT. PRODS. DETECTOR F-2 SPECTRUM 46220

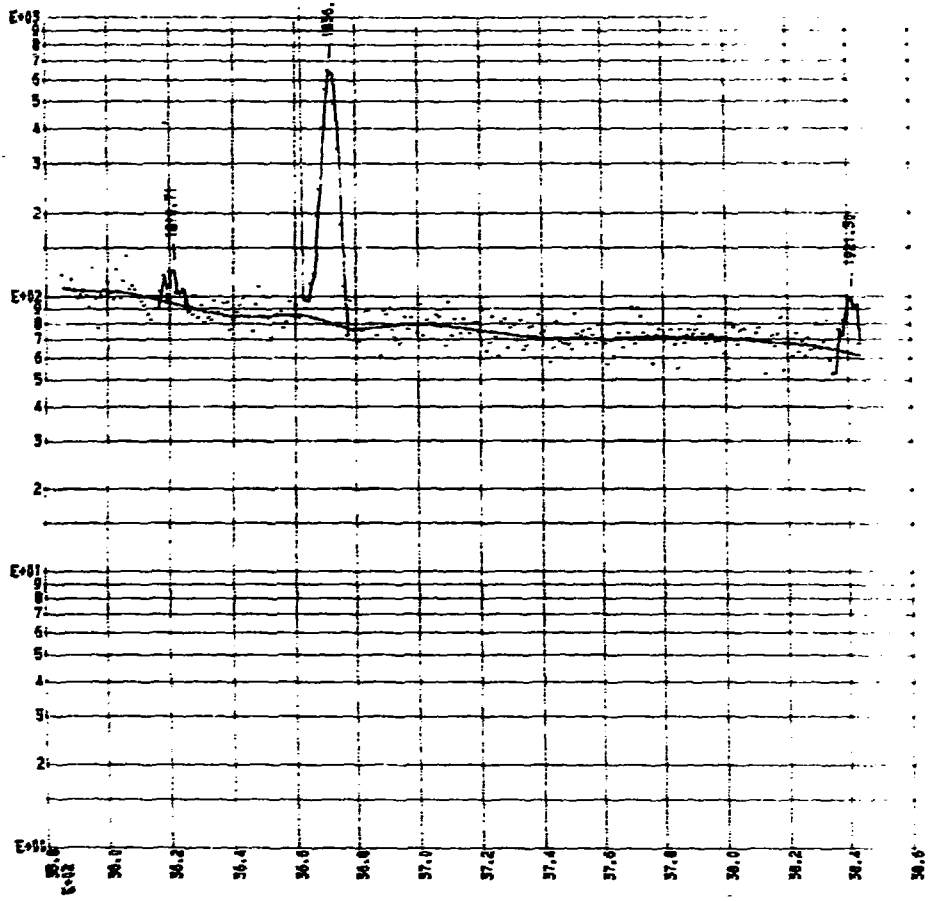

FISS. +ACT. PRODS. DETECTOR F-2 SPECTRUM 462201

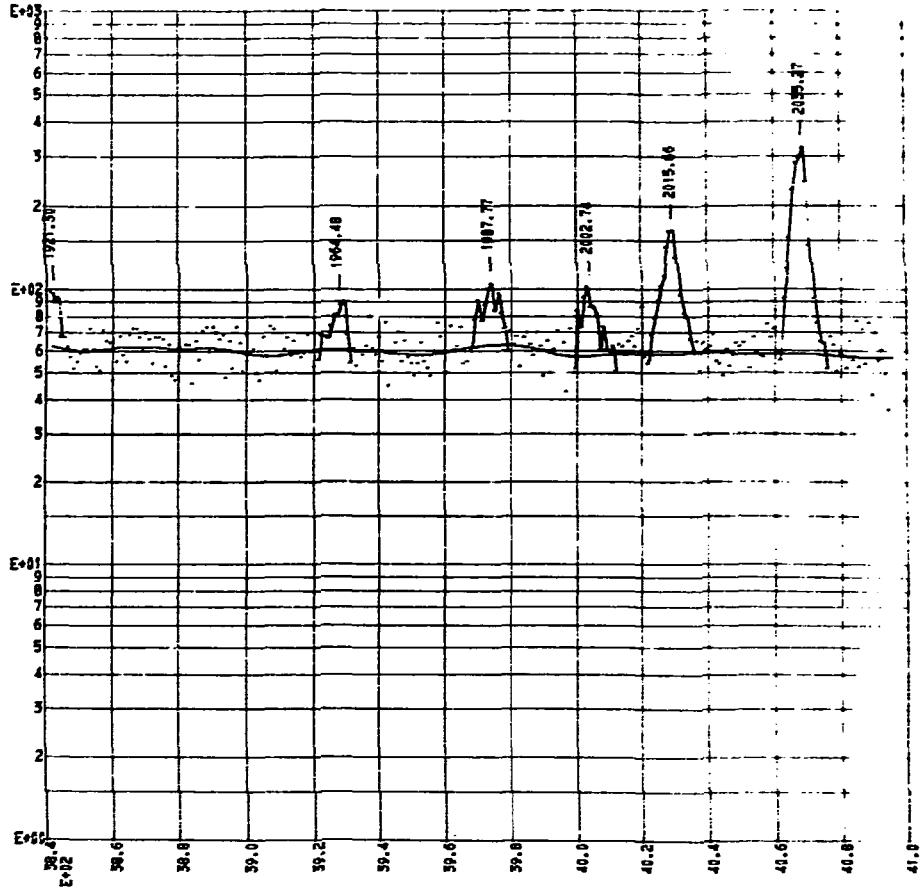

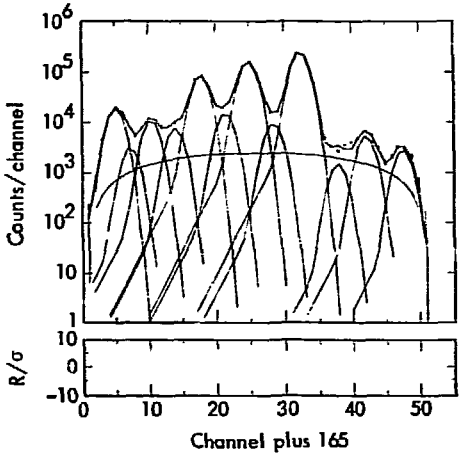

Fig. B-2. Peak fitting of the 90 keV region of the spectrum presented in Appendix A. Two of the peaks are due to uranium K_α x rays. Their anomalous shape frequently causes satellite peaks to be inserted near the bases of these peaks. A slight parabolic increment to the background can also be seen in the figure.

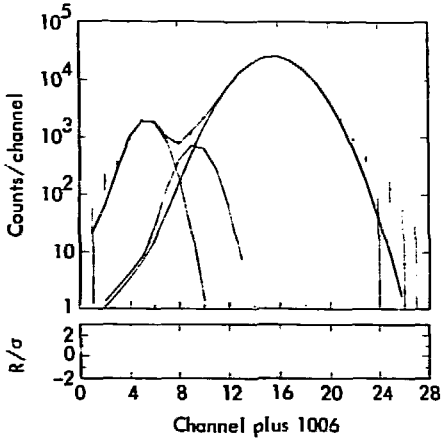

Fig. B-3. Fitting of the 511 keV peak region. Since the 511 keV radiation resulting from β^+ annihilation is Doppler broadened, its width is allowed to be greater than would otherwise be calculated for a gamma ray of this energy.

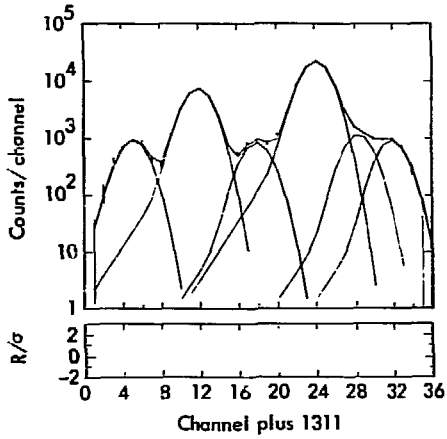

Fig. B-4. Peak fitting of a typical gamma ray multiplet. The 669 keV peak shown as the fifth member of thie multiplet is not discernible of normal methods of peak detection (see Fig. B-1) but was found by GAMANAL through an examination of the residuals.

Appendix C

Printouts of a Peak Shape Analysis

The various parameters used for describing the peak shape as a function of energy may be determined from a given spectrum by making an appropriate call to SHAPE. The peaks specified on the Type 3 card will be used for the characterization and will result in a detailed printout, such as that shown in Table C-1, for each peak or peak grouping examined. The correlation of the results is summarized in a printout such as that shown in Table C-2, which lists the new shape parameters and the results of the overall fit.

Table C-1. Printout showing the characterization of some of the shape parameters for the 1596 keV peak in the fission product spectrum shown in Appendix A. Starting with the input estimates shown on the first line, an iterative process is used to find a set of values for the shape parameters which will give the best fit. The results of the fit are then indicated.

```
1        FITTING OF DATA USING  1 PEAKS ALPHA =  -C.151 (FWHM =   4.284) PLUS A  0 ORDER POLYNOMIAL

 CFIT  FWHM   SKEW1 SKEW2 SKEW3 PKPOS  PKPOS  PKPLS  PKPLS  PKPCS  PKPCS  PKPOS  PKPOS  PKPUS
                                / PKHT / PKHT / PKHT / PKHT / PKHT / PKHT / PKHT / PKHT / PKHT

       4.284 0.850 0.540 0.400  10.970
                                4475.

 0.83  4.412 0.850 0.540 0.400  11.067
                                4377.

 0.84  4.399 0.850 0.540 0.400  11.069
                                4386.

 0.85  4.336 0.907 0.551 0.400  11.116
                                4365.

 0.88  4.336 1.005 0.568 0.400  11.115
                                4365.

 0.89  4.346 1.109 0.585 0.400  11.109
                                4367.

 0.90  4.358 1.168 0.593 0.400  11.100
                                4371.

 0.90  4.366 1.178 0.595 0.400  11.094
                                4373.

 0.84  4.366 1.183 0.596 0.400  11.093
                                4374.

          CHANNEL  ERROR  FWHM   SKEW1  SKEW2  SKEW3  C/AREA    P/AREA   ERROR
   1  3181 +  11.093  0.028  4.366  1.183  0.596  0.400  21965.0   21940.7  1.12


          YNET   RESIDUAL  CY1     CY2      WTF          WTD. RES
   1      0.     -12.0     0.      0.    0.086387        -1.1
   2     11.5    -11.2     0.64   -0.26  0.044001        -0.5
   3     14.7    -26.2     3.36    2.26  0.043967        -1.2
   4     94.3     20.0     4.01   -1.61  0.041042         0.8
   5    115.4    -25.7     7.71    4.77  0.040469        -1.0
   6    329.9     34.8    15.65    2.84  0.034920         1.2
   7    684.8     18.7    23.20    6.08  0.029245         0.5
   8   1428.8    -12.7    31.68    5.51  0.022898        -0.3
   9   2638.1    -13.0    31.38   -0.47  0.017932        -0.2
  10   3797.5    -61.1    21.10   -3.85  0.013317        -0.9
  11   4475.0    104.5     0.90   -9.62  0.010238         1.5
  12   3878.5     -3.6   -22.58   -6.04  0.015198        -0.1
  13   2526.0    -56.3   -34.31    1.24  0.018349        -1.0
  14   1304.3     19.6   -34.48    5.14  0.023961         0.5
  15    497.4     18.7   -27.51    7.49  0.032816         0.6
  16    119.3    -14.1   -15.34    7.07  0.042849        -0.6
  17     25.0     -2.8    -5.22    2.18  0.047404        -0.1
  18      0.      -4.3     0.      0.    0.096337        -0.4
```

Table C-2. A portion of the printout summarizing the results of the peak shape analysis. The new values for the various parameters may be used to describe the shapes of all the peaks found in the current spectrum and subsequent spectra taken on the same detector and system.

RESULTS OF PEAK SHAPE ANALYSIS USING 6 PEAKS IN THE SPECTRUM

SHAPE PARAMETERS ARE , S(1) = 1.106 S(3) =-2.979E+00 S(5) = 1.192
S(2) = 2.212E-03 S(4) = 1.999E-03 S(6) = 0.400

PEAK POSITION	PEAK ENERGY	MEASURED FWHM	CALC. FWHM	MEASURED SKEW1	CALC. SKEW1
281.0	140.4	2.502	2.476	C.C78	0.067
457.0	228.2	2.613	2.628	C.128	0.080
1545.0	772.7	3.462	3.425	C.115	0.238
1693.0	846.8	3.462	3.519	C.382	0.276
2476.0	1238.3	3.988	3.981	C.73C	0.604
3192.0	1596.2	4.366	4.361	1.183	1.235

Printed in USA. Available from the National Technical Information Center, National Bureau of Standards, U. S. Department of Commerce, Springfield, Virginia 22151
Price: Printed Copy $3.00; Microfiche $0.65.